KfK 3068
Oktober 1980

Annual Report

Teilinstitut Kernphysik des Instituts für Angewandte Kernphysik (July 1, 1979 - June 30, 1980)

Editors:
F. Dickmann, A. Hanser
Institut für Angewandte Kernphysik

Kernforschungszentrum Karlsruhe

KERNFORSCHUNGSZENTRUM KARLSRUHE

Institut für Angewandte Kernphysik

KfK 3068

ANNUAL REPORT

Teilinstitut Kernphysik
des Instituts für Angewandte Kernphysik

(July 1, 1979 - June 30, 1980)

Editors: F. Dickmann and A. Hanser

Kernforschungszentrum Karlsruhe GmbH, Karlsruhe

Kernforschungszentrum Karlsruhe
ISSN 0303-4003
ISSN 0171-2926

Abstract

The activities of the Nuclear Physics Section of the Institute of Applied Nuclear Physics from mid 1979 to mid 1980 are surveyed. The research program comprises both contributions to fundamental and applied nuclear research. The activities on the application of nuclear methods mainly concentrate on the application of gamma-ray spectrometry to nuclear fuel assay problems, the development of a proton microbeam for elemental analysis, and the production of radioisotopes for medical application. The study of nuclear reactions induced by alpha particles, ^{6}Li ions and fast neutrons, and the measurement of optical hyperfine structure using high-resolution laser spectroscopy form the major part of the fundamental research work. In addition, the operation of the Karlsruhe Isochronous Cyclotron is briefly reviewed.

Zusammenfassung

Es wird über die Tätigkeit des Teilinstituts Kernphysik des Instituts für Angewandte Kernphysik von Mitte 1979 bis Mitte 1980 berichtet. Das Forschungsprogramm beinhaltet sowohl Anwendungen der Kernphysik auf Probleme der Kernenergie als auch grundlagenphysikalische Arbeiten. Schwerpunkte der angewandten Arbeiten bilden die Anwendung gammaspektrometrischer Meßverfahren zur Spaltstoffbestimmung, die Entwicklung einer Protonenmikrosonde für die Elementanalyse sowie die Erzeugung von Radioisotopen für medizinische Anwendungen. Zu den grundlagenphysikalischen Arbeiten gehören Untersuchungen von Kernreaktionen mit Alpha-Teilchen, ^{6}Li-Ionen und schnellen Neutronen sowie die Messung der optischen Hyperfeinstruktur mittels hochauflösender Laserspektroskopie. Ferner wird der Betrieb des Karlsruher Isochronzyklotrons kurz geschildert.

The Institute of Applied Nuclear Physics of the Karlsruhe Nuclear Research Centre is engaged in research in fundamental nuclear physics and its applications to problems of nuclear energy, solid state physics, medicine, and analysis. This report gives a survey of the work of the Nuclear Physics Section from mid 1979 to mid 1980. Progress of the Nuclear Solid State Section is reported separately.

Most of the experimental research makes use of the two accelerators of our institute, a 3.7 MV single stage Van de Graaff employed mainly for neutron time-of-flight work, and the Karlsruhe Isochronous Cyclotron. The latter accelerates protons, deuterons, α particles, and ^{6}Li ions to 26 MeV/nucleon.

A number of important changes occurred or were initiated around the isochronous cyclotron. By January 1, 1980, a group engaged in the activation of machine parts for wear studies was transferred to the cyclotron laboratory from the Laboratory of Isotope Technology of the Research Centre. The steadily increasing demand of machine time for applied work, mainly in mechanical engineering and isotope production for nuclear medicine, has led to the decision late in 1979 to order a second, compact cyclotron. This will be a 42 MeV negative hydrogene ion machine and is expected to take over most of the applications in 1982. Meanwhile the work on the MAFIOS ion source for completely stripped carbon, nitrogene, oxygene and, hopefully, neon ions has proceeded succesfully. Construction of the annex to the cyclotron building for this ion source has started, and planning of the building for the compact cyclotron is under way.

In most fields, research work proceeded along the lines indicated by the work of previous years. The measurement of nuclear radii and moments by laser spectroscopy has been extended to nine calcium isotopes. The analysis of α particle scattering with the aim of determining neutron distributions in nuclei has been further refined. Measurements of neutron capture cross sections of relevance to the s-process of nucleosynthesis have been extended, and their analysis yielded improved parameters of the flux distribution pre-

vailing during this process. The system for measuring the enrichment of uranium on-line during the production process in a fuel fabrication plant has been installed in the factory and completed the first six months of operation successfully.

In June 1980, the institute was host of the 17th European Cyclotron Progress Meeting attended by 125 participants from 15 European countries, Canada and the USA. It was considered to be a successful meeting, in spite of a post-conference hike to the Black Forest drowned in pouring rain.

Gerd Schatz

Das Institut für Angewandte Kernphysik des Kernforschungszentrums Karlsruhe beschäftigt sich zu etwa gleichen Teilen mit Grundlagenuntersuchungen zur Kernphysik und ihrer Anwendung auf Probleme der Kernenergie, Festkörperphysik, Medizin und Analyse. Der vorliegende Bericht gibt einen Überblick über die Tätigkeit des Teilinstituts Kernphysik von Mitte 1979 bis Mitte 1980. Über die Tätigkeit des Teilinstituts Nukleare Festkörperphysik wird getrennt berichtet.

Die meisten experimentellen Arbeiten nutzen die beiden Beschleuniger unseres Institutes, einen einstufigen Van-de-Graaff von 3,7 MV, der hauptsächlich für Flugzeitmessungen von Neutronen eingesetzt wird, und das Karlsruher Isochronzyklotron. Das Zyklotron beschleunigt Protonen, Deuteronen, α-Teilchen und ^{6}Li-Ionen auf 26 MeV/Nukleon.

Am Zyklotron wurden einige wichtige Änderungen durchgeführt oder eingeleitet. Anfang 1980 trat die Gruppe, die sich mit der Aktivierung von Maschinenteilen für Verschleißuntersuchungen beschäftigt, vom Laboratorium für Isotopentechnik des Kernforschungszentrums in das Zyklotronlaboratorium über. Die stetig ansteigenden Strahlzeitanforderungen von Seiten der Anwendungen, vor allem im Maschinenbau und der Isotopenproduktion für die Nuklearmedizin, führten zu dem Entschluß, ein zweites Zyklotron zu bestellen. Es handelt sich hierbei um eine Maschine, die negative Wasserstoffionen auf 42 MeV beschleunigt. Sie soll ab 1982 den größten Teil der Anwendungen übernehmen. In der Zwischenzeit kommen die Arbeiten an der MAFIOS-Ionenquelle, die "nackte" Ionen der Elemente Kohlenstoff, Stickstoff, Sauerstoff und evtl. Neon liefern soll, gut voran. Ein Anbau an das Zyklotrongebäude für diese Ionenquelle wurde begonnen, und die Planung des Gebäudes für das neue Zyklotron ist im Gange.

Auf den meisten Gebieten folgten die Forschungsarbeiten den Linien, die durch die Arbeit der vorhergehenden Jahre vorgezeichnet waren. Die Messungen von Kernradien und -momenten mit Hilfe der Laserspektroskopie wurden auf neun Kalziumisotope ausgedehnt. Die Analyse der Streuung von α-Teilchen mit dem Ziel, die Verteilung der Neutro-

nen in Kernen zu bestimmen, wurde weiter verfeinert. Die Messungen von Neutroneneinfangquerschnitten, die für den s-Prozeß der Nukleosynthese von Bedeutung sind, wurden ausgedehnt und haben verbesserte Parameter für die Flußverteilung ergeben, die während des s-Prozesses herrschte. Das System zur on-line-Messung der Urananreicherung während der Brennelementproduktion wurde in der Fabrik installiert und hat die ersten sechs Betriebsmonate erfolgreich bestanden.

Im Juni 1980 war das Institut Gastgeber des 17th European Cyclotron Progress Meeting, das von 125 Teilnehmern aus 15 europäischen Staaten, Canada und den USA besucht wurde. Das Treffen war sehr erfolgreich, trotz eines total verregneten Ausflugs in den Schwarzwald.

Gerd Schatz

CONTENTS

1. NEUTRON PHYSICS

1.1 FUNDAMENTAL RESEARCH

1.1.1 The Number of Prompt Fission Neutrons $\nu(A)$ for Fast Neutron Induced Fission of ^{235}U and ^{237}Np

A.A. Naqvi, R. Müller[+], F. Käppeler

First results from the 4-parameter experiment for the determination of kinetic energies and velocities from correlated fragments were reported in previous progress reports (1). The measurements were carried out on ^{235}U at neutron energies of .5 and 5.5 MeV and on ^{237}Np at .8 and 5.5 MeV.

The last and most difficult step in data analysis concerns the number of prompt fission neutrons as a function of fragment mass. This quantity is calculated from the fragment mass difference before and after neutron evaporation. Primary fragment masses are derived from the fragment velocities and secondary masses result from the observed kinetic fragment energies. During analysis it turned out that the common calibration scheme of Schmitt et al. (2) for the conversion of detector pulse height to fragment kinetic energy yields too large values for E_{kin}. Therefore a correction to the respective parameters was applied which was determined from comparison of our results with radiochemical data. Fig. 1 shows the saw-tooth curve for $\nu(A)$ for ^{235}U and ^{237}Np at the different neutron energies.

The curves in Fig. 1 exhibit two interesting points:

- The increase of ν with excitation energy is observed for the heavy fragments only. There is no easy theoretical explanation for this behaviour (see contrib. 4.4 to this report).
- The excitation of the near doubly magic fragments around A=132 appears to be so low that they do not evaporate neutrons even at rather high saddle point excitations. For example, fission of ^{235}U with neutrons of 0.5 MeV energy corresponds to a saddle point excitation of about 1.5 MeV. This indicates that there is probably no complete statistical equilibrium between various degrees of freedom during the deformation from saddle to scission.

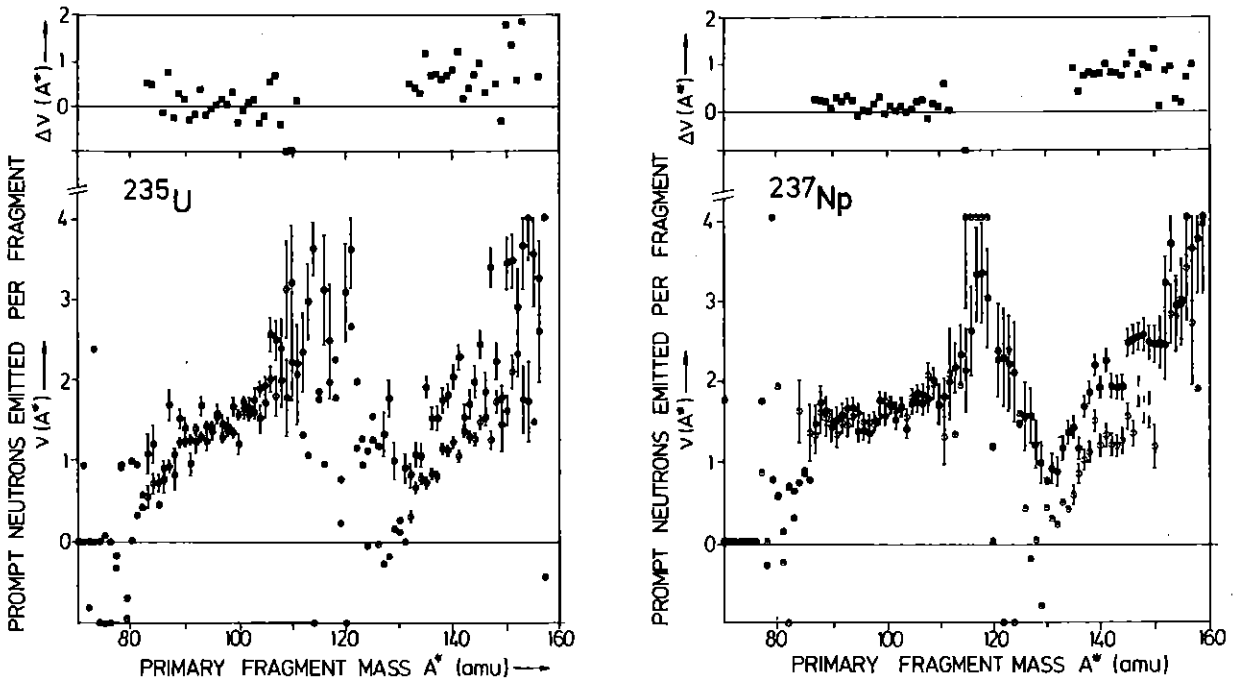

Fig. 1: The number of prompt fission neutrons as a function of fragment mass for fast neutron induced fission of ^{235}U and ^{237}Np (o E_n=.5 MeV, • E_n=5.5 MeV). Obviously for both isotopes the increase in ν with excitation energy is restricted to a corresponding increase in the heavy fragments only.

References

(1) R. Müller, A.A. Naqvi, F. Käppeler, KfK-Report 2686 (Oct. 1978) p. 11
A.A. Naqvi, F. Käppeler, R. Müller, KfK-Report 2868 (Oct. 1979) p. 17

(2) H.W. Schmitt, W.E. Kiker, C.W. Williams, Phys. Rev. B137 (1965) 837

+University of Tübingen, present adress: Siemens, München

1.1.2 Improvements in the Systematics of s-Process Nucleosynthesis

F. Käppeler, H. Beer, K. Wisshak, R.L. Macklin+, D.D. Clayton++, R. Ward+++

The description of nucleosynthesis under weak neutron irradiations (s-process, s ≙ slow neutron capture) requires knowledge of the Maxwellian averaged capture cross sections of the nuclei concerned and

some assumptions about the neutron flux. Since the s-process was formulated (1,2) several attempts were made to establish a model for calculating the isotopic abundances produced in this process. As a result it was found that probably an exponential distribution of time integrated neutron fluxes reproduces best the abundance pattern of pure s-process nuclei (3,4). It also turned out that beside the pure s-process nuclei in particular those nuclei with closed neutron shells (N=50,82, 128) are very important for the model. The existing investigations suffered from the fact that for these relevant cases experimental cross sections were either very uncertain or entirely lacking.

This situation was improved considerably during the past three years (see also contributions 1.1.4, 1.1.5 and 1.1.6 to this report) and we therefore tried to reanalyse the s-process which is characterized by the product $N_s\langle\sigma\rangle$ of the s-process abundance N_s and the Maxwellian-averaged capture cross section $\langle\sigma\rangle$ for thermal energies of kT=30 keV. The result is shown in Fig. 1 where the solid lines represent the $N_s\langle\sigma\rangle$ curve calculated with the following flux distribution:

$$\rho(\tau) = \frac{G_1}{\tau_{o1}} \exp(-\tau/\tau_{o1}) + \frac{G_2}{\tau_{o2}} \exp(-\tau/\tau_{o2}) \qquad (1)$$

G_i is the respective ^{56}Fe seed abundance and τ_{oi} means the respective mean neutron fluence. The comparison with empirical values for $N_s\langle\sigma\rangle$ of pure s-process nuclei and of those which are produced predominantly in this way clearly indicates that there is quite good agreement within an error band of about $\pm$ 20 %. The error bars on the black squares correspond to the cross section uncertainties only and do not account for the respective uncertainties of the abundances.

For the stronger flux component our calculations yield parameters G_2 and τ_{o2} which are similar to the results of Ref. (4). The build-up of nuclei with A 90 requires a ^{56}Fe seed which is only 0.1 % of the solar ^{56}Fe abundance and an average neutron fluence of τ_{o2}=0.220 neutrons per mb. The corresponding values of Ref. (4) are 0.34 % and 0.25 neutrons per mb.

However, for the weak flux component which is responsible for most of the s-process abundances in the mass region $56 < A < 90$ come to very different conclusions. Interpreting ^{58}Fe as being predominantly produced in the s-process we find that 2.5 % of the solar

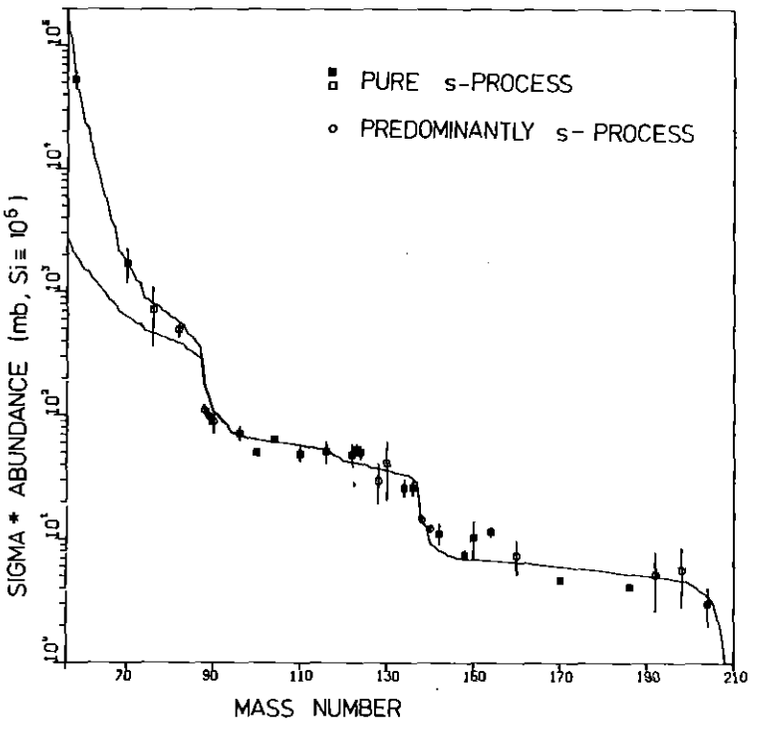

Fig. 1: The calculated Nσ-curve (solid lines) which now represents a rather accurate basis for s-process systematics. For comparison, empirical values are shown for pure s-process nuclei and also for those nuclei which are produced predominantly in this process.

^{56}Fe abundance has to be irradiated with a mean fluence of 0.059 neutrons per mb whereas the previous numbers of Ref. (4) were 130 % and 0.05 neutrons per mb, respectively.

As the abundances of isotopes with A>70 are normally composed of contributions from the s- and the r-process (r = rapid neutron capture) the Nσ-curve of Fig. 1 allows to determine also the abundance pattern for the r-process which is known to be a rather smooth function of A. Fig. 2 shows the abundances of pure r-process nuclei together with the r-process abundances which were determined from solar abundances by subtraction of the s-process component. The two data sets are in good agreement which is an additional confirmation of the derived s-process systematics.

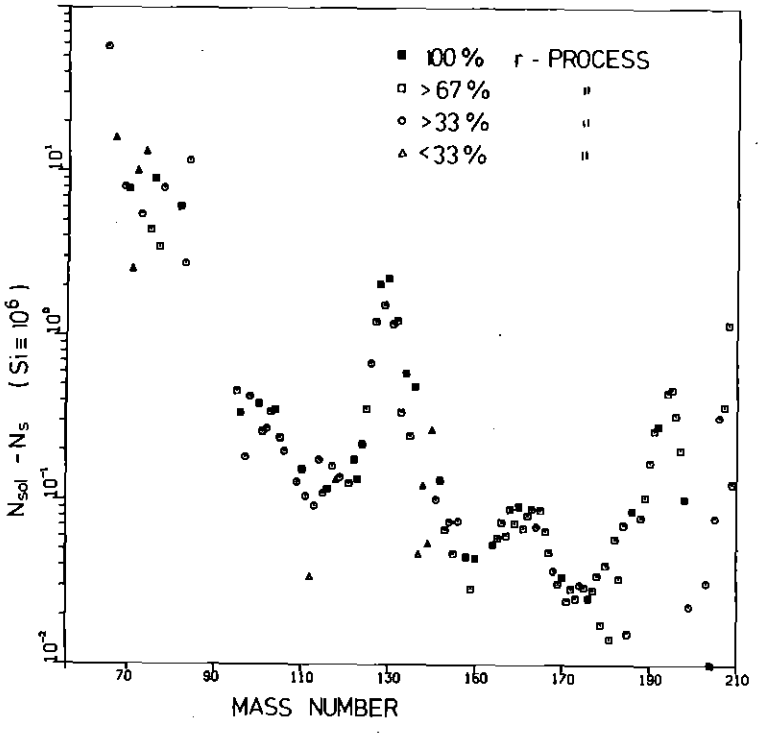

Fig. 2: The abundance pattern synthesized by rapid neutron capture (r-process). The pure r-process nuclei (black squares) fit well to those values, which were derived from s-process systematics.

References

(1) E.M. Burbridge, G.R. Burbridge, W.A. Fowler, F. Hoyle, Rev. Mod. Phys. 29 (1957) 547

(2) D.D. Clayton, W.A. Fowler, T.E. Hull, B.A. Zimmermann, Annals of Physics 12 (1961) 331

(3) P.A. Seeger, W.A. Fowler, D.D. Clayton, Astrophysical Journal 98 (1965) 121

(4) R. Ward. M. Newman, Astrophysical Journal 219 (1978) 195

+ Oak Ridge National Laboratory, Tennessee / USA

++ MPI für Kernphysik Heidelberg, Univ. of Houston, Texas / USA

+++ MPI für Physik und Astrophysik München

1.1.3 Total Neutron Cross Sections of the Neon Isotopes in the Energy Range from 5 to 900 keV

J. Almeida, F. Käppeler

The neutron cross sections of neon isotopes in the keV region are of great importance for the nucleosynthesis of heavy elements with A 60. In the stellar environment where the so called s-process takes place the reaction $^{22}Ne(\alpha,n)$ is believed to be the major neutron source. Simultaneously, neutron capture in the very abundant ^{22}Ne is probably the most important neutron sink. For a quantitative investigation of the neutron balance experimental information about the neutron capture cross section of ^{22}Ne is required. As no such measurements have been performed so far in the energy range of interest, we have initiated a systematic study of total and capture cross sections on all neon isotopes.

In a first step, transmission measurements were carried out on natural neon and on isotopically enriched samples. The energy region from 5 to 800 keV was covered in several runs. Neutrons were produced via the $^{7}Li(p,n)$ reaction using thick metallic lithium targets which provided a neutron energy spread of $\sim$300 keV. Neutron energies were measured by time-of-flight at a flight path of 3 m and a resolution of $\sim$0.4 ns/m.

The samples were contained in stainless steel cylinders with 0.5 mm thick walls under pressures of up to 150 bar. Except for ^{21}Ne, where only 1 l of gas was available, the sample thicknesses were approximately 0.03 at/barn corresponding to 6.6 l of gas at standard conditions. The samples were natural neon (90.5 % ^{20}Ne, 9.2 % ^{22}Ne), and enriched ^{21}Ne (95.4 %) and ^{22}Ne (99.9 %).

For all three isotopes the various experimental runs were analyzed and the total cross sections calculated. Fig. 1 shows part of the results for ^{22}Ne in the energy range from 150 to 750 keV. These data will be further investigated by resonance analysis.

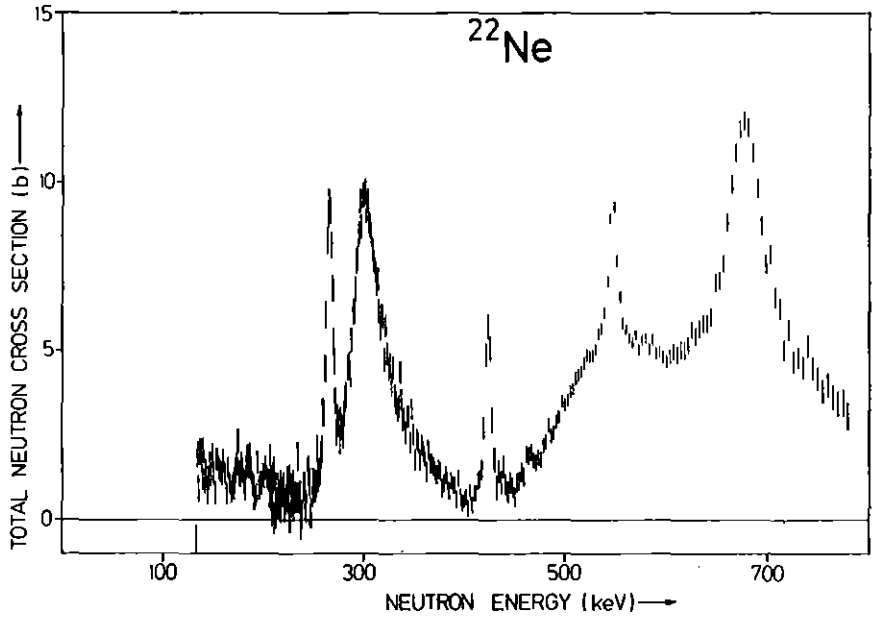

Fig. 1: The total neutron cross section of ^{22}Ne in the energy range from 150 to 750 keV.

1.1.4 Neutron Capture Cross Sections on ^{138}Ba, ^{140,142}Ce, ^{175,176}Lu, and ^{181}Ta at 30 keV: Prerequisite for Investigation of the ^{176}Lu Cosmic Clock*

H. Beer and F. Käppeler

The capture cross sections of ^{138}Ba, ^{140,142}Ce, ^{176}Lu, ^{181}Ta and the capture cross section of ^{175}Lu to the 3.68 h isomeric state in ^{176}Lu have been determined at 30 keV neutron energy using the activation technique. Neutrons were generated via the ^{7}Li(p,n) reaction just above the reaction threshold at a 3 MV pulsed Van de Graaff accelerator. The capture cross sections are of importance to stellar nucleosynthesis. With the ^{138}Ba and ^{140}Ce cross sections the time integrated average neutron flux for the s-process was determined to 0.22 mb^{-1}. This result, the capture cross section of ^{176}Lu and the ^{175}Lu cross section to the 3.68 h isomeric state in ^{176}Lu were used to analyze the ^{176}Lu cosmic clock. The mean s-process age of solar matter before the solidification of the solar system was estimated to 6 x 10^{9} a. In addition the Hf/Lu abundance ratio was determined.

*Phys. Rev. C21 (1980) 534

1.1.5 ^{176}Lu: A Cosmic Clock or a Stellar Thermometer?

R.A. Ward[+], H. Beer, F. Käppeler, K. Wisshak

Since the β^--decay of the long-lived ground state of ^{176}Lu ($t_{1/2} = (3.6 \pm 0.16) \times 10^{10}$ a) to ^{176}Hf can potentionally be used as a chronometer of galactic s-process nucleosynthesis (1) it is important to calculate the rate at which stellar photons can induce transitions between the ground state of ^{176}Lu and the much shorter-lived β^--decaying isomeric state ($T_{1/2}$ = 3.68 h) at 126.5 keV. The problem is of astrophysical interest because if internal thermal equilibrium is attained at the s-process temperature, then the effective half-life of the entire ^{176}Lu nucleus against β^--decay can be shortened considerably.

Figure 1 shows the properties of the first 20 excited states of ^{176}Lu that can be of importance for providing intermediate coupling between the ground and isomeric states of ^{176}Lu. The fraction of the stellar ($\sim$30 keV) neutron captures on the $7/2^+$ ground state of ^{175}Lu that initially populate the long-lived ground state is denoted as B, with the remaining fraction 1-B following gamma cascades that ultimately lead to ^{176}Lu^m (3.68 h). These lowest-lying states have also been separated according to their rotational band structure in order to emphasize the possible importance of K-selection rules in determining interband electromagnetic transition rates. The inhibition factor $f = 10^{-2\,(|\Delta K| - \lambda)}$ given in Figure 1 was chosen because of the empirical observation (2) that for $|\Delta K| > \lambda$ every degree of K-forbiddenness corresponds to a retardation by a factor of $\sim$ 100 relative to that predicted by using theoretical Weisskopf single-particle transition rates.

To ascertain whether or not the ground state and the isomer are in fact able to maintain their separate identities under stellar conditions, we have used the formalism of Ward and Fowler (3) to integrate numerically the coupled set (in this case 20) of first order differential equations describing the complete time evolution at constant stellar temperature and free-neutron density of the population of each state of ^{176}Lu shown in Fig. 1.

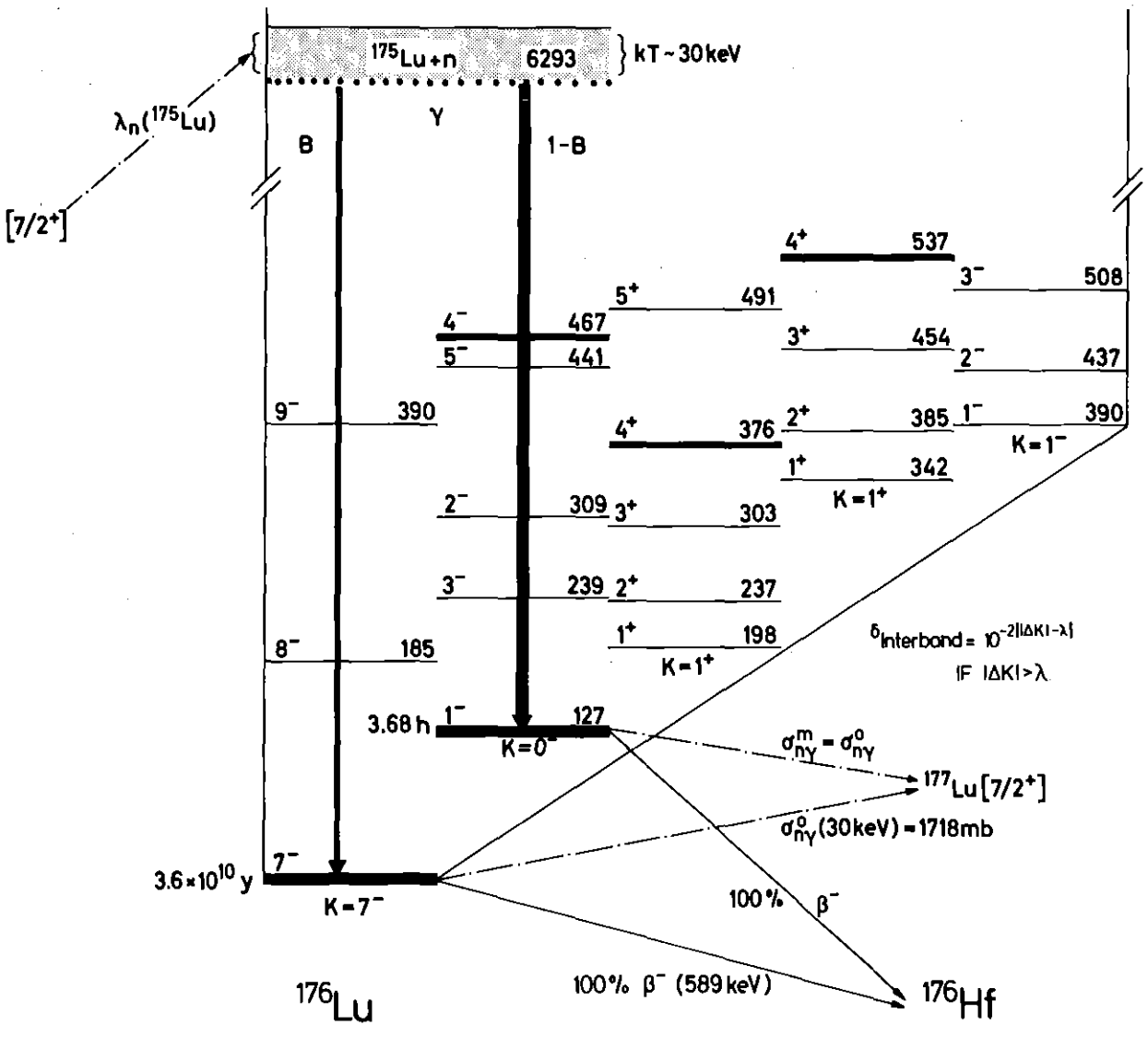

Fig. 1: Level scheme of the first 20 states of ^{176}Lu. For both, the ground and the isomeric state at 127 keV the possible branchings due to neutron capture and beta decay are indicated.

With this procedure we can calculate the resulting neutron capture branching ratio $\langle f_n \rangle$ as a function of temperature and neutron density. Fig. 2 shows the variation of $\langle f_n \rangle$ for different input values B=0.01, 0.36 and 0.99 and a neutron density of 10^7 neutrons per cm^3 where B=0.36 corresponds to the experimental value (4) and the neutron density of 10^7 cm^{-3} is the typical mean neutron density estimated from various s-process branches (5). The families of solid curves show how $\langle f_n \rangle$ evolves from the low-temperature limit into thermal equilibrium. Each curve is labeled with the appropriate value of δ. For temperatures $T_8 \leqq 1.7$ (kT = 15 keV) B is not disturbed by thermal effects ($\langle f_n \rangle \equiv$ B) and therefore ^{176}Lu can be regarded as a cosmic clock, whereas for

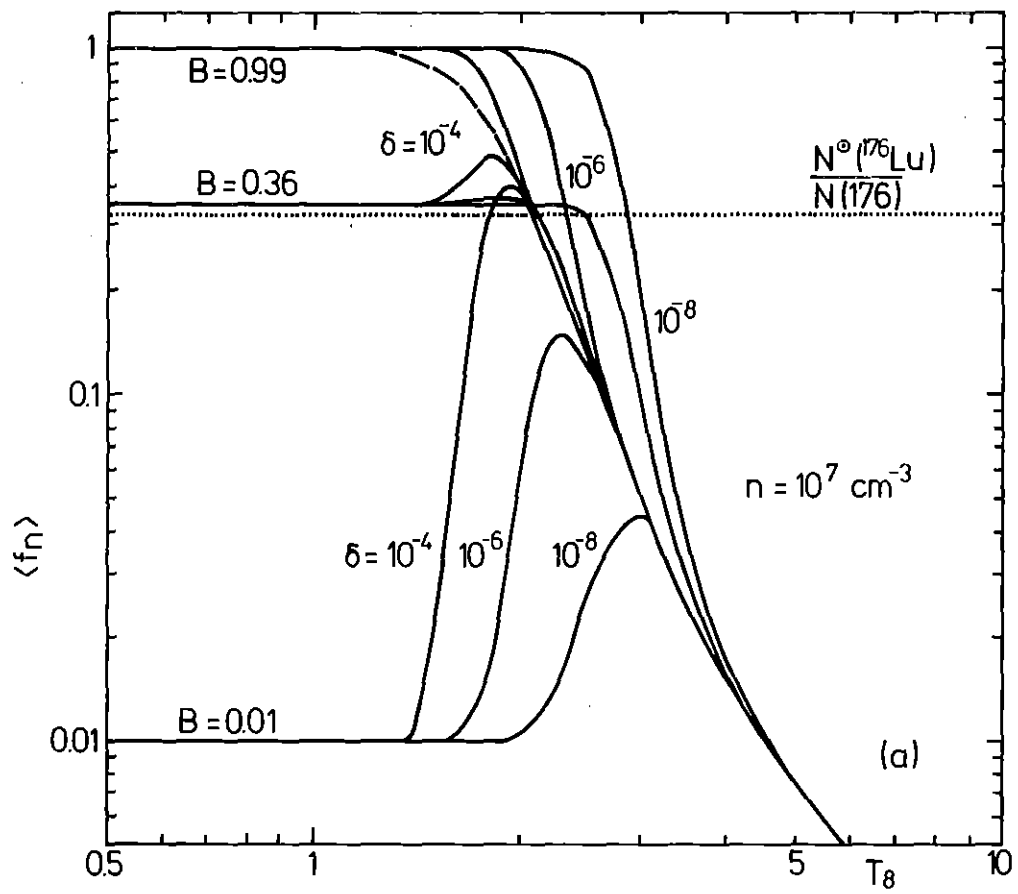

Fig. 2: The neutron capture branching ratio $\langle f_n \rangle$ as a function of the stellar temperature $T_8 \equiv T/10^8$ K for the constant free neutron density $n=10^7\ cm^{-3}$. Each family of three curves emerges from a common value B as indicated, and they separate according to the value of δ (the internal electromagnetic rate scaling factor) with which they are labeled. The dashed curve gives the value of $\langle f_n \rangle$ appropriate to thermal equilibrium, and the additional horizontal dotted line gives the observed present-day value of $N_o(^{176}Lu)/N(176) = 0.33$.

$T_8 > 3$ (kT = 26 keV) the ^{176}Lu ground and isomeric levels are equilibrated so that ^{176}Lu is an s-process thermometer. The intermediate region is determined by the detailed properties of the ^{176}Lu decay scheme.

In the present discussion ^{176}Lu was studied under the simplifying assumptions of both a constant stellar temperature and neutron density. However, in a realistic model for the site of the s-process one must actually follow the detailed time dependence of the neutron density and

temperature during and after the neutron irradiation in order to account for the important "freeze out" of the neutron capture and β^--decay rates.

References

(1) H. Beer, F. Käppeler, Phys. Rev. C21, 534 (1980)

(2) K.E.G. Löbner, Phys. Lett. 26B, 369 (1968)

(3) R.A. Ward, W.A. Fowler, Ap. J. 238 (1980)

(4) H. Beer, F. Käppeler, K. Wisshak, and R.A. Ward, Ap. J. (to be published)

(5) R.A. Ward, M.J. Newman, D.D. Clayton, Ap. J. Suppl. 31, 33 (1976)

+MPI für Physik und Astrophysik, München

1.1.6 Measurement of the Neutron Capture Reactions $^{152}Gd(n,\gamma)$, $^{151}Eu(n,\gamma)^{152}Eu^m$ and $^{152}Sm(n,\gamma)$ to Investigate the ^{151}Sm s-Process Branching

H. Beer and F. Käppeler

An important parameter in s-process nucleosynthesis which until now is only vaguely known is the mean neutron flux. Its determination provides major insight in the site and neutron capture time scale of the s-process. Several s-process branching points have been proposed to determine the neutron flux (1,2,3); however, for an accurate analysis experimental capture cross sections are often too uncertain or even completely lacking. This is also true for the branching of ^{151}Sm which is shown in Fig. 1.
Evidence for the ^{151}Sm branching is given by the fact that the ^{152}Gd abundance cannot be reproduced in p-process calculations (4). The s-process capture path leads from ^{150}Sm to ^{151}Sm with a 93 a half life. Some of the synthesized ^{151}Sm nuclei are expected to decay to ^{151}Eu. For this branch a complicated decay in ^{152}Eu occurs both from a 9.3 h isomeric state ($I\beta^-$: 77 %, I_{EC}: 23 %) and from the 12.4 a ground state ($I\beta^-$: 24%, I_{EC}: 76 %) feeding partly ^{152}Gd and ^{152}Sm. In principle there are two possibilities to determine the mean average neutron flux Φ from this branching, either by comparing the σN-value for A=152 with that of ^{152}Gd (which is shielded against the r-process) or with that of ^{152}Sm.

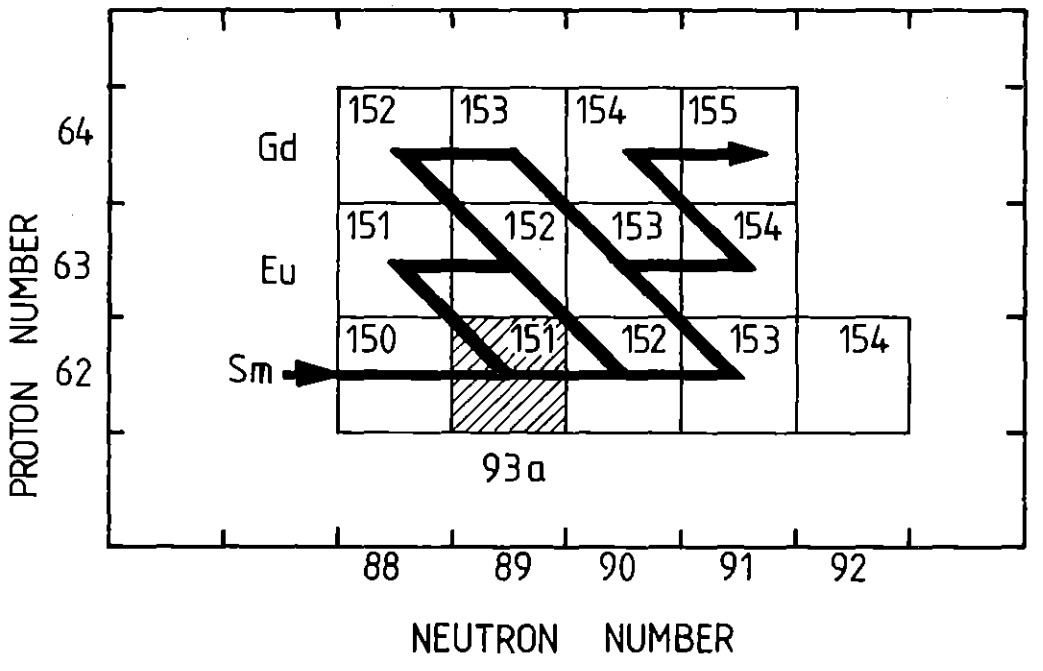

Fig. 1: The s-process path in the Sm-Eu-Gd region.

In the latter case a correction for the r-process contribution to the ^{152}Sm abundance has to be made by interpolation. This should be possible in this mass region as the solar Nd/Sm ratio is known to 1 % (12).

Relevant cross sections for the analysis of the branching at ^{151}Sm taken from literature are summarized in Table 1. The cross section and abundance of ^{148}Sm are relatively well-known and serve to determine σN(152). The important ^{151}Sm cross section appears to be well established due to two consistent theoretical calculations. However, there exists no experimental information of the highly important ^{152}Gd cross section and for ^{152}Sm two experimental values disagree (Table 1).

A detailed study of the ^{151}Sm branching must also consider the problem whether or not the two decay modes of ^{152}Eu are in thermal equilibrium under s-process conditions. For that purpose the initial population of ground and isomeric state have to be determined because they are important input parameters. The capture cross section of ^{151}Eu to the isomeric 9.3 h state and the total capture cross section can yield these relative populations.

Table 1: Capture cross sections and abundances for the s-process branching at ^{151}Sm from literature. Values without errors are calculated theoretically.

A_Z	$\sigma(^AZ)$ (mb)	A_Z	$\sigma(^AZ)$ (mb)
^{148}Sm	258 ± 48 [a] 281 ± 23 [b]	^{150}Nd	147 [c]
^{151}Sm	1990 [c] 2130 [d]	^{154}Sm	219 [c]
^{151}Eu	4822 ± 740 [e]	^{152}Gd	983 [c]
^{152}Sm	682 ± 54 [b] 411 ± 71 [a]	^{152}Eu	5180 [c] 5235 [f]

a) Ref. (5), b) Ref. (6), c) Ref. (7), d) Ref. (8), e) Ref. (9), f) Ref. (10)

In view of the above situation we have measured Maxwellian average capture cross sections for $^{152}Gd(n,\gamma)$, $^{152}Sm(n,\gamma)$ and $^{151}Eu(n,\gamma)^{152}Eu^m$ using the activation technique (11). The ^{152}Gd and ^{152}Sm cross sections can also be determined via detection of the prompt capture γ-rays. This technique was applied to ^{152}Sm (Table 1) so that the activation measurement provides an independent check with a different method. In the case of ^{152}Gd the activation technique was suitable as only a small sample amount with moderate enrichment of this highly expensive rare nucleus was available (34 mg enriched in ^{152}Gd to 50 %). The experimental data are now under analysis.

References

(1) J.B. Blake and D.N. Schramm, Ap. J. 197, 615 (1975)
(2) R.A. Ward, M.J. Newman and D.D. Clayton, Ap. J. Suppl. 31, 33 (1976)
(3) R.L. Macklin, R.R. Winters, Ap. J. 208, 812 (1976)
(4) S.E. Woosley, W.M. Howard, Ap. J. Suppl. 36. 285 (1978)
(5) R.L. Macklin, J.H. Cribbons, T. Inada, Nature 197, 369 (1963)

(6) V.N. Kononov, B.D. Yurlov, E.D. Poletaw, V.N. Timokhov, S.J. Nucl. Phys. 27, 5 (1978)
(7) J.A. Holmes, S.E. Woosley, W.A. Fowler, B.A. Zimmerman, Atomic Data Nucl. Data Tables 18, 305 (1976)
(8) H. Gruppelaar. Report ECN-33, 1977, Vol. 2
(9) M.C. Moxon, D.A.J. Endacott, J.E. Jolly, Ann. Nucl. Eng. 3, 399 (1976)
(10) ENDF/B-V data file for ^{152}Eu evaluated by H. Takahashi
(11) H. Beer, F. Käppeler, Phys. Rev. C21, 534 (1980)
(12) S.B. Jacobsen and G.J. Wasserburg, Lunar and Planetary Science XI, p. 502 (1980)

1.1.7 Optimized Set-up for the Measurement of Capture Cross Sections of Noble Gas Isotopes

J. Almeida, D. Erbe, G. Rupp, F. Käppeler

The set-up for capture cross section measurements on gaseous samples was described in previous progress reports (1). For the neon isotopes, which are important with respect to the neutron balance in s-process environments (see also contribution 1.1.3), very small capture cross sections are expected. Therefore the properties of the set-up and possible further improvements were investigated in detail in order to reduce the experimental background. The resulting changes are:

- High pressure gas samples: The relatively heavy valves were replaced by a completely new and surprisingly simple design which is integrated in the inlet tube of the spherical samples. That means, the mass and the dimensions of the samples, as they are mounted on the sample changer are reduced to 6 % and 44 %, respectively. In addition, the samples are now mounted only on two 0.1 mm thick stainless steel wires which replace the formerly used more massive aluminium tubes. In this way, background from scattered neutrons is considerably reduced.
- Shielding of the detectors: The smaller dimensions of the samples and their mounting allow to use a narrower through-hole in the lead shield, resulting in a smaller contribution from room-background. The background due to capture of scattered neutrons was

further reduced by surrounding the detector volume with a 5 mm thick layer of $^{6}LiCO_{3}$.

- Neutron collimation: Beside some technical changes in the fabrication of the collimator with respect to density and homogeneity the solid angle of the collimator was reduced by a factor 2. This should improve the background situation in general. It also allows for a smaller distance between samples and detectors, resulting in a better signal to background ratio.

Overall, we hope that these amendments increase the experimental sensitivity by about 50 %.

1.2 NUCLEAR DATA

1.2.1 The Neutron Capture Cross Section of ^{184}W

H. Beer, F. Käppeler, K. Wisshak

The neutron capture cross section of ^{184}W has been measured at the 3 MV pulsed Van de Graaff accelerator between 5 and 200 keV. The experimental arrangement which is characterized by very short flight paths for the neutron time-of-flight determination and by the use of a Moxon-Rae detector for recording the capture events is described elsewhere (1,2). In this experiment an enriched sample of WO_3 was measured relative to a gold reference sample (for details see Table 1).

Table 1: Sample characteristics of ^{184}W and Au.

Chemical composition	Isotopic composition (%)	Weight (g)	Thickness (at/b) x 10^4	(MS·SS)
WO_3	(180) 0.05, (182) 1.91, (183) 1.87, (184) 94.3, (186) 1.91	3.245	11.235	1.02
Au(metallic)	-	6.666	28.833	1.04

The capture cross section was calculated from

$$\frac{C_W}{C_{Au}} = \frac{N_W}{N_{Au}} \quad \frac{(MS\cdot SS)_W}{(MS\cdot SS)_{Au}} \quad \frac{\sum_i \sigma_i H_i E_{B,i}}{\sigma_{Au} E_{B,Au}} \qquad (1)$$

where C_i denotes the background subtracted count rate, (MS·SS) the correction for multiple scattering and self-shielding and N the sample thickness in atoms per barn. The subscripts W and Au refer to the tungsten and gold reference sample, respectively. The index i stands for the various tungsten isotopes with cross section σ, abundance H and neutron binding energy E_B. The binding energy E_B accounts for a specific property of the Moxon Rae detector: the linear dependence of the efficiency on the γ-ray energy.

In Fig. 1 the present capture cross section is shown in comparison with various results from previous work. The solid line represents a least squares fit of the present data with the statistical model. The parameters deduced are given in Table 2.

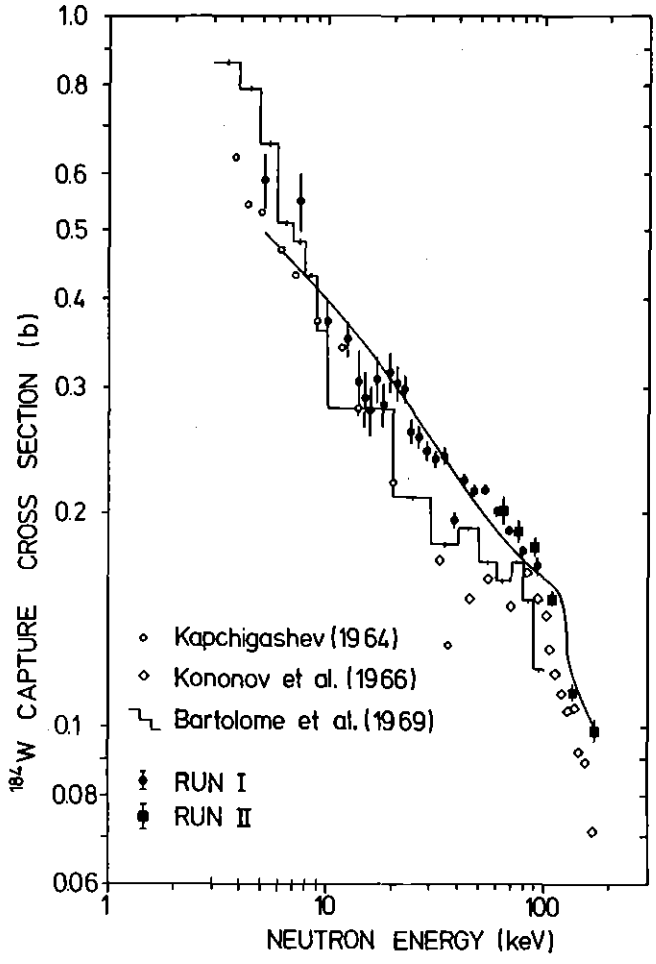

Fig. 1: Experimental results for the neutron capture cross section of ^{184}W (full black symbols: RUN I with the $^{7}Li(p,n)$, Run II with the T(p,n) reaction) compared to previous work (Ref. 3-5).

Table 2: Average resonance parameters for the statistical model fit of ^{184}W.

Strength function $S_1 x 10^4$	S_o=2.37	S_1=1.72	S_2=0.5
Radiation width Γ_1 (meV)	Γ_o=36.96	Γ_1=78.16	Γ_2=23.79
Average level spacing D_1 (eV)	D_o=126.3	D_1=44.76	D_2=30.35
Effective nuclear radius R (fm)		R=7.3	

References

(1) H. Beer, F. Käppeler, K. Wisshak, Proc. Conf. on Nucl. Cross Sections for Technology, Knoxville, TN, Oct. 1979

(2) K. Wisshak, F. Käppeler, Nucl. Sci. Eng. 66, 363 (1978), and Nucl. Sci. Eng. 69, 39 (1979)

(3) S.P. Kapchigashev, Russian Compilation 1964, CCDN Data Bank Paris

(4) V.N. Kononov, Yu.Ya. Stavisskij, V.E. Kolesov, A.G. Dobenko, V.S. Nesterenko, V.I. Soroka, S.J. Nucl. Phys. 4, 204 (1967)

(5) Z.M. Bartolome, R.W. Hockenbury, W.R. Moyer, J.R. Tatarczuk, R.C. Block, Nucl. Sci. Eng. 37, 137 (1969)

1.2.2 Determination of the Capture Width of the 27.7 keV s-Wave Resonance in ^{56}Fe*

K. Wisshak and F. Käppeler

The capture width of the 27.7 keV s-wave resonance in ^{56}Fe has been determined using a setup completely different from most of the previous experiments. A pulsed 3 MV Van de Graaff accelerator and the ^{7}Li(p,n) reaction served as a neutron source. Capture gamma-rays were observed by a Moxon-Rae detector and gold was used as a standard. The samples were positioned at a flight path of only 7.6 - 8.0 cm. This allowed the use of very thin samples avoiding large multiple scattering corrections. Three metallic discs enriched in ^{56}Fe were used with a thickness between 0.6 and 0.15 mm. Events due to capture of resonance neutrons scattered into the detector or by surrounding material were completely eliminated by time-of-flight. The result for the capture width is Γ_γ = 1.01 eV with a statistical uncertainty of 1.3 % and a systematic uncertainty of $\sim$5 %.

*Accepted for publ. in Nucl. Sci. Eng.

1.2.3 The Neutron Capture Cross Section of Nb, Ta and Rh in the Energy Range from 10 to 70 keV

K. Wisshak, F. Käppeler, and G. Reffo[+]

The neutron capture cross sections of Nb, Ta and Rh have been measured in the energy range from 10 to 70 keV using the same experimental setup as in contribution 1.2.2. A pulsed 3 MV Van de Graaff accelerator and the ^{7}Li(p,n) reaction served as a neutron source. The proton energy was adjusted slightly above the reaction threshold in order to produce kinematically collimated neutrons. The samples were positioned at a flight path of only 77-80 mm. Capture gamma-rays were observed by a Moxon-Rae detector and gold was used as a standard.

Preliminary data for the capture cross section of Ta are given in Fig. 1. The statistical accuracy of the data points is 3-5 % in the energy range from 20 to 50 keV and increases up to $\sim$20 % at higher and lower energies. The systematic uncertainty is 3-4 % in the respective energy range and increases up to 15 % at higher and lower energies. In the present evaluation a systematic uncertainty due to a possible deviation of the detector efficiency from the assumed linear increase with gamma energy is not yet included. To evaluate this uncertainty detailed calculations of the gamma-ray spectra will be performed for the respective isotopes. However, it was pointed out in contribution 1.2.2 at the example of a relative measurement of ^{56}Fe and gold that this correction is only of the order of 2-3 %. Similar or even smaller corrections are expected in the present case. In Fig. 1 comparison is made to recent results of Le Rigoleur et al. (1) and Yamamuro et al. (2). The overall agreement is quite sufficient but final conclusions cannot be drawn until the data evaluation is finished completely.

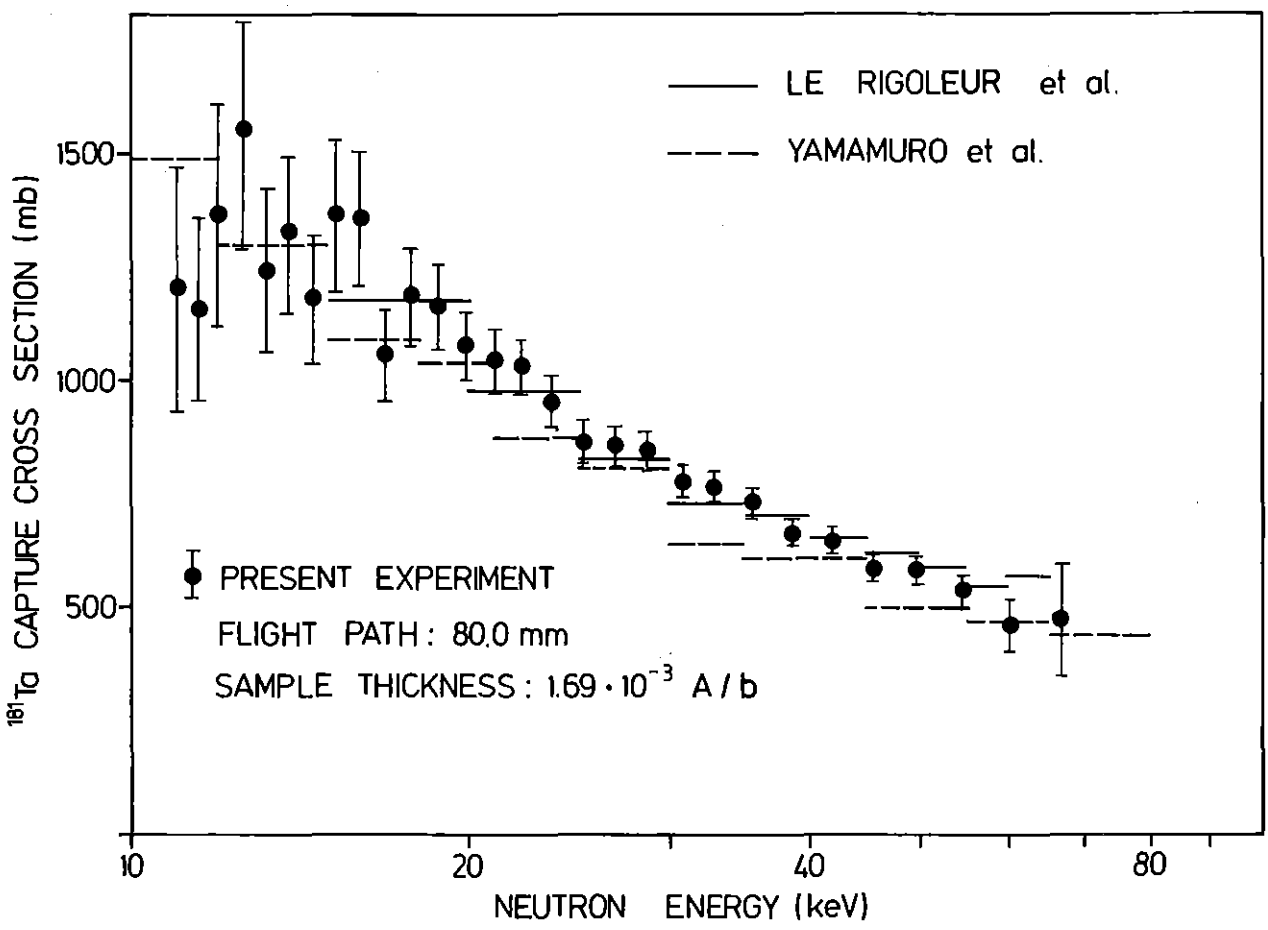

Fig. 1: Preliminary data for the neutron capture cross section of tantalum. The experimental ratios have been converted to absolute values using the ENDF/B-IV evaluation for the cross section of gold.

References

(1) C. Le Rigoleur, A. Arnaud, and J. Taste, Report CEA-R-4788, Commissariat a l'energie atomique, Gif-sur-Yvette, France (1976)

(2) N. Yamamuro, K. Saito, T. Emoto, and T. Wada, submitted for publ. to Journal of Nuclear Science and Technology

+CNEN Centro di Calcolo Bologna

1.2.4 The Isomeric Ratio in ^{242}Am Following Neutron Capture in ^{241}Am at 14.75 meV and 30 keV

K. Wisshak, J. Wickenhauser, and F. Käppeler

Neutron capture in ^{241}Am populates not only the ground state, but also an isomeric state of ^{242}Am. While the ground state has a half life of only 16 h the life time of the isomeric state is 152 years. In the neutron flux of a reactor ^{242g}Am will decay predominantly to ^{242}Cm via β-decay, whereas ^{242m}Am may be transformed to ^{243}Am in a second capture event. The partial capture cross section to the ground state determines essentially the amount of ^{242}Cm produced in a reactor during burn up. This nucleus, however, is of interest because of its high specific neutron activity due to spontaneous fission.

The present experiment is the first attempt to determine the partial capture cross section to the ground state in ^{242}Am in a differential measurement (1,2). A thin ^{241}Am sample ($\sim$200 µg weight, 7 mm diameter) is activated with monoenergetic neutrons for a period of $\sim$ 20 h. The number of ^{242g}Am nuclei produced is determined directly via the electrons emitted in beta decay. The beta spectrum was observed with a mini orange spectrometer (3,4) which offers the possibility of a selective detection of electrons in a high background of alpha-, gamma- and X-ray radiation. The measurements were performed relative to gold.

At thermal energies monoenergetic neutrons of 14.75 meV were provided from a triple axis spectrometer at the Karlsruhe FR2 reactor. The fast flux was obtained from our 3 MV Van de Graaff accelerator using the ^{7}Li(p,n) reaction. The proton energy was adjusted 25 keV and in a second experiment 10 keV above the reaction threshold. The neutron spectrum produced is slightly asymmetric and has an energy of 30 $^{+35}_{-20}$ keV and 25 $^{+25}_{-15}$ keV, respectively. For the narrower distribution the neutron flux is a factor of three lower.

The preliminary results obtained until now are compiled in Table 1. The capture cross section to the ground state in ^{242}Am could be determined relative to gold with a total accuracy of $\sim$ 5 % at all energy points. The statistical accuracy of the measurement is $\sim$1 %. For the determination of the isomeric ratio IR from the experi-

mental data the total capture cross sections of ^{241}Am and gold are required. The respective values are given in the second part of Table 1. The data at 14.75 meV were calculated from the 2200 m/sec values (625 b for ^{241}Am (5) and 98.8 b for gold (6)) assuming a 1/v-dependence of the cross sections. For the keV energy runs weighted cross sections for the experimentally determined energy distribution were calculated from the data given in Ref. 7 and from the ENDF/B-IV gold cross section.

Preliminary results for the capture cross section to the ground state in ^{241}Am and for the isomeric ratio are given in the third part of Table 1.

Table 1: Preliminary results for the capture cross section $^{241}Am(n,\gamma)^{242g}Am$ and for the isomeric ratio IR.

Neutron Energy	$\frac{\sigma_\gamma, ^{242g}Am}{\sigma_\gamma, Au}$	Adopted cross sections for the determination of IR	$\sigma_\gamma, ^{242g}Am$	IR
$30\ ^{+35}_{-20}$ keV	2.86±0.14	σ_γ,Am=2.46 ± 0.12 b σ_γ,Au=0.580 ± 0.015 b	1.66 ± 0.09 b	0.67 ± 0.05
$25\ ^{+25}_{-15}$ keV	3.06±0.17	σ_γ,Am=2.67 ± 0.13 b σ_γ,Au=0.624 ± 0.015 b	1.91 ± 0.12 b	0.72 ± 0.06
14.75 meV	5.87±0.3	σ_γ,Am=818 ± 26 b σ_γ,Au=129 ± 0.4 b	756 ± 39 b	0.92 ± 0.06

References

(1) K. Wisshak, J. Wickenhauser, and F. Käppeler, Proc. of a Int. Conf. on Nuclear Cross Sections for Technology, Knoxville, Tennessee, October 1979, to be published

(2) K. Wisshak, F. Käppeler, J. Wickenhauser, and W. Hage, Proc. of the 2nd Technical Meeting on the Nuclear Transmutation of Actinides Ispra, April 1980, to be published

(3) J. van Klinken and K. Wisshak, Nucl. Instr. Methods 98 (1972) 1

(4) J. van Klinken, S.J. Feenstra, and G. Dumont, Nucl. Instr. Methods 151 (1978) 433

(5) B. Goel, Proc. of a Specialists Meeting on Nuclear Data of Plutonium and Americium Isotopes for Reactor Applications, Brookhaven BNL 50991, NEANDC L-116 p. 177 Brookhaven National Laboratory (1978)

(6) S.F. Mughabghab and D.J. Garber, BNL-325, 3rd ed. Brookhaven National Laboratory (1973)

(7) K. Wisshak and F. Käppeler, accepted for publ. in Nucl. Sci. Eng.

1.2.5 Fission Cross Section Measurement of ^{241}Am in the Energy Range from 10 to 1030 keV*

W. Hage[+], K. Wisshak, and F. Käppeler

The neutron fission cross section of ^{241}Am was measured in the energy range from 10 to 1030 keV using ^{235}U as a standard. The measurements were carried out at the Karlsruhe 3 MV pulsed Van de Graaff accelerator with ^{7}Li targets for the generation of a continuous neutron spectrum below 140 keV and monoenergetic neutron spectra between 120 and 1030 keV. Fission events were detected by measuring the prompt fission neutrons with a NE 213 liquid scintillator with pulse shape discrimination. The flight path was as short as 60 mm in measurements with continuous neutron spectra leading to a moderate energy resolution of 23 ns/m. The statistical uncertainty was between 0.8 % and 10 % and the systematic uncertainty between 3 % and 7.5 %. Discrepancies were found comparing our results with those of other experiments.

*Submitted for publ. in Nucl. Sci. Eng.

[+]Commission of the European Communities, Joint Research Centre, Ispra, Varese, Italy

2. CHARGED PARTICLE REACTIONS AND NUCLEAR SPECTROSCOPY

2.1 POLARIZED DEUTERONS

2.1.1 Nuclear Shape Effects in the Scattering of Tensor-Polarized Deuterons

W. Stach[+], W. Kretschmer[+], H. Löh[+], W. Schuster[+], P. Urbainsky[+], M.B. Wango[+], and H.G. Rebel

The influence of the nuclear shape on the vector analyzing power of deuteron elastic and inelastic scattering have been demonstrated by Clement et al. (1). It is the purpose of the present investigation to show whether there are similar effects in the tensor analyzing powers (TAP).

We have measured T_{20}, T_{21} and T_{22} for the elastic and inelastic scattering of tensorpolarized deuterons on ^{46}Ti (prolate) and ^{50}Ti (spherical) at an incident energy of 10 MeV (2,3). The tensor observables were determined simultaneously in 4π geometry with the polarized beam of the Erlangen Lamb-shift source (for details see ref. 3). The elastic scattering TAP, shown in the upper part of fig. 1, are grossly reproduced by optical model calculations including tensor potentials. The calculations have been performed with the code DDB written by Ramirez and Thompson, which was modified with the fitting routine MINUIT. The best fit optical potentials are very similar to the results of Goddard and Haeberli (4) for ^{46}Ti(d,d_o) and of Bürgi et al. (5) for ^{50}Ti(d,d_o), where compared to refs. 4 and 5 only the imaginary spin orbit potential and the complex tensor (T_R) potential have been changed slightly. The TAP for the inelastic scattering to the first 2^+ state are shown in the lower part of fig. 1 with some lines to guide the eye. Both T_{20} and T_{21} show some sign effect, whereas T_{22} is shifted by about 10°. An extended analysis of elastic and inelastic scattering with the code CHUCK, modified by H. Clement (6) for the inclusion of tensor potentials, is in progress.

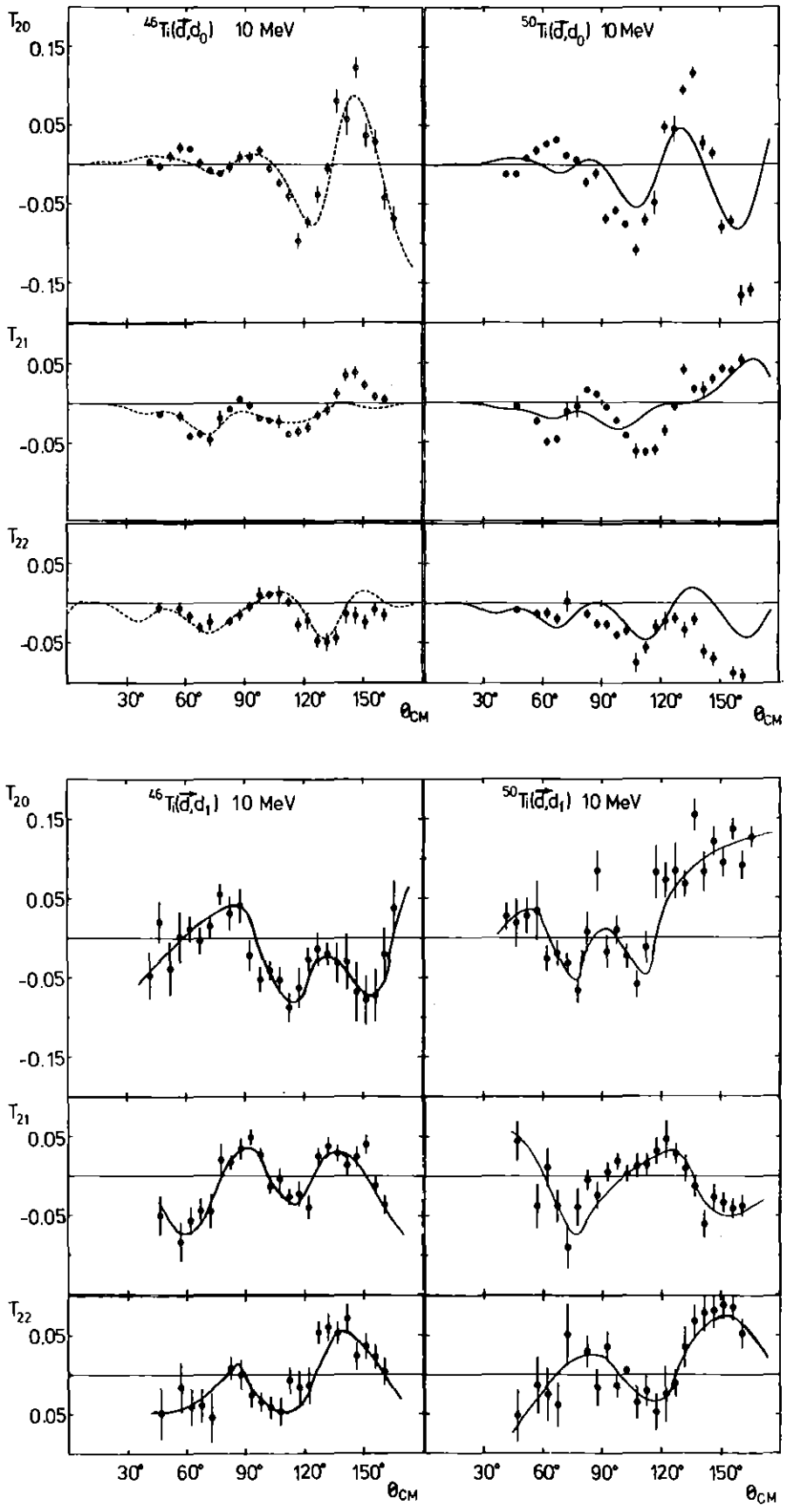

Fig. 1: Tensor analyzing power for deuteron scattering on ^{46}Ti and ^{50}Ti with optical model curve (for d,d_o) and with guide lines (for d,d_1).

References

(1) H. Clement, G. Graw, W. Kretschmer, and W. Stach, J. Phys. Soc. Japan 44 Suppl. (1978) 570

(2) W. Stach, W. Kretschmer, M.B. Wango, and H.G. Rebel, Proc. XII. Masurian School in Nuclear Physics, Nukleonika Vol 25 (1980) no. 2

(3) M.B. Wango, Diplom thesis, Erlangen 1980

(4) R.P. Goddard and W. Haeberli, Nucl. Phys. A316 (1979) 116

(5) H.R. Bürgi, W. Grüler, J. Nurzynski, P.A. Schmelzbach, R. Risler, B. Jenny, and R.A. Hardekopf, Nucl. Phys. A334 (1980) 413

(6) H. Clement, University of Munich, private communication

+Tandemlabor der Universität Erlangen-Nürnberg

2.1.2 The Optical Potential for Vector-Polarized Deuterons of 52 MeV*

G. Mairle+, K.T. Knöpfle++, H. Riedesel+, G.J. Wagner+, V. Bechtold, and L. Friedrich

The vector analysing power for elastic scattering of 52 MeV polarized deuterons was measured for ^{12}C, ^{16}O, ^{20}Ne, ^{28}Si, ^{32}S, ^{40}Ar, ^{58}Ni, ^{90}Zr and ^{197}Au. The data were analysed together with previously measured differential cross sections in the framework of the optical model. Best-fit and average optical-model parameters were obtained both for surface and volume absorption. Fits with surface absorption are superior to those with volume absorption, especially for heavier nuclei. Typical parameters of the spin-orbit part of the best-fit potentials are found to be $V_{s.o.} \simeq 5.5$ MeV, $r_{s.o.} \simeq 1.15$ fm and $a_{s.o.} \simeq 0.4$ fm, and there is no evidence for an imaginary component. The volume integrals and rms radii of real, imaginary and l·s potentials show a smooth mass dependence and differ insignificantly for different sets of potentials.

* Nuclear Physics A339 (1980) 61

+ Max-Planck-Institut für Kernphysik, Heidelberg, Germany

++Supported by Deutsche Forschungsgemeinschaft

2.1.3 Spins of Deeply-Bound Hole States in ^{89}Y and ^{143}Pm from $(\vec{d},\tau)$ Reactions and the Spin-Orbit Splitting in the 1f and 1g Shells

A. Stuirbrink[+], K.T. Knöpfle[+], G. Mairle[+], H. Riedesel[+], K. Schindler[+], G.J. Wagner[+], V. Bechtold, and L. Friedrich

Using vector-polarized deuterons of 52 MeV from the Karlsruhe cyclotron and using techniques described previously (1) we have measured differential cross sections and vector-analyzing powers of the $(\vec{d},^3He)$ reactions on ^{90}Zr and ^{144}Sm. The spectra measured with an overall resolution of about 200 keV determined mainly by the beam energy spread show deeply-bound proton hole states in ^{89}Y and ^{143}Pm peaking near 6.8 MeV (see Fig. 1) and 5.0 MeV, respectively. The latter has been identified as a 1g hole state previously (2) from the differential cross sections. The vector-analyzing powers now allow us to determine for the first time the total spins of deeply-bound hole states. They are identified as a dominant $1f_{7/2}$ hole state in ^{89}Y and a $1g_{9/2}$ hole state in ^{143}Pm. Zero-range DWBA calculations yield satisfactory fits to the data (see fig. 2) and spectroscopic factors which other than in neutron pick-up reactions (3) exhaust the shell model strengths. This allows us to determine the 1f and 1g spin-orbit splitting ε_{so} in ^{89}Y abd ^{143}Pm, respectively. In table 1 the experimental values are compared to various calculations. While the Woods-Saxon (λ_{so} = 25) and semi empirical predictions (4) yield reasonable results, the Brueckner-Hartree-Fock theory (5) yields nearly a vanishing ε_{so} if contributions from spin-saturated and non-spin-saturated shells are added.

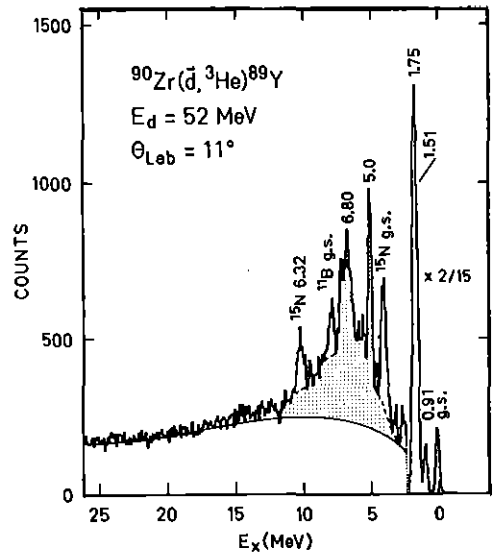

Fig. 1: Spectrum of the ^{90}Zr($\vec{d}$,^{3}He)^{89}Y reaction.

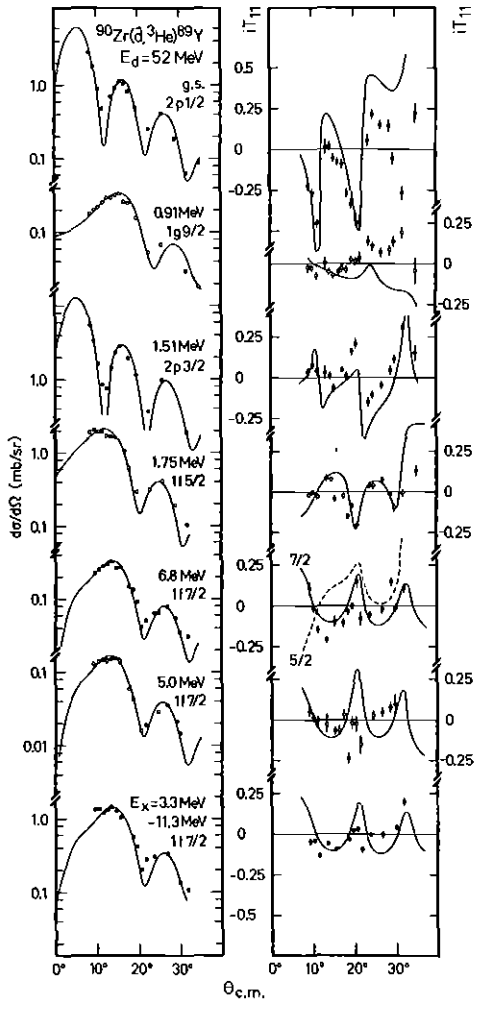

Fig. 2:
Differential cross sections and vector-analyzing powers for the ^{90}Zr($\vec{d}$,^{3}He) reaction together with DWBA results.

Tab. 1: Spin-orbit Splitting ε_{so} (MeV).

A_Z	$n\ell$	exp	W.-S.	semi- (3,4) emp.	BHF (4,5) ss + nss
^{90}Zr	1f	5.1	4.0	6.1	3.9 - 2.5
^{144}Sm	1g	4.7	4.1	5.7	3.9 - 3.9

References

(1) V. Bechtold et al., Phys. Lett. 72B (1977) 169

(2) P. Doll et al., Phys. Lett. 82B (1979) 357

(3) E. Gerlic et al., Phys. Rev. C21 (1980) 124 and refs. therein

(4) M.A.K. Lohdi and B.T. Waack, Phys. Rev. Lett. 33 (1974) 431

(5) R.R. Scheerbaum, Nucl. Phys. A257 (1976) 77

+Max-Planck-Institut für Kernphysik, D-69 Heidelberg, Germany

2.1.4 Search for States with Stretched Configurations by Means of the $(\vec{d},\alpha)$ Reaction at 52 MeV

G. Mairle+, Liu Ken Pao+, K.T. Knöpfle+,
H. Riedesel+, K. Schindler+, G.J. Wagner+,
V. Bechtold, J. Bialy, and L. Friedrich

Spectroscopic investigations by means of the (d,α) reaction are usually limited, because the observed angular distributions are unstructured and the a priori knowledge of suitable two-particle formfactors is required to describe them in the framework of the DWBA. It has been shown (1,2), however, that analyzing powers of $(\vec{d},\alpha)$ reactions are sensitive as to the coupling of the deuteron spin to the transferred angular momentum L. This allows spin determinations at least for states excited with an unique L-value. The method, therefore, is excellently suited to study stretched two particle configurations.

In fig. 1 the analyzing powers of some states observed in the $^{18}O(\vec{d},\alpha)^{16}N$ reaction are shown. For states of known spin J and unique L they show consistently large negative values at forward angles for J = L+1, large positive values for J = L-1 and small positive values for J = L. The measured analyzing powers for negative parity states at 0.0, 0.297 and 6.17 MeV are consistent with the spins 2^-, 3^- and 4^-, respectively, if L = 3 transfer is assumed in the DWBA calculations. For the g.s. transition L = 1 is also allowed; L = 3 is unique for 3^- and 4^- states in the frame of the simple shell model. A spin 4^- for the 6.17 MeV state is in agreement with results of

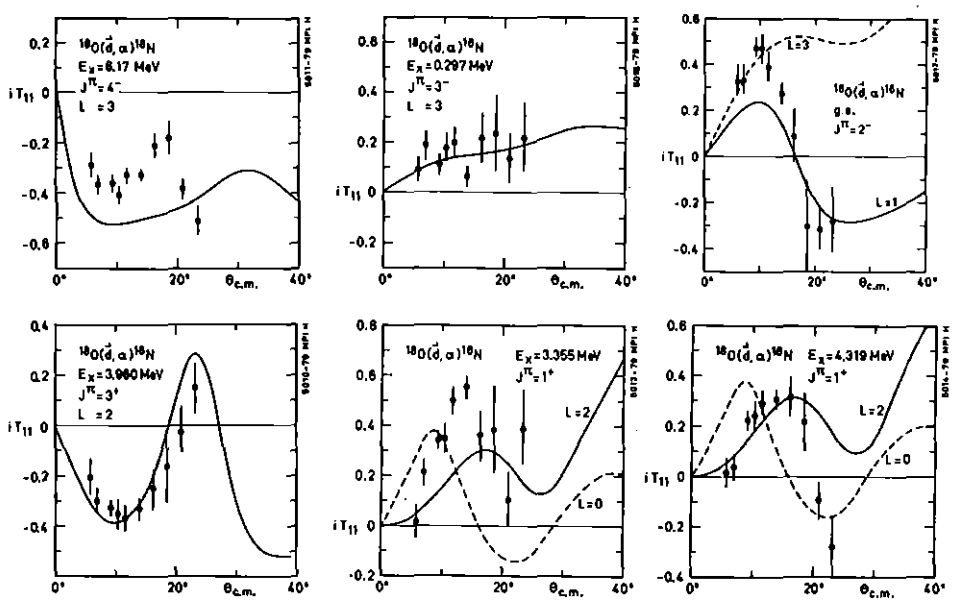

Fig. 1: Vector analyzing powers measured in the $^{18}O(\vec{d},\alpha)^{16}N$ reaction compared to DWBA calculations assuming pick-up of a deuteron cluster of given L.

$^{17}O(d,\tau)$, $^{17}O(\vec{d},\tau)$ and $^{16}O(p,p')$ experiments (3,4,5). The analyzing power for the 3^+ state at 3.96 MeV (unique L) is in perfect agreement with a DWBA calculation assuming L = 2. For the 1^+ states at 3.355 MeV and 4.319 MeV a mixture of L = 0 and L = 2 would be consistent with the data.

The analyzing powers observed in the $^{12}C(\vec{d},\alpha)^{10}B$ and $^{34}S(\vec{d},\tau)^{32}P$ are not shown for brevity. At least for states of maximum spin there is a clear-cut situation with negative values of the analyzing power at forward angles. This is e.g. the case for the 3^+ states at 0.0 and 4.77 MeV in ^{10}B (L = 2) and for strongly excited states at 7.76 and 8.09 MeV in ^{32}P which are described by DWBA calculations assuming L = 4 pick-up, with the consequence of a spin 5^+ for these to-date unknown states.

From a shell model point of view, the considered states are characterized by their stretched configurations:

$$^{10}B: \quad (1P^{-2}_{3/2})_{J=3^+,T=0}$$

^{16}N: $(1d_{5/2}\ 1p_{3/2}^{-1})_{J=4^-,T=1}$ and

$|(1d_{5/2}^{2})_{0,1}\ (1p_{3/2}^{-2})_{3,0}|_{J=3^+,T=1}$

^{32}P: $|(1d_{3/2}^{2})_{0,1}\ (1d_{5/2}^{-2})_{5,0}|_{J=5^+,T=1}$

The energies of these states represent a valuable information on effective interactions and hence for shell model calculations.

References

(1) J.D. Crossairt et al., Nucl. Phys. A287, 13 (1977)
(2) P.G. Ikossi et al., Nucl. Phys. A297, 1 (1978)
(3) G. Mairle et al., Nucl. Phys. A299, 39 (1978)
(4) G. Mairle et al., Contribution to Fifth International Symposium on Polarization Phenomena in Nuclear Physics, Santa Fe, USA August 1980
(5) R.S. Henderson et al., Australian J. of Phys. 32, 411 (1979)

+Max-Planck-Institut für Kernphysik, 69 Heidelberg, Germany

2.1.5 Purity of Particle-Hole States in ^{16}O and ^{16}N Studied by the $(\vec{d},t)$ and $(\vec{d},\tau)$ Reaction on ^{17}O

G. Mairle+, K.T. Knöpfle+, H. Riedesel+, K. Schindler+, G.J. Wagner+, V. Bechtold, and L. Friedrich

The simultaneous measurement (1) of the $^{17}O(d,t)^{16}O$ and $^{17}O(d,\tau)^{16}N$ reactions at 52 MeV has yielded a wealth of spectroscopic information on states which have a large overlap with $(1d_{5/2}\ 1p_{1/2}^{-1})_{2^-,3^-}$ and $(1d_{5/2}\ 1p_{3/2}^{-1})_{1^-,2^-,3^-,4^-}$ multiplets both for T = 0 and T = 1. A remaining problem were the relative $1p_{1/2}$ and $1p_{3/2}$ contributions in transitions to 2^- and 3^- states. We report on an attempt to disentangle these contributions using the vector analyzing powers (VAPs) of the $(\vec{d},t)$ and $(\vec{d},\tau)$ reactions on ^{17}O. We utilize the slow Q- and A-dependence of the VAPs found (2) for ℓ = 1 pick-up in $(\vec{d},\tau)$ reactions on nuclei between ^{12}C and ^{28}Si.

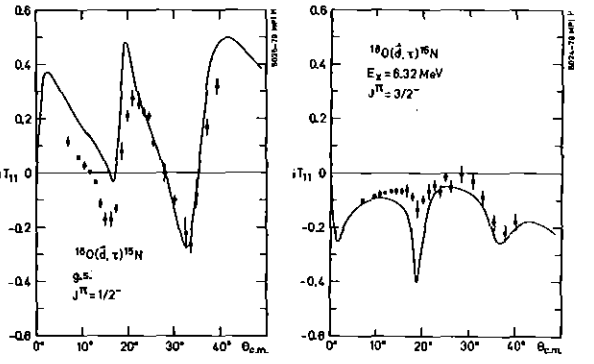

Fig. 1: Analyzing power for $1p_{1/2}$ and $1p_{3/2}$ pick-up from ^{16}O compared to DWBA calculations.

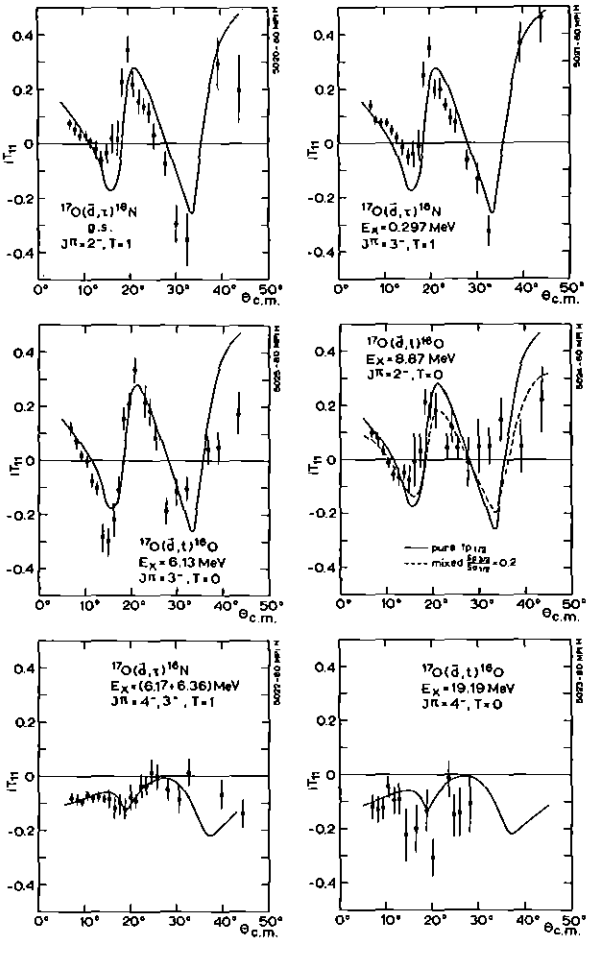

Fig. 2: Analyzing power of some selected states compared to VAPs of pure $1p_{1/2}$ or $1p_{3/2}$ pick-up (smooth curves drawn through the data points of fig. 2).

In fig. 1 measured VAPs for $1p_{1/2}$ and $1p_{3/2}$ pick-up observed in the $^{16}O(\vec{d},\vec{\tau})^{15}N$ reaction are displayed together with DWBA calculations, which show satisfactory agreement. Since the DWBA description, however, is not perfect, we use experimentally determined VAPs (smooth curves drawn through the data points of fig. 1) to deduce the degree of j-mixing in the 2^- and 3^- states of ^{16}O and ^{16}N. This is justified because of the negligible mass difference and the moderate Q-value differences. In fig. 2 we present the VAPs of some states strongly excited in pick-up reactions from ^{17}O compared

to VAPs of pure $1p_{1/2}$ and $1p_{3/2}$ pick-up from ^{16}O. T=1 states: Generally the data obtained for ^{16}N states agree with those of their analog (T=1) states in ^{16}O; we, therefore, discuss only results for ^{16}N states. In detail, we observe VAPs typical for $1p_{1/2}$ pick-up in the case of the 2^- g.s. and the 3^- state at 0.297 MeV. For the 2^- state the forward angle behaviour is indicative for some small $1p_{3/2}$ admixture ($R=S(p_{3/2})/S(p_{1/2})<0.1$). The agreement for the 3^- state, however, cannot be improved by $1p_{3/2}$ contributions ($R<0.05$). The VAP of the highly excited group comprising the 4^- and 3^- states at 6.17 and 6.36 MeV, respectively, shows no significant deviation from a pure $1p_{3/2}$ VAP. This is consistent with the $1d_{5/2}\ 1p_{3/2}^{-1}$ nature of these states (1). T=0 states: The VAP of the 3^- state at 6.13 MeV of ^{16}O shows the typical features of $1p_{1/2}$ pick-up. Due to the very pronounced structure, the agreement with the VAP of the pure $1p_{1/2}$ pick-up cannot be improved by $1p_{3/2}$ contributions ($R<0.15$). In contrast, the structure of the VAP of the 2^- state at 8.87 MeV in ^{16}O is obviously damped ($0.1<R<0.2$). The evaluation of the highly-lying state at 19.79 MeV is more difficult due to the increased background. Nevertheless, the observed VAP is compatible with pure $1p_{3/2}$ pick-up as required for a 4^- state.

DISCUSSION

The strongly excited particle-hole states in ^{16}O and ^{16}N show rather pure configurations in qualitative agreement with results of the shell model calculations of Gillet and Vinh Mau (4) and Hsieh (5). If the spectra are interpreted as $1d_{5/2}\ 1p_{1/2}^{-1}$ and $1d_{5/2}\ 1p_{3/2}^{-1}$ multiplets, they can be used to extract matrix elements of the related effective interactions as has been done in ref. 1. Since j-mixing in the 2^- and 3^- states has proved to be small, the conclusion (1) of different $1d_{5/2}\ 1p_{1/2}^{-1}$ and $1d_{5/2}\ 1p_{3/2}^{-1}$ interactions remains unchanged.

References

(1) G. Mairle et al., Nucl. Phys. A299, 39 (1978)

(2) G. Mairle et al., to be published

(3) G. Mairle et al., Nucl. Phys. A339, 61 (1980)

(4) V. Gillet and N. Vinh Mau, Nucl. Phys. 54, 321 (1964)

(5) S.T. Hsieh et al., Nucl. Phys. A243, 380 (1975)

+Max-Planck-Institut für Kernphysik, 6900 Heidelberg, Germany

2.2 ^{4}HE- AND ^{3}HE-PARTICLES

2.2.1 Elastic Scattering of 104 MeV Alpha Particles from ^{40,42,44,48}Ca and Determination of the Optical Potentials*

H.J. Gils, E. Friedman[+], H. Rebel, J. Buschmann, S. Zagromski, H. Klewe-Nebenius[++], B. Neumann, R. Pesl, and G. Bechtold

Differential cross sections for elastic scattering of 104 MeV α particles from ^{40,42,44,48}Ca have been measured with high angular accuracy over a wide angular range. Optical model analyses using different approaches for the potential form including a Fourier-Bessel description of the real potential reveal isotopic differences which, in particular for ^{48}Ca, indicate a small neutron skin. The model dependence of the extracted quantities is discussed in detail.

* KfK-Report 2838; Phys. Rev. C21 (1980) 1239

[+] The Racah Institute of Physics, The Hebrew University, Jerusalem, Israel

[++] Kernforschungszentrum Karlsruhe GmbH, Institut für Radiochemie

2.2.2 Nuclear Density Distributions of ^{40,42,44,48}Ca from Elastic Scattering of 104 MeV Alpha Particles*

H.J. Gils, E. Friedman[+], Z. Majka[++], and H. Rebel

The elastic scattering of 104 MeV α particles from ^{40,42,44,48}Ca has been analyzed by a single folding model with a density dependent effective interaction. Nuclear density distributions have been extracted using various descriptions including Fourier-Bessel series which distinctly reduces the model dependence of the results and enables realistic estimates of errors. Differences of the density shapes of the Ca-isotopes are well determined showing evidence for a neutron skin in ^{48}Ca. The resulting root mean square radii are compared to the results obtained from other methods. The sensitivity and limitations of various methods are discussed.

* KfK-Report 2839; Phys. Rev. C21 (1980) 1245

+ The Racah Institute of Physics, The Hebrew University of Jerusalem, Jerusalem, Israel

++Institute of Physics, Jagellonian University, Cracow, Poland

2.2.3 Saturation Effect and Determination of Nuclear Matter Density Distribution from Optical Potential*

Z. Majka+, H.J. Gils, and H. Rebel

A refined double folding procedure with density dependence of the effective nucleon-nucleon interaction included is used to calculate the real part of the alpha particle-^{48,40}Ca potentials. We show that the experimentally determined difference between rms radii of the (real) potentials implies a larger size of the nuclear matter distribution of the ^{48}Ca nucleus as compared to the ^{40}Ca nucleus.

*Acta Physica Pol. B11 (1980) 227

+Institute of Physics, Jagellonian University, Cracow, Poland

2.2.4 Elastic and Inelastic Alpha Particle Scattering from ^{48}Ca, ^{50}Ti, ^{52}Cr and the Response of the Excess Protons to the Total Matter Distributions

R. Pesl, H.J. Gils, H. Rebel, J. Buschmann, H. Klewe-Nebenius+, B. Neumann+, and S. Zagromski

The alpha-particle scattering studies in the Ca region (1) have been continued by measuring the differential cross sections of elastic and inelastic scattering of 104 MeV alpha particles for the isotone series ^{48}Ca-^{50}Ti-^{52}Cr. The data were measured with high angular accuracy, and their angular range exceeds the nuclear rainbow region thus enabling a refined optical model analysis and a

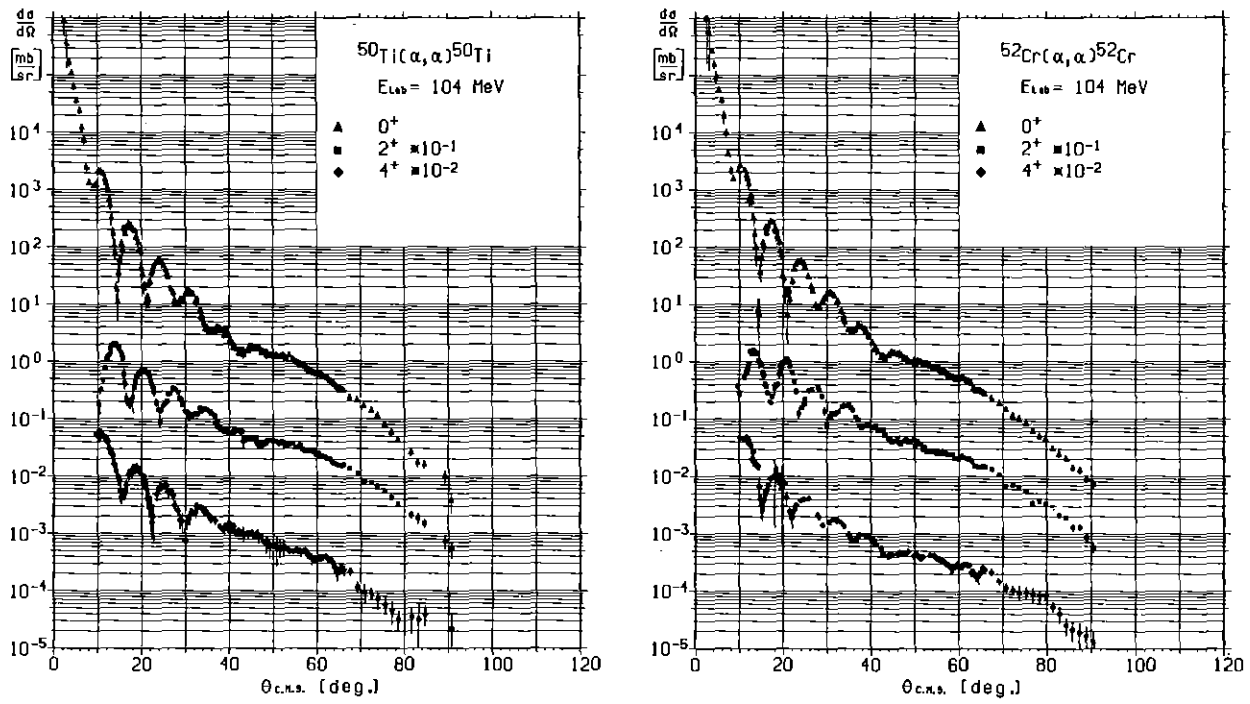

Fig. 1: Differential cross sections of elastic and inelastic scattering of 104 MeV alpha particles from ^{50}Ti and ^{52}Cr.

unique determination of the real part of the optical potential. For the analysis the radial shape of the real part has been represented by a Fourier Bessel (FB) series added to a Saxon-Woods squared form (2). In addition to the flexibility of the FB-method realistic estimates of the uncertainties could be provided. Tab. 1 presents some results of integral quantities of the potential and Fig. 2 displays differences of the real part of the considered isotone series. The results lead to the following conclusions:

a) While in ^{48}Ca the neutron excess strongly polarises the ^{40}Ca proton core, the additional protons in ^{50}Ti and ^{52}Cr seem to reduce this effect.

b) The excess protons in ^{50}Ti and ^{52}Cr, however, affect the ^{48}Ca neutron core and "pull" neutrons to smaller radial distances. As a consequence the radii of the neutron distributions in ^{50}Ti and ^{52}Cr prove to be slightly smaller than in ^{48}Ca.

	$\langle r_v^2 \rangle^{1/2}$ |fm|	$-J_v/4A$ |MeV fm^3|	$\langle r_w^2 \rangle^{1/2}$ |fm|	$-J_w/4A$ |MeV fm^3|
^{40}Ca	4.37 ± 0.06	327 ± 2	4.94	103
^{48}Ca	4.49 ± 0.09	319 ± 5	5.09	96
^{50}Ti	4.46 ± 0.05	306 ± 5	5.05	93
^{52}Cr	4.48 ± 0.05	303 ± 4	5.08	96

Tab. 1: Integral quantities of the FB-Potential.

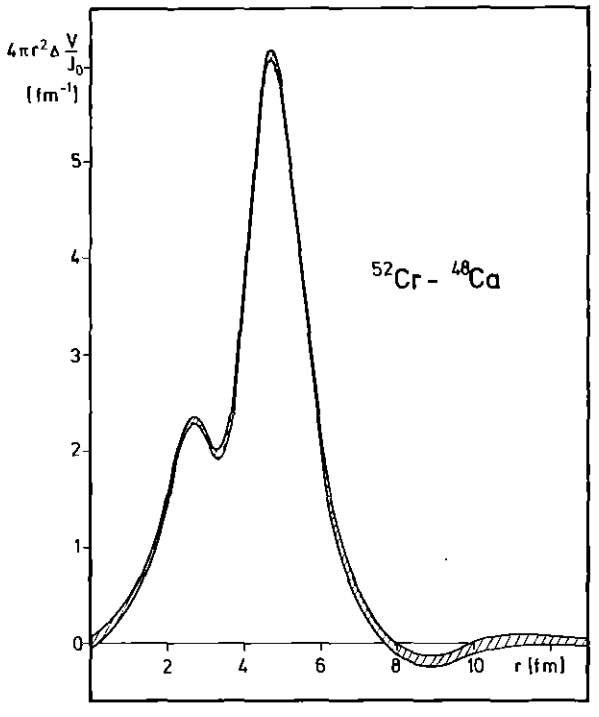

Fig. 2:
Radial differences of the real part of the optical potentials for 104 MeV alpha particle scattering from ^{48}Ca, ^{50}Ti and ^{52}Cr.

References

(1) H.J. Gils, E. Friedman, H. Rebel, J. Buschmann, S. Zagromski, H. Klewe-Nebenius, B. Neumann, R. Pesl, and G. Bechtold, Phys. Rev. C21 (1980) 1239

(2) E. Friedman and C.J. Batty, Phys. Rev. C17 (1978) 34

+Institut für Radiochemie, Kernforschungszentrum Karlsruhe

2.2.5 Fourier-Bessel Description of the Imaginary Part of the Alpha-Nucleus Optical Potential

H.J. Gils and K. Feißt

The "model independent" description of the *real* part of the alpha particle-nucleus optical potential by a Fourier-Bessel series (FB) (1) has proven to be a most successful method providing interesting information about the radial shape of the potential. In addition, the method enables realistic estimates of the uncertainties of the potential and its integral quantities. Even if presently the detailed shape of the *imaginary* part of the potential may - for itself - be of minor interest it seems to be important to get rid off undesirable constraints given by the form factor used. In particular when studying possible couplings and ambiguities between real and imaginary part of the optical potential this problem arises. For these reasons we have introduced the additional flexibility of the FB-method also into the description of the imaginary part when analyzing 104 MeV alpha particle scattering from ^{12}C and ^{40}Ca. 25 different combinations of cut-off radii and number of parameters (2,3) generated in a random procedure have been studied. When comparing the results with corresponding ones where only the real part was described by the FB-series the following statements can be made:

1. When comparing cases with equal number of total varied parameters (FB only in the real part compared to FB in the real and imaginary part) the experimental cross sections were equally well reproduced. Convergence of the fit procedure is worse when including the FB-method in the imaginary part, even for small numbers of parameters.

2. The extracted averaged slope (2) of the real potential and the values of the integral moments are not affected by the detailed form of the imaginary potential.
3. The averaged error band of the real potential and its integral quantities are not affected by the additional flexibility in the imaginary part, provided that the total number of parameters does not exceed the region of stability.
4. The averaged slope of the FB-imaginary potential does not deviate from the conventional Saxon-Woods parametrization.
5. The integral quantities of the imaginary potential are determined with nearly the same accuracy as that of the real part whereas the slope of the potential is not at all determined at radii smaller than about 2 fm.

In view of the investigations of radii of nuclear matter distributions the second and third statement are most important confirming previous results (2). The Saxon-Woods form seems to be an adequate description of the imaginary optical potential of alpha-particle scattering. This is also the result of microscopic treatments of the imaginary optical potential (4). It must, therefore, not be replaced by more flexible forms since the added flexibility only leads to convergence problems but does not affect the results.

References

(1) E. Friedman and C.J. Batty, Phys. Rev. C17 (1978) 34

(2) H.J. Gils, E. Friedman, H. Rebel, J. Buschmann, S. Zagromski, H. Klewe-Nebenius, B. Neumann, R. Pesl, and G. Bechtold, Phys. Rev. C21 (1980) 1239
KfK 2838 (1979)

(3) H.J. Gils, KfK 3063 (1980)

(4) N. Vinh Mau, Phys. Lett. 71B (1977) 5

2.2.6 Fine Structure of Inelastic Scattering Angular Distributions?*

V. Corcalciuc[+], R. Dumitrescu[+], A. Ciocanel[+], H.J. Gils, H. Rebel, W. Stach[++], and S. Zagromski

The angular distributions of 29 MeV ^{3}He particles elastically and inelastically scattered from a ^{68}Zn target has been measured with high angular resolution. A fine structure of the diffraction oscillation observed could not be detected. Various suggestions for the origin of such a fine structure seen in α-particle scattering experiments are discussed.

* Rev. Roum. Physique (in print)

[+] Institute for Physics and Nuclear Engineering, Bucharest, P.O.B. 5205, Romania

[++]Physikalisches Institut der Universität Erlangen-Nürnberg, Erlangen, Federal Republic of Germany

2.2.7 Decay of the Isoscalar Giant Resonances in ^{208}Pb*

W. Eyrich[+], A. Hofmann[+], U. Scheib[+], S. Schneider[+], F. Vogler[+], and H. Rebel

The decay of the giant-resonance region in ^{208}Pb has been studied in a α'-γ angular correlation experiment via the reaction chain $^{208}\mathrm{Pb}(\alpha,\alpha')^{208}\mathrm{Pb}^{GR}(n)^{207}\mathrm{Pb}^{*}(\gamma)^{207}\mathrm{Pb}$. The correlation functions are in agreement with the assumption of predominant $E2$ strength for the resonance around E_x=10.9 MeV, but require considerable strengths of excitation modes higher than $E0$ for the resonance around E_x=13.7 MeV. The coincident α-particle spectra show significant fine structure in the giant-resonance region.

*Phys. Rev. Lett. 43 (1979) 1369

[+]Physikalisches Institut der Universität Erlangen-Nürnberg, Erlangen, Germany

2.2.8 Investigation of the Neutron Decay of the Isoscalar Giant Resonances in ^{208}Pb

W. Eyrich[+], A. Hofmann[+], U. Scheib[+], R. Stamminger[+], H. Steuer[+], and H. Rebel

In the preceeding annual report we described an α-γ-angular correlation experiment where the n-decay of the isoscalar giant resonances (GR) in ^{208}Pb was studied indirectly by observation of the subsequent γ-decay in the residual nucleus ^{207}Pb. Furthermore we reported on test-measurements for the direct investigation of the neutron decay of the giant resonances in ^{208}Pb via an α-n-coincidence measurement.

In the meantime the α-n-correlation-measurements have been continued. To resolve the neutron decay into the individual states in ^{207}Pb an overall energy resolution of about 300 keV is necessary which could be achieved roughly in our experiment. In figure 1 neutron spectra coincident to the central part of the GQR in ^{208}Pb are shown for two

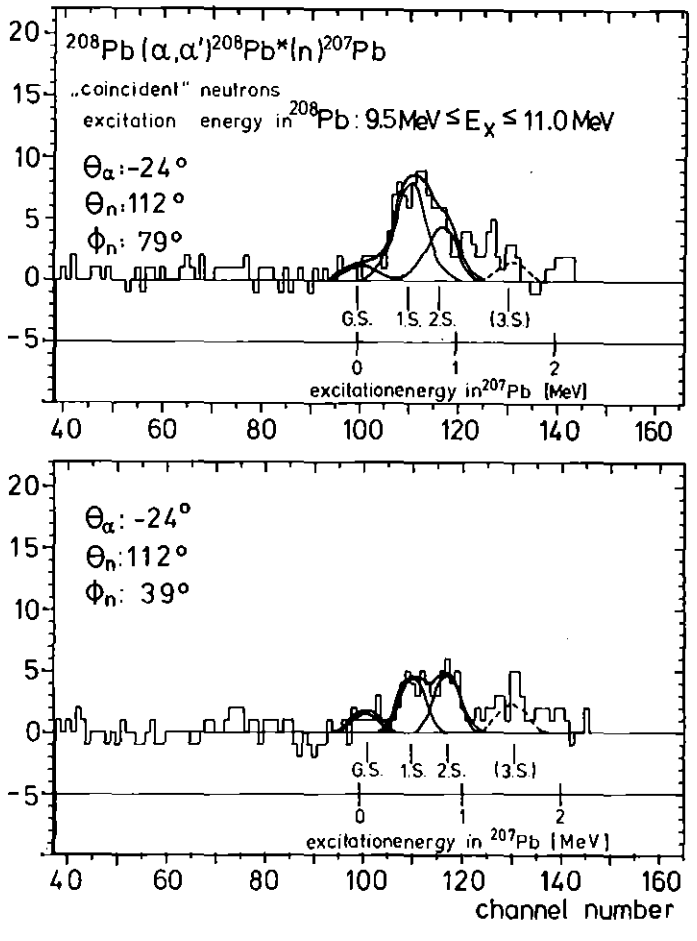

Fig. 1:
Neutron spectra coincident to α-particles scattered from the central region of the GQR in ^{208}Pb at two different positions of the neutron detector.

different positions of the n-detectors for an α-scattering angle corresponding to a maximum of the angular distribution of the GQR. Although the statistical errors are still large the neutron groups corresponding to the decay into different states of ^{207}Pb can be identified.

As a first result this α-n-coincidence experiment in agreement with the α-γ-work (1) shows that the GR-region in ^{208}Pb ($9 \leq E_x \leq 15$ MeV) decays predominantly to the lowest states in ^{207}Pb ($E_x \leq 2.5$ MeV). This is true also for the upper part of the GR-region ($E \approx$ 13-14 MeV), whose large widths for the decay into these states indicate that the decay cannot be described by the statistical model alone.

To get quantitative values for the branching ratios of the n-decay we are extending our α-n-correlation measurements to additional angles of the n-detectors observing the α-particles at angles corresponding to maxima and minima of the α-angular distribution of the GR's order to distinguish between the decay of the resonances and the underlying continuum. Our aim is to obtain the branching ratios of the different fine structure components separately. This fine structure which was found in our α-γ-work (1) as well as in a recent (e,e')-experiment (2) could be observed again in the α-n-coincidence spectra.

References

(1) W. Eyrich et al., Phys. Rev. Lett. 43 (1979) 1369

(2) A. Richter, Verh. DPG (VI) 15 (1980) 1042

+Physikalisches Institut der Universität Erlangen-Nürnberg, Germany

2.2.9 A Study of the Giant Resonance Region of ^{40}Ca by Inelastic Scattering of 104 MeV α-Particles*

H. Rost[+], W. Eyrich[+], A. Hofmann[+], U. Scheib[+], F. Vogler[+], and H. Rebel

Inelastic α-scattering experiments have been performed on ^{40}Ca at E_α=104 MeV in the angular range θ_{lab}=4°-16°. From the angular distributions of the giant resonance structures in the excitation energy region E_x=13.3-21.8 MeV the contributions of different L-transfers have been determined.

*Phys. Lett. 88B (1979) 51

[+]Physikalisches Institut der Universität Erlangen-Nürnberg, Erlangen, Germany

2.2.10 Isoscalar Dipole Excitations in the Giant Resonance Region Observed in the Small Angle Scattering of 104 MeV α-Particles

H. Rost[+], W. Eyrich[+], A. Hofmann[+], H. Rebel, U. Scheib[+], H. Steuer[+]

Studying the giant resonance region in ^{40}Ca by the aid of inelastic scattering of 104 MeV α-particles at small angles ($4° \leq \Theta_L \leq 16°$) we found strong indications for collective isoscalar dipole states at excitation energies between 13.3 MeV and 16.7 MeV (1). In this energy region the cross sections show a typical rise at forward angles, which can be described in the framework of the conventional DWBA only if beside some L = 2 excitation also L = 1 excitation is assumed. In order to investigate whether such L = 1 excitations occur also in the giant resonance region of other light nuclei we extended our measurements of small angle α-particle scattering to the nuclei ^{24}Mg, ^{28}Si and ^{58}Ni. Whereas in ^{24}Mg no remarkable dipole strength could be observed, in ^{28}Si some L = 1 strength was found at 14.1 MeV. In ^{58}Ni at 7.3 MeV and around 10.2 MeV isoscalar dipole states were found with strengths comparable to those of ^{40}Ca.

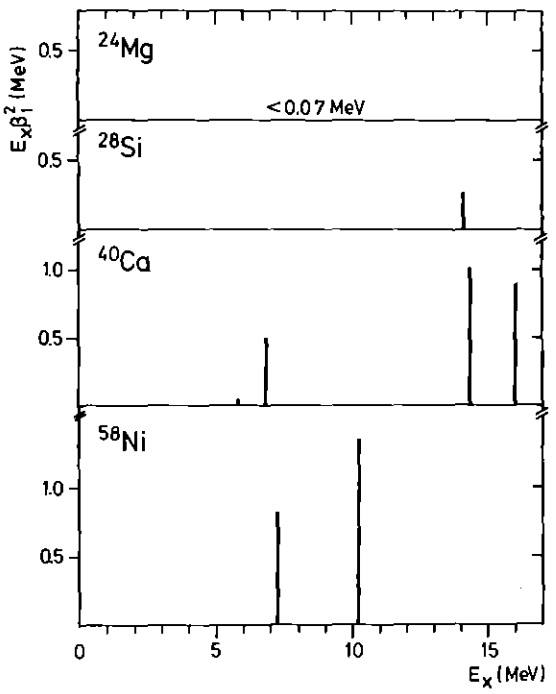

Fig. 1:
Isoscalar dipole strengths, observed in the nuclei ^{24}Mg, ^{28}Si, ^{40}Ca, ^{58}Ni at excitation energies $E_x \leq 22$ MeV.

In our DWBA calculations we used a transition density, which was given by Satchler (2) extending the collective optical model to dipole diffuseness oscillations. This transition density has a node at r = R', where R' is given by the constraint of a fixed centre of mass.

In fig. 1 the deformation parameters extracted from these DWBA analyses versus the excitation energy are plotted as products $\beta^2 E_x$.

Of course these deformation parameters cannot be related to a sum rule on the basis of the usual dipole operator $r\, Y_{1\mu}$. But using the next higher moment on the dipole operator $r^3\, Y_{1\mu}$ an approximate energy weighted sum rule can be derived immediately (3). In this sum rule the third moments of the transition densities are connected with the fourth moment of the ground state density. We calculated these moments for the used Woods-Saxon-potentials neglecting terms of the order $\exp(-\frac{R}{a})$.

Thereby the total dipole sum turns out to depend to a certain extent on the ratio a/R. In our case a/R changed from 0.25 leading to a total sum of (14 ± 6) MeV. In column 3 of table 1 the fractions of this isoscalar E1 energy weighted sum rule are shown. A sum rule with center of mass correction for the application to electron scattering

Table 1: Percentages of isoscalar E1 energy weighted sum rules.

Nucleus	E_x (MeV)	% E1 EWSR a)	% E1 EWSR b)
^{24}Mg	< 22	< 0.7 %	< 0.8-2 %
^{28}Si	14.1	2 %	3-8 %
^{40}Ca	5.9	0.3 %	0.5-1 %
	6.95	4 %	6-14 %
	13.3-15.3	7 %	12-29 %
	15.3-16.7	6 %	11-26 %
^{58}Ni	7.3	6 %	10-23 %
	9.2-11.2	10 %	17-39 %

a) From $\sum_n E_n \beta_1^2(n) = 14$ MeV according to the E1 EWSR

$$\sum_{n\mu} E_n \left| \langle n, 1\mu | r^3 Y_{1\mu} | 0 \rangle \right|^2 = \frac{33\hbar^2}{2m} \frac{A}{4\pi} \langle r^4 \rangle$$

b) Adjusted from the value for the 6.95 MeV state in ^{40}Ca from ref. (4).

connecting transition form factors with the elastic form factor has been derived by Deal (4). He investigated the 6.95 MeV in ^{40}Ca in electron scattering finding that this state exhausts 6-14 % of his sum rule. If we use this state to normalize our dipole strengths we find the values of column 4 in table 1, which are in qualitative agreement with the values of column 3. An extension of our analyses to more sophisticated transition densities in connection with folding model calculations is in preparation.

References

(1) H. Rost et al., Phys. Lett. 88B, (1979) 51

(2) G.R. Satchler, Nucl. Phys. A100 (1967) 481

(3) A. Bohr, B.R. Mottelson, Nuclear Structure (W.A. Benjamin Inc., 1975) Vol. II, p. 401

(4) T.J. Deal, Nucl. Phys. A217, (1973) 210

+Physikalisches Institut der Universität Erlangen-Nürnberg

2.2.11 Inelastic Alpha Particle Scattering Experiments Using the Jülich Magnetic Spectrograph "Big Karl" for Measuring the $(0^+-4^+_1)$-Hexadecapole Transition Rate on ^{204}Pb

W. Stach[+], H.J. Gils, S. Zagromski, H. Rebel, S. Martin[++], G. Berg[++], J. Meißberger[++], T. Sagefka[++], and R. de Swiniarski[+++]

There is considerable evidence for collective hexadecapole motion in spherical and quasi-spherical nuclei. Inelastic alpha particle scattering (1) in the 100 MeV region showed a high sensitivity to magnitude and phase of the L = 4 transition amplitudes and revealed a correlation between a strong lowering of the energy level ratio $E_{4^+_1}$ / $E_{2^+_1}$ and an enhancement of the $4^+_1 \rightarrow 0^+$ hexadecapole transition. It is desirable to compare electromagnetic transition rates with the isoscalar rates induced by alpha particle scattering as there might be interesting differences, in particular for nuclei with large neutron excess. Furthermore, as the analysis of the scattering cross sections is necessarily based on a specific reaction model, a comparison may shed some light to the model dependence of the extracted isoscalar transition rates.

The specific case of the $0^+ \rightarrow 4^+_1$ transition in ^{204}Pb provides a favourable situation since Signorini and Morinaga (2) suceeded in measuring the $4^+_1 \rightarrow 0^+$ γ-transition in presence of the dominating $4^+_1 \rightarrow 2^+ \rightarrow 0^+$ cascading transitions. We have started measurements of inelastic alpha particle scattering from ^{204}Pb in order to provide precise differential cross sections for a detailed theoretical analysis. Test runs using the 104 MeV alpha particle beam of the Karlsruhe Isochronous Cyclotron demonstrated that - due to restricted resolution and nuclear reactions in the solid state material - a semiconductor detector is not suited to measure the relatively low 4^+_1-peak (in presence of the dominating elastic scattering tail).

In order to do so we took advantage of the qualities of the magnetic spectrograph "Big Karl" at the Jülich Isochronous Cyclotron. Fig. 1 displays a spectrum of inelastically scattered alpha particles

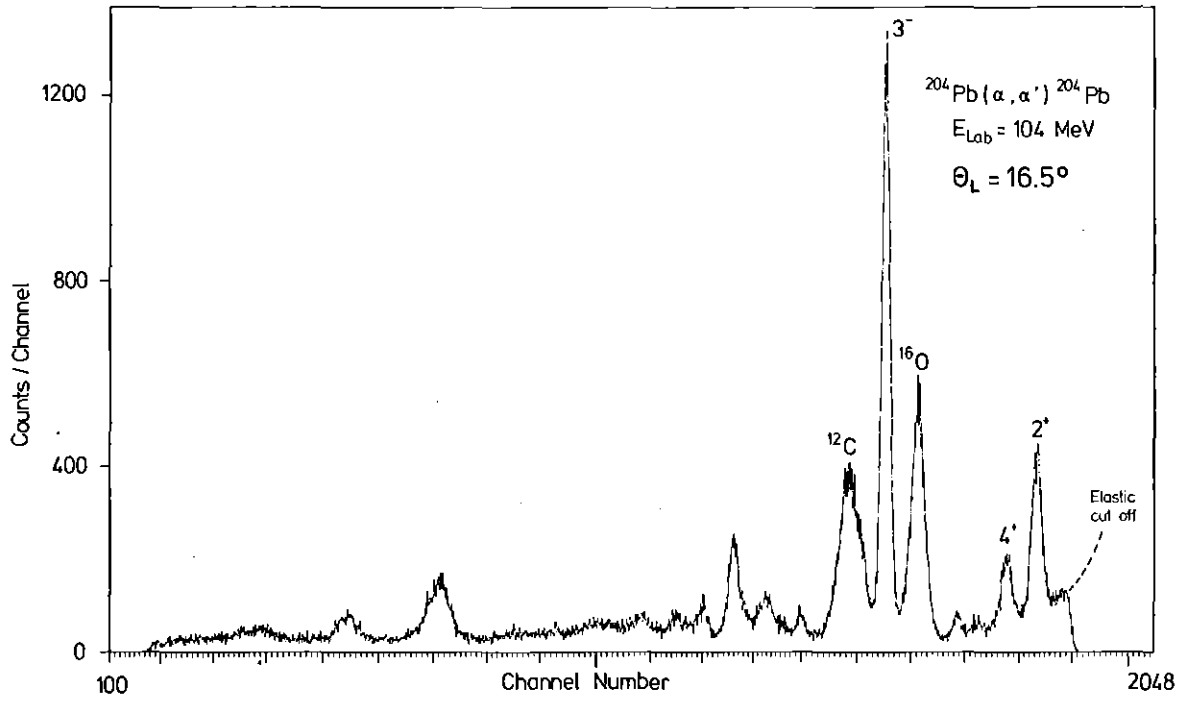

Fig. 1: Spectrum of alpha particles inelastically scattered from a ^{204}Pb target (with C and O impurities).

from a ^{204}Pb target (2.04 mg/cm^2 thick) where the peak of interest is clearly identified. The intensity of the peak is strongly varying with the scattering angle. Up to now spectra for seven angles between Θ_L = 9° and 18.5° have been taken for E_{Lab} = 104 MeV. Further runs are in preparation.

References

(1) H. Faust, A. Hanser, H. Klewe-Nebenius, H. Rebel, J. Buschmann, and H.J. Gils, J. Phys. 6, Nucl. Phys. 4 (1978) 247

(2) C. Signorini and H. Morinaga, Phys. L. 40B (1972) 549

(3) G. Berg, A. Hardt, S. Martin, J. Meißburger, and T. Sagefka, Annual Report 1978/79 KfA Jülich

+ Tandemlaboratorium Universität Erlangen

++ Institut für Kernphysik der KfA Jülich

+++ Institut des Sciences Nucléaires, Université de Grenoble

2.3 ^{6}LI-PARTICLES

2.3.1 Transfer of ^{6}Li Break-Up Fragments at ^{6}Li Projectile Energies far above the Coulomb Barrier*

B. Neumann, J. Buschmann, H. Klewe-Nebenius[+], H. Rebel, and H.J. Gils

Transfer of beam-velocity fragments has been experimentally investigated in ^{6}Li induced reactions on ^{208}Pb and ^{209}Bi in the energy range E_{Li} = 60-156 MeV. The experimental techniques involve the observation of the target residues and measurements of the recoil ranges of heavy residual nuclei produced by charged particle bombardment. The determination of the recoil energy enables the discrimination of different reaction paths leading to the same residual nuclei. (^{6}Li, xn+p) excitation functions prove to be very similar to (α, (x-1)n) reactions at $E_{\alpha} \approx \frac{2}{3}E_{Li}$. The results present experimental evidence for a particular reaction type indicated in previous experiments: Dissociation of the ^{6}Li projectile with capture of the beam-velocity α-particle indicating an (α, xn) reaction ("internal break-up").

*Nuclear Physics A329 (1979) 259

[+]Institut für Radiochemie, Kernforschungszentrum Karlsruhe

2.3.2 Projectile Break-Up in Continuous Particle Spectra from Nuclear Reactions Induced by 156 MeV ^{6}Li*

B. Neumann, H. Rebel, J. Buschmann, H.J. Gils, H. Klewe-Nebenius[+], and S. Zagromski

The break-up of 156 MeV ^{6}Li ions colliding with ^{12}C, ^{60}Ni, ^{90}Zr, ^{120}Sn and ^{208}Pb has been experimentally studied. It was found that the break-up cross section decreases rapidly with increasing emission angles of the fragments and increases with increasing target mass. It comprises a fairly large fraction of the total reaction cross section. The observed features suggest that the ^{6}Li fragmentation is mainly a

peripheral process, and is dominated by the cluster properties of the incident projectile. A simple plane-wave break-up model gives a rather good description of the shapes of the break-up bumps. The angular distributions of the fragments emitted in the ^{6}Li + ^{208}Pb reaction reveal the transition from peripherial break-up to incomplete fusion processes by which beam-velocity fragments are captured by the target nucleus. In addition to the (α+d) dissociation the (^{3}He + t) break-up has been observed, but the triton spectra appear to be rather complex indicating further components due to more complicated reaction paths.

*Z. Physik A (in print)

+Institut für Radiochemie, Kernforschungszentrum Karlsruhe

2.3.3 Continuous Particle Spectra from (^{6}Li + ^{40}Ca) Reactions at E_{Li}=156 MeV and the Complex Structure of the Triton Component

B. Neumann+, J. Buschmann, H.J. Gils, H. KLewe-Nebenius+, H. Rebel, S. Zagromski, and K. Feißt

Our previous experiments (1,2) investigating ^{6}Li induced nuclear reactions at E_{Li}=25 MeV/nucleon have given an overview of the main features of inclusive energy spectra of light particles emitted after ^{6}Li bombardment and have established the dominant contribution of the projectile break-up components. For more detailed studies of the reaction meachanism and of the relative importance of various channels the system ^{6}Li on ^{40}Ca has been chosen and measurements of the energy spectra for p,d,t,^{3}He,^{4}He,^{6}Li and ^{7}Li ejectiles at emission angles between θ_{Lab}=9° and 90° have been performed. The detector consisted of a 300 µm thick silicon E detector followed by a 20 mm thick high-purity germanium detector. The obtained energy spectra show distinct bumps of beam-velocity particles, strongly decreasing in intensity with the emission angle. The ^{3}He and triton spectra confirm the conspicuosly different structure of the triton and ^{3}He spectra which has been already observed when bombarding a ^{208}Pb target (2). In addition to a component which may be associated with the quasi-free

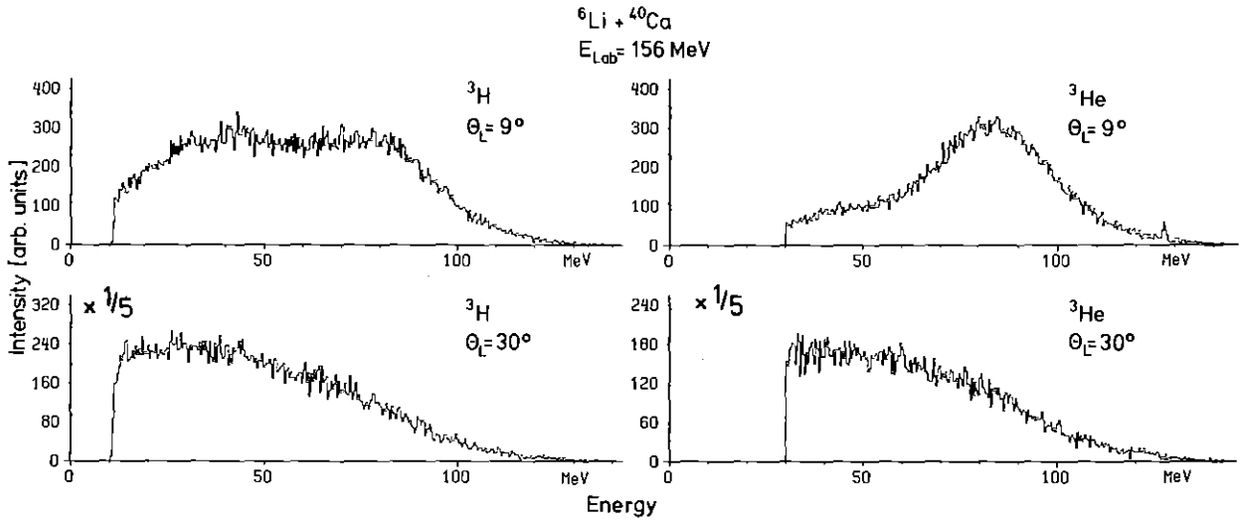

Fig. 1: Continuous ^{3}He and triton energy spectra after bombarding ^{40}Ca by 156 MeV ^{6}Li ions.

(^{3}He + t) break-up and which is exponentially decreasing with emission angle (see fig. 1) we may recognize further rather intensive components at lower energies covering the region of the optimum Q-value of ^{3}He transfer reactions. This might be also an indication for the role of "incomplete fusion" processes. In addition the triton spectra may contain - besides of the precompound decay - contributions due to two-step processes involving break-up followed by neutron-pick-up by the break-up deuteron. Nevertheless, the triton spectrum, and in particular its difference from the ^{3}He spectrum remains somewhat puzzling and has to be clarified by more detailed (exclusive) experiments.

References

(1) B. Neumann, J. Buschmann, H. Klewe-Nebenius, H. Rebel, and H.J. Gils, Nucl. Phys. A329 (1979) 259

(2) B. Neumann, H. Rebel, J. Buschmann, H.J. Gils, H. Klewe-Nebenius, and S. Zagromski, Z. Physik A296 (1980) 113

+Institut für Radiochemie des KfK

2.3.4 Investigation of Fusion and Partial Fusion in the $^{6}Li + ^{40}Ca$ Reaction at E_{Li}=156 MeV

K. Grotowski[+], Z. Majka[+], R. Planeta[+], J. Buschmann, H. Klewe-Nebenius[++], H.J. Gils, B. Neumann[++], H. Rebel, and S. Zagromski

In order to obtain information on fusion and partial fusion cross sections and the respective reaction mechanisms when bombarding ^{40}Ca by 156 MeV ^{6}Li ions, in-beam γ-ray spectra have been measured using a Ge(Li) detector. The experimental set-up is shown in fig.1.

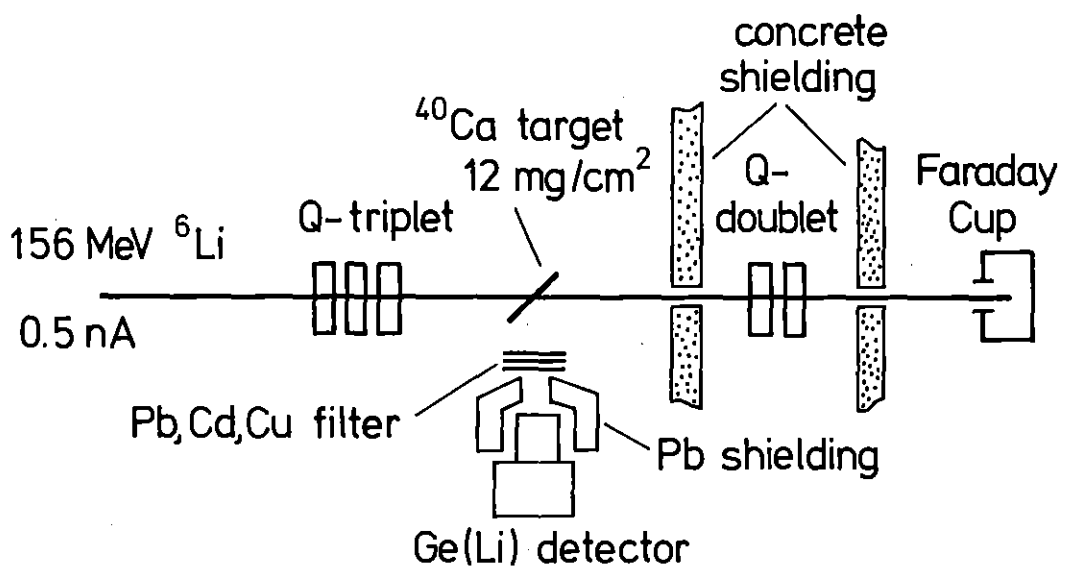

Fig. 1: Schematic view of the experimental set-up.

An example of the γ-spectra which have been measured in coincidence with the cyclotron RF pulses is shown in fig. 2. By analysing the spectra by means of the "SAMPO" code about 260 γ-lines could be identified. About 80 % of these lines have been assigned to the residual nuclei quoted in tab. 1 by at least one unique and one additional γ-transition. Transitions not feeding the respective ground states are marked by an asterisk. Some reaction products lighter than sulfur may also be due to reactions of ^{6}Li or neutrons with ^{27}Al of the beam tube. A more detailed analysis and comparison with statistical model calculations are in progress.

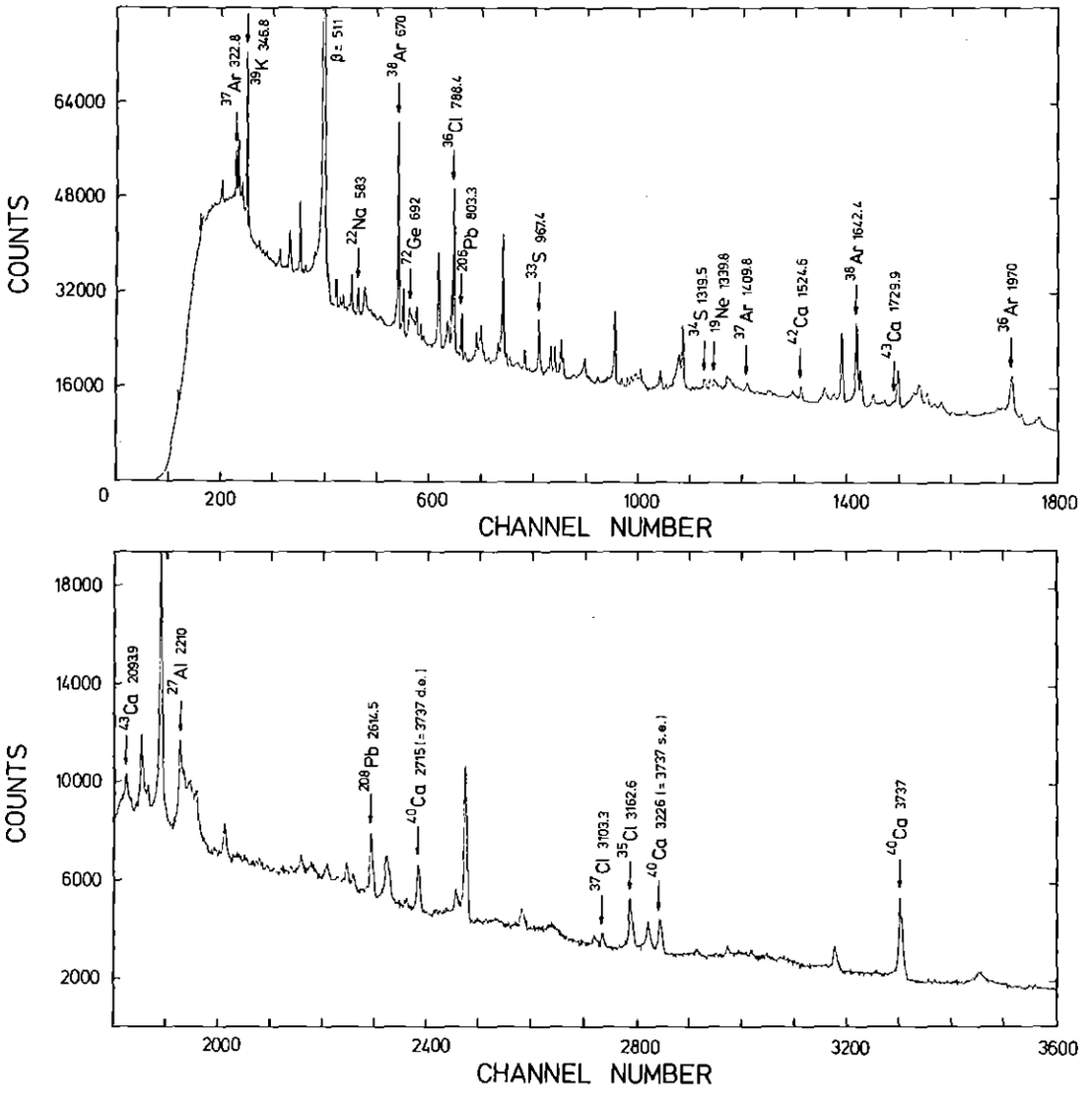

Fig. 2: Inclusive γ-ray spectrum from the $^{6}Li + ^{40}Ca$ reaction at E_{Li}=156 MeV.

Table 1: Residual nuclei identified in the ^{6}Li + ^{40}Ca reaction together with the most prominent transitions.

Nuclide	E_γ keV	Nuclide	E_γ keV	Nuclide	E_γ keV
^{43}Sc	845.3	^{37}K	1379.	^{27}Al	2210.
^{43}Ca	2093.9	^{37}Ar	1409.1	^{25}Mg	974.8
^{42}Ca	1524.6	^{37}Cl	3103.3	^{24}Al	2380.
^{41}Ca	2605.	^{36}Ar	1970.	^{24}Na	2563.
^{41}K	850.5*	^{36}Cl	788.4	^{23}Na	627.3*
^{40}Ca	3737.	^{35}Cl	3162.6	^{23}Ne	1017. *
^{40}K	843.6	^{35}S	1992.	^{22}Na	583.
^{39}K	783.3*	^{34}S	3303.5	^{21}Ne	350.7
^{39}Ar	1267.2	^{33}P	3490.	^{19}Ne	1339.8*
^{39}Cl	1301.5	^{32}Si	2292.6*	^{19}F	1348.6*
^{38}K	3420.	^{29}Si	754.9*	^{11}Be	3890.0
^{38}Ar	1642.4*	^{28}Al	1014.	^{10}B	718.3

+ Institute of Nuclear Physics and Jagellonian University, Krakow, Poland

++Institut für Radiochemie des Kernforschungszentrums Karlsruhe

2.3.5 Cluster Folding Model Description of 156 MeV ^{6}Li Elastic Scattering from ^{12}C

Z. Majka+, H. Rebel, and H.J. Gils

The elastic scattering of 156 MeV ^{6}Li ion from ^{12}C has been analyzed by single folding models (target and projectile folding) and by refined double folding model (1). The calculations indicate that such approaches are not able to describe satisfactorily the experimental differential cross sections in this specific case.

Taking into account the cluster structure of the projectile (^{6}Li=α+d) (2) and of the target nucleus (^{12}C = 3 α-particles) (3) the real part of ^{6}Li-^{12}C potential has been contructed using α-α and α-d interactions. The resulting real potential improves the description of ^{12}C(^{6}Li,^{6}Li)^{12}C experimental data.

These investigations indicate that the inclusion of clusterisation effects is important for the ^{6}Li-^{12}C system.

References

(1) Z. Majka, H.J. Gils, H. Rebel, Z. Physik A288 (1978) 139

(2) V.G. Neudatchin et al., Nucl. Phys. A163 (1971) 316

(3) W. Wadia, S. Moharram, Phys. Rev. C12 (1975) 2050

+Institute of Nuclear Physics and Jagellonian University, Krakow, Poland

3. LASER SPECTROSCOPY AND PHOTON SCATTERING

3.1 Atomic Beam Laser Spectroscopy of Neutron Deficient Ba-Nuclides*

H. Rebel, K. Bekk, G. Nowicki, and G. Schatz

Isotope shifts and hyperfine structure of the BaI $6s^2\ ^1S_o$ - $6s6p\ ^1P_1$ resonance transitions (λ = 553.6 nm) in neutron deficient Ba nuclides (N < 82) have been measured by observing the resonance fluorescence induced by a high resolution tunable CW dye laser in a well collimated atomic beam. The experimental results, now available for 17 Ba isotopes and isomers with A = 140 - 124, are used to deduce differences of rms charge radii, magnetic dipole and electric quadrupole moments. While the groundstates display a pronounced odd-even staggering the h $11/2^-$ isomers ^{135m}Ba and ^{133m}Ba show a decreased staggering. Conspicuously the isomer shift of the g $7/2^+$ isomer ^{129m}Ba proves to be negative. The nuclear structure information is discussed in the context of gamma-spectroscopic studies of transition nuclei with $50 \leq N,Z < 82$ and on the basis of a quasi-particle-plus-triaxial rotor model. The isotope shift discrepancy observed is fairly well described by the droplet model.

*Nukleonika 25 (1980) 145

3.2 Measurements of Isotope Shifts and Hyperfine Structure Splitting of the $4s^2\ ^1S_o$ - $4s\ 4p\ ^1P_1$ Atomic Resonance Transition for the Ca Isotopes

A. Andl, K. Bekk, G. Nowicki, and A. Hanser

Isotope shifts (IS) and hyperfine structure (A- and B-factors) of the CaI resonance line at λ = 422.7 nm have been measured for stable and radioactive Ca nuclides between A = 40 and A = 48. The measurements are based on the observation of the resonance fluorescence induced in a well-collimated atomic beam by the light of high resolution tunable CW dye lasers. The experimental method and set-up

are similar to those in ref. 1. The main modification introduced is a new jet-stream laser operated with a stilben dye. For the sample preparation quantities of 0.05 - 10 ng of the Ca isotope of interest were implanted into the inner surface of the atomic beam oven by means of an electromagnetic mass seperator. Details as to the instable isotopes are given in contribution 3.3. The results on ^{47}Ca were obtained using a sample of only 20 pg at the beginning of the measurement which demonstrates once more the sensitivity of the method. Fig. 1 displays a fluorescence spectrum of a sample containing ^{41}Ca

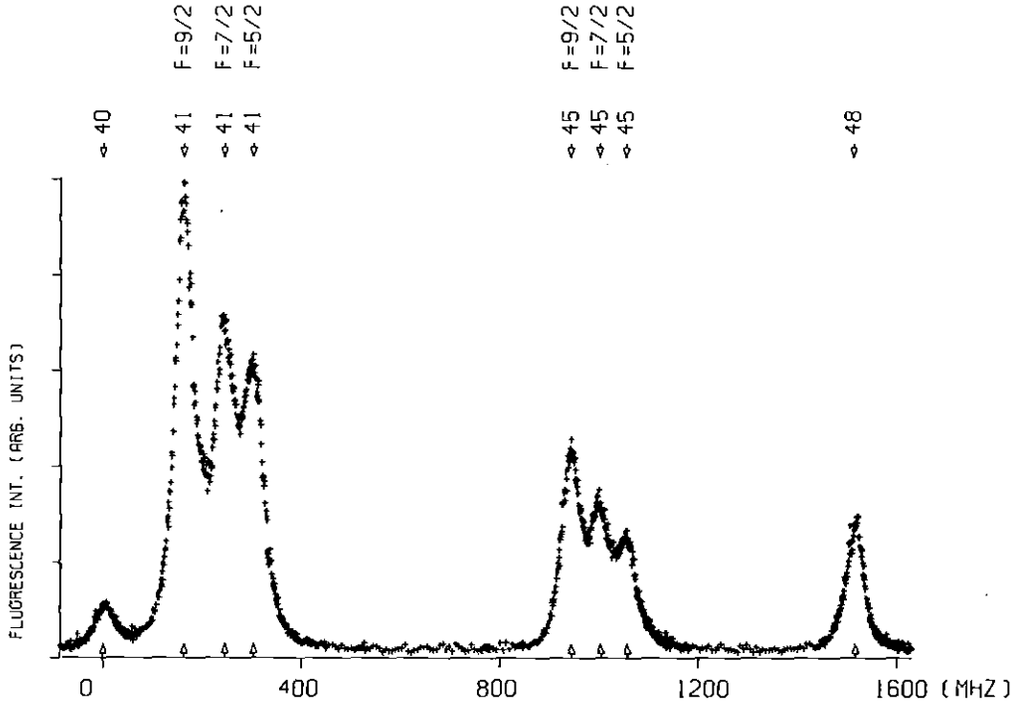

Fig. 1: Fluorescence spectrum measured with a $^{41,45}Ca$ sample.

and ^{45}Ca. The experimental line-width was about 42 MHz (FWHM) which exceeds the natural line-width by ca. 20 %. The counting rate far off the resonances was about 100 counts/s. From the hyperfine splittings A- and B-factors have been determined which are given in tab. 1 in addition to the isotope shifts relative to the transition in the ^{40}Ca atom.

Table 1: Observed IS and hyperfine structure constants A and B in the Ca isotopic chain.

Atomic number	Isotope shift (MHz)	A (MHz)	B (MHz)
41	221.3 (2.8)	-17.65 (27)	-3.13 (2.78)
42	393.9 (1.1)	-	-
43	613.6 (1.3)	-14.25 (5)	-3.52 (50)
44	777.2 (2.5)	-	-
45	991.2 (1.4)	-13.96 (8)	+3.70 (76)
46	1166.0 (1.1)	-	-
47	1351.2 (3.2)	-15.73 (30)	+2.46 (2.90)
48	1518.8 (1.8)	-	-

References

(1) K. Bekk, A. Andl, S. Göring, A. Hanser, G. Nowicki, H. Rebel, G. Schatz, Z. Physik A291 (1979) 219

3.3 Samples of Instable Ca Isotopes with Low Contamination by Stable Ca

B. Feurer and A. Hanser

For laserspectroscopic measurements (see contribution 3.2) instable Ca isotopes were produced via the reactions $^{40}Ca(n,\gamma)^{41}Ca$, $^{44}Ca(n,\gamma)^{45}Ca$, $^{46}Ca(n,\gamma)^{47}Ca$, and $^{48}Ca(d,2n+p)^{47}Ca$. In order to isolate instable Ca isotopes from stable Ca target material, an electromagnetic mass separation with a high separation factor is required. The thermal ion source used successfully in the foregoing barium experiments yields high separation factors. But the ionization potential of Ca is higher and the decomposition temperature of the oxid lower than the corresponding values of Ba, both decreasing the ionization process yield. Therefore, a new oven ampoule for the thermal ion source was developed (fig. 1) with which even at the necessary high ion current output practicable yields for the mass separation process (up to 5 %)

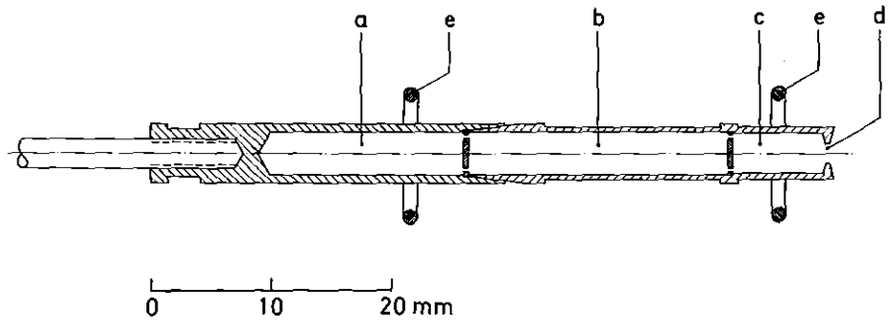

Fig. 1: New tantalum oven ampoule for the thermal ion source, suitable for Ca separations.

a: decomposition and vaporization chamber; b: connecting tube; c: ionization chamber; d: ion extraction orifice; e: filaments for electron impact heating.

are achieved. For a further decrease of the contamination by stable Ca, care was taken for good vacuum inside the mass separator ($\sim 1 \cdot 10^{-6}$ Torr), and a tube of 22 cm length was set in front of the collector diaphragm in order to screen against scattered ions and neutrals.

Samples containing both $\sim$ 20 ng ^{41}Ca ($\tau_{1/2} = 1.3 \cdot 10^5$ a) and $\sim$5 ng ^{45}Ca ($\tau_{1/2}$ = 163 d) have been prepared from natural Ca and enriched ^{44}Ca, respectively, irradiated for about 1 1/2 years in the Karlsruhe Research Reactor. Contamination by the stable target isotopes originating from the mass separation process was quite negligible in this case. To prepare samples of ^{47}Ca ($\tau_{1/2}$ = 4.5 d) firstly 1.5 mg oxide of ^{48}Ca enriched to 95 % was irradiated with 38 MeV deuterons for 3 1/2 days in the Karlsruhe Isochronous Cyclotron yielding a ^{47}Ca/^{48}Ca ratio of $4.5 \cdot 10^{-6}$. The electromagnetic separation of the ^{47}Ca resulted in a sample of 0.08 ng (measured via the γ-radiation) contaminated by $\sim$0.11 ng ^{48}Ca (as seen in the laserspectroscopic measurement). From this a separation factor of $\sim 1.6 \cdot 10^5$ can be deduced. As the separation of a lower mass from a heavier one is the more unfavourable case for electromagnetic mass separation, in a second experiment 2.6 mg carbonate of very expensive highly enriched ^{46}Ca (43 %) was irradiated in the Karlsruhe Reactor for 20 days. In this case the mass separation resulted in a sample of 0.5 ng

^{47}Ca. From the measurement of the ^{46}Ca mass line tailing the separation factor and the contamination by ^{46}Ca can be estimated to $\sim 6 \cdot 10^5$ and $\sim$0.04 ng, respectively. For calibration purposes a trace of a noninterfering stable Ca isotope has been added to every sample.

3.4 The Charge ms-Radii of Stable and Radioactive Ca Isotopes

A. Andl, K. Bekk, G. Nowicki, H. Rebel, and G. Schatz

The measured hyperfine structure splitting factors and isotope shifts of the Ca I resonance transition (λ = 422.7 nm) have been considered in view of their information on nuclear moments and on the variation of the charge radii of the Ca isotopes. The contribution of the "specific mass effect" to the observed isotope shifts has been ruled out by comparison with results from muonic X-ray (1) and electron scattering studies (2). Fig. 1 displays the variation of the ms-radii of the charge distributions and compares with results of different experiments (1,3,4). The error bars quoted for the laserspectroscopic results are dominated by the remaining (systematic) uncertainty due to the specific mass effect. Fig. 1 reveals a remarkable behaviour of the charge distributions of the Ca nuclei

- the charge ms-radii of ^{40}Ca and ^{48}Ca are equal whereas the even nuclei in between have a charge radius larger in size by about 1 %
- there is a considerable odd-even staggering
- the ms-charge radii of ^{41}Ca and ^{40}Ca are equal whereas those of ^{47}Ca ($T_{1/2}$ = 4.54 d) and ^{48}Ca differ slightly.

It is interesting to note that there are conspicuously similar trends in the quadrupole transition strengths inferred from inelastic alpha particle scattering (5) in the B(E2;0-2_1)-values as well as in the transition radii measured (6) for 0_1^+-0_2^+ monopole transitions in even Ca nuclei. Therefore, in a phenomenological way the observed variation may be ascribed to a deformation effect via

$$\delta\langle r^2\rangle = \delta\langle r^2\rangle_{Ca-40} + \delta\langle\tilde{r}^2\rangle + \frac{5}{4\pi}\langle r^2\rangle_{Ca-40}\delta\langle\beta^2\rangle$$

including a small breathing (monopole polarizibility) $\delta\langle\tilde{r}^2\rangle$ of the ^{40}Ca

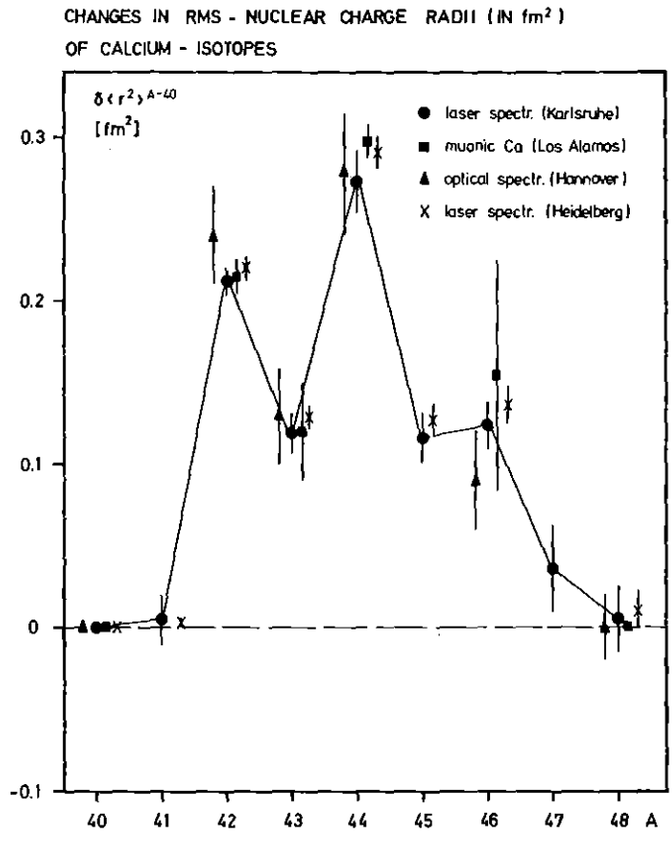

Fig. 1:
Variation of ms-radii of the nuclear charge distributions of Ca isotopes

core. The required ms deformation values $\langle\beta^2\rangle$ are consistent with the observed B(E2) values, but can hardly be related to the observed quadrupole moments without further nuclear structure information.

References

(1) H. Wohlfahrt, E. Shera, M. Hoehn, Y. Yamazaki, G. Fricke, and R. Steffen, Phys. Lett. 73B (1978) 131

(2) R.F. Frosch, R. Hofstadter, J.S. McCarthy, G.K. Nöldecke, K.J. van Oostrum, B.C. Clark, R. Herman, D.G. Ravenhall, Phys, Rev. 174 (1968) 1380

(3) E. Bergmann, P. Bopp, Ch. Dorsch, J. Kowalski, and F. Träger, Z. Physik A294 (1980) 319

(4) H.W. Brandt, K. Heilig, M. Knöckel, and A. Steudel, Z. Physik A288 (1978) 241

(5) M.J.A. De Voigt, D. Cline, and R.N. Horoshko, Phys. Rev. C10 (1974) 1798

(6) H.D. Gräf, H. Feldmeier, P. Manakos, A. Richter, and E. Spamer, Nucl. Phys. A295 (1978) 319

3.5 Coulomb Correction to Delbrück Scattering Investigated at Z = 94*

P. Rullhusen[+], F. Smend[+], M. Schumacher[+], A. Hanser, and H. Rebel

Differential cross sections for the elastic scattering of 2.754 MeV photons by Pu were measured for angles ranging from 45 to 120° and interpreted in terms of Delbrück, nuclear Thomson, Rayleigh and nuclear resonance scattering. It is shown that the largest part of the discrepancy between experiment and the lowest-order Delbrück theory can be removed by introducing a $(Z\alpha)^4$-dependent Coulomb correction term. Evidence is obtained for additional Coulomb corrections terms of higher order in $(Z\alpha)$.

*Z. Physik A293 (1979) 287

[+]II. Physikalisches Institut der Universität Göttingen, Göttingen, Federal Republic of Germany

4. THEORY

4.1 Calculation of Nuclear Reaction Parameters with the Generator Coordinate Method and their Interpretation*

R. Beck, M.V. Mihailović[+], and M. Poljšak[+]

Collisions between complex nuclei are described variationally in terms of the GCM with the aim to provide an evidence that it is a managable calculational procedure. The variational principle of Kohn and Kato is used to derive the expression for the K matrix. The space of scattering states is spanned entirely by antisymmetrized products of shell model wave functions describing separate clusters; the generator coordinate is the separation between the two shell model potentials. Scattering boundary conditions are enforced by solving an integral equation for the channel GC amplitude in each open channel separately. The main part of evaluation of collision parameters is performed by calculating double integrals of a form factor between channel GC amplitudes. A theorem about a property of the form factors is proved which allows to reduce the amount of work needed to calculate double integrals.

The application of the method to the elastic ^{3}H to ^{4}He scattering has shown the feasibility of the calculation.

It is shown how an analysis of calculated scattering parameters and corresponding scattering states in terms of quasibound states enables one to make a consistent comparison with experiment and to extract some knowledge of the reaction mechanism.

Finally a comparative list of the calculational procedures of the GCM and RGM for reactions is made.

*Submitted to Nuclear Physics

[+]J. Stefan Institute, E. Kardelj Institute, Ljubljana, Yugoslavia

4.2 The Three-Cluster Structures in ^{7}Li*

R. Beck, R. Krivec, and M.V. Mihailović[+]

A model is derived for the structure of light nuclei which includes two- and three-cluster configurations. The model is applied to the nucleus ^{7}Li by including the two-cluster configuration (^{4}He-^{3}H) and the three-cluster configurations $(^{4}\text{He}-(^{2}\text{H}_{\text{Id}}-^{1}\text{n}))_{\text{I}}$, $\text{I}_{\text{d}} = 0,1$ and $\text{I} = \frac{1}{2},\frac{3}{2}$. A significant improvement has been obtained compared to the model which contained two-cluster configurations only with 1s- and 1p-fragments.

*Submitted to Nuclear Physics

[+]J. Stefan Institute, E. Kardelj University, Ljubljana, Yugoslavia

4.3 Calculation of Two-Particle Transfer Reactions in ^{7}Li

R. Beck, R. Krivec, and M.V. Mihailović[+]

The reaction

$$^{4}\text{He} + {}^{3}\text{H} \longrightarrow \begin{matrix} ^{4}\text{He} + {}^{3}\text{H} \\ ^{6}\text{Li} + \text{n} \end{matrix}$$

is studied in the framework of the reaction theory (1) of the Generator Coordinate Method. The vector space is spanned by the basis

$$\Phi_1^{JM\pi}(\underset{\sim}{X},\underset{\sim}{S}_1) = P^{JM\pi}_{A}\{\Phi_{^{4}\text{He}}(\underset{\sim}{X},\underset{\sim}{S}_{^{4}\text{He}})\Phi_{^{3}\text{H}}(\underset{\sim}{X},\underset{\sim}{S}_{^{3}\text{H}})\}$$

$$\Phi_2^{JM\pi}(\underset{\sim}{X},\underset{\sim}{S}_2) = P^{JM\pi}_{A}\{\Phi_{^{6}\text{Li}}(\underset{\sim}{X},\underset{\sim}{S}_{^{6}\text{Li}})\Phi_{^{1}\text{n}}(\underset{\sim}{X},\underset{\sim}{S}_{\text{n}})\}$$

where $\Phi_{^{4}\text{He}}(\underset{\sim}{X},\underset{\sim}{S}_{^{4}\text{He}})$, $\Phi_{^{3}\text{H}}(\underset{\sim}{X},\underset{\sim}{S}_{^{3}\text{H}})$ and $\Phi_{^{1}\text{n}}(\underset{\sim}{X},\underset{\sim}{S}_{\text{n}})$ are Slater determinants built from 1s-single particle harmonic oscillator functions centered at $\underset{\sim}{S}_{^{4}\text{He}}$, $\underset{\sim}{S}_{^{3}\text{H}}$ and $\underset{\sim}{S}_{^{1}\text{n}}$, respectively. The function $\Phi_{^{6}\text{Li}}(\underset{\sim}{X},\underset{\sim}{S}_{^{6}\text{Li}})$ is a two-center function of the type (^{4}He-^{2}H). The distances $\underset{\sim}{S}_1 = \underset{\sim}{S}_{^{4}\text{He}} - \underset{\sim}{S}_{^{3}\text{H}}$ and $\underset{\sim}{S}_2 = \underset{\sim}{S}_{^{6}\text{Li}} - \underset{\sim}{S}_{^{1}\text{n}}$ are the generator coordinates.

The trial function is of the type

$$\psi_j^t(\underset{\sim}{X}) = \sum_p c_{jp}^{(1)t} \Phi_1^{JM\pi}(\underset{\sim}{X}, \underset{\sim}{S}_{jp}) + \sum_p c_{jp}^{(2)t} \Phi_2^{JM\pi}(\underset{\sim}{X}, \underset{\sim}{S}_{2p})$$
$$+ \int d\underset{\sim}{s}\, f_j(\underset{\sim}{S}) \Phi_j^{JM\pi}(\underset{\sim}{X}, \underset{\sim}{S})$$
$$+ \sum_{j'=1}^{2} K_{jj'}^t \int d\underset{\sim}{s}\, g_{j'}(\underset{\sim}{S}) \Phi_{j'}^{JM\pi}(\underset{\sim}{X}, \underset{\sim}{S}); \quad (j=1,2)$$

The coefficients $c_{jp}^{(1)t}$, $c_{jp}^{(2)t}$ and $K_{jj'}^t$, are the variational parameters. The index $j = \{JM\pi Ilk\}$ comprises all channel quantum numbers.

The generator coordinate amplitudes $f_j(\underset{\sim}{S})$ and $g_j(\underset{\sim}{S})$ are defined by the following equation

$$\begin{pmatrix} F_j(k_j r_j) \\ G_j(k_j r_j) \end{pmatrix} \frac{Y_{lm}(\hat{r}_j)}{r_j} = \int d\underset{\sim}{s}\, \exp\left[-\frac{\beta_j'}{2}(\underset{\sim}{r}_j - \underset{\sim}{S})^2\right] \begin{pmatrix} f_{lm}(\underset{\sim}{S}) \\ g_{lm}(\underset{\sim}{S}) \end{pmatrix},$$

where F_j and G_j are the regular and the irregular Coulomb functions, respectively.

The reduced oscillator parameters β_j' are given by $\beta_1' = \frac{12}{7}\beta$ and $\beta_2' = \frac{6}{7}\beta$, where β is the oscillator parameter.

The matrix $K_{jj'}^t$ is determined by the Kato-Kohn variational method

$$K_{j'j} \quad w_j = -\langle F_{j'}|\Delta|F_j\rangle + \sum_{ii'} \langle G_i|\Delta|F_{j'}\rangle$$
$$* \langle G_i|\Delta|G_{i'}\rangle^{-1} \langle G_{i'}|\Delta|F_j\rangle ,$$

where W_j is the Wronskian of the functions F_j and G_j.

$$\Delta = \bar{H} - \bar{H} \sum_{pp'} |\Phi(\underset{\sim}{S}_p)\rangle \langle \Phi(\underset{\sim}{S}_p)|\bar{H}|\Phi(\underset{\sim}{S}_{p'})\rangle^{-1} \langle \Phi(\underset{\sim}{S}_{p'})|\bar{H}$$

$$\bar{H} = H - E$$

The method of calculation of the matrix elements $\langle F_j|\Delta|F_{j'}\rangle$, $\langle G_j|\Delta|G_{j'}\rangle$ and $\langle G_j|\Delta|F_{j'}\rangle$ is described in ref. (1).

Reference

(1) Calculation of nuclear reaction parameters with the Generator Coordinate Method and their interpretation, R. Beck, M.V. Mihailović, and M. Poljsak. Submitted to Nucl. Phys.

+J. Stefan Institute, E. Kardelj University, Ljubljana, Yugoslavia

4.4 Comparison of the Scission-Point Model of Nuclear Fission with Experimental Data

F. Dickmann, A.A. Naqvi, F. Käppeler

The scission-point model is used to test different hypotheses concerning the interplay of the collective modes relevant for the fission process and their coupling to internal degrees of excitation prior to scission (1-3). In all versions of the model the deformability of the nascent fragments is essential because, by influencing the Coulomb interaction of the fragments, it is a contributory determinant of the measurable kinetic energy (2) and of the energy available for collective and internal excitation.

The so far most successful version (3) is based on the assumption of a statistical equilibrium between the collective degrees of freedom and a weak coupling of these modes to internal excitations. It explains the gross features of fission such as the fragment yields, the kinetic energy distribution and the neutron emission from the fragments. This is achieved without extensive parameter fitting. The distance d between the half density surfaces of the fragments in the scission configuration, e.g., is independent of the mass ratio. In contrast to this the assumption of a complete statistical equilibrium leads to disagreement with the mass yield curve unless d is adjusted (1).

However also the model of Wilkins et al. (3) runs into difficulties upon a detailed comparison with new experimental data (4). The theoretical number of neutrons emitted by the heavy fragment is low. Furthermore we conclude from the published results that the observed asymmetric increase of the neutron-emission curve with excitation energy (see Fig. 1 of ref. 4) is outside the scope of the model in its present version, although calculations emphasizing this point don't exist. We suggest that the inclusion of octupole deformations for the nascent fragments will help to brooden the mass yield curves which are too narrow due to overstimation of shell effects.

References

(1) R.E. Pepping, A Statistical Model Investigation of Nuclear Fission, Report LA-4047-T (1979), unpublished

(2) F. Dickmann and K. Dietrich, Nucl. Phys. A129 (1969) 241-258

(3) B.D. Wilkins, E.P. Steinberg, and R.R. Chasman, Phys. Rev. C14 (1976) 1832-1863

(4) A.A. Naqvi, R. Müller, and F. Käppeler, contribution 1.1.1 to this report

5. APPLIED NUCLEAR PHYSICS

5.1 NUCLEAR FUEL AND ELEMENTAL ANALYSIS

5.1.1 Assay of Uranium and Plutonium in Solution by K-Edge Photon Absorptiometry Using a Continuous X-Ray Beam*

H. Eberle, P. Matussek, I. Michel-Piper, and H. Ottmar

K-edge absorptiometry of a continuous X-ray spectrum is examined and evaluated with respect to the nondestructive analysis of uranium and plutonium in feed and product solutions of a reprocessing plant. Random and systematic errors associated with the technique are carefully analyzed and experimentally verified. The data presented show that K-edge densitometry allows to determine SNM materials at concentration levels above 50 g/ℓ with an accuracy of 0.2 % in any type of solution, including highly gamma active feed solutions.

*Proceedings of the 2nd Annual ESARDA Symposium on Safeguards and Nuclear Material Management, 26th/28th March, 1980, Edinburgh, Scotland, ESARDA Report No. 11, p. 372, edited by JRC Ispra, Italy

5.1.2 Status of the Gamma Densitometer for Uranium and Plutonium Analysis in Solutions

H. Eberle, P. Matussek, I. Michel-Piper, and H. Ottmar

The K-edge gamma absorptiometry system has now been equipped with a new D.C. high voltage X-ray generator which is powered by a 150 kV / 20 mA high voltage supply with a stability of 0.1 %. Compared to the previously used A.C. generator the new set-up provides better high voltage stability, better pile-up behaviour and significantly reduced measurement times at the same integral countrate. The new X-ray tube can also be operated at low X-ray energies for L-edge densitometry.

Measurements have been performed on uranium nitrate solutions with uranium concentrations ranging from 50 to 500 grams U/litre. Accuracies of about 0.2 % could be achieved within assay times of 20 minutes (1). Qualitative test measurements have also been carried out on some plutonium solutions and a reprocessing input tank solution. The quantitative

assay of those solutions is planned for the near future. In order to allow the handling of the highly radioactive samples, a glove box has been added to the densitometry system. Two locks serve as input and output for shielded radioactive solution containers to and from the measurement position inside the glove box. The X-ray generator, the primary collimator and the Ge detector are positioned outside the glove box. The collimated X-ray beam enters and leaves the glove box through thin Be windows.

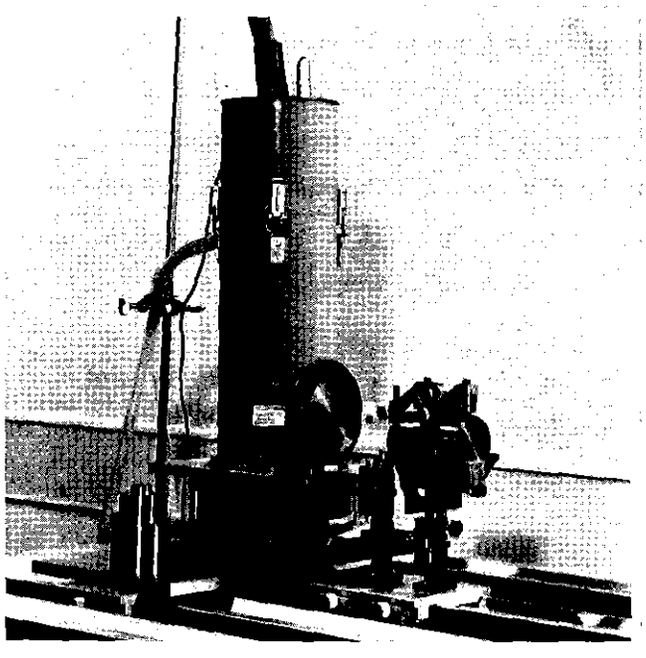

Fig. 1:
Details of the X-ray densitometer system showing the X-ray tube, the primary collimator, the sample cell and the secondary collimator. Sample shielding and glove box are removed.

All elements of the system are mounted on a distortion free table. The generator, the measuring cell and the collimators are fixed on an optical bank in order to assure the proper alignment of the extremely narrow beam geometry. The system components including the HV generator with the associated control electronics are combined into a transportable unit.

The Ge detector signals are processed with a standard NIM amplifier and pile-up rejector to a computer-based data aquisition and evaluation system (ND 6600) equipped with 224 kByte memory, a 10 MByte harddisk and a magnetic tape unit. The data evaluation programs are written in FORTRAN. They comprise Compton and pile-up background correction routines, calculation of the heavy element concentration using least squares fit procedures and treatment of measurement errors (1).

The dialog between operator and system takes place on a question and answer basis via the system console or the fast teletype. The accumulated spectra will be routinely recorded on magnetic tape. The calculated heavy element concentrations along with the relevant system parameters and calibration constants are printed out and are also saved on magnetic tape.

The evaluation of the densitometer system is part of the joint program on the technical development and further improvement of IAEA safeguards between the gouvernment of the Federal Republic of Germany and the IAEA. After final tests the equipment will be transferred to the radiochemistry division where the measurements on plutonium and reprocessing input tank solutions will be performed.

References

(1) H. Eberle, P. Matussek, I. Michel-Piper, H. Ottmar, Proc. of the 2nd Annual Symposium on Safeguards and Nuclear Material Management, 26th/28th March, 1980, Edinburgh, Scotland, ESARDA Report No. 11, p. 372, edited by JRC Ispra, Italy

5.1.3 Branching Intensity of the 43.40 keV Gamma Line from ^{241}Am

M.R. Iyer[+] and H. Ottmar

The low energy region 26 to 60 keV in the gamma spectrum of plutonium provides finger prints of all major plutonium isotopes (except ^{241}Pu) and their daughter products of interest for the NDA of Pu isotopic composition using high resolution gamma-ray spectrometry. The low energy region is ideal for the isotopic assay in solutions. The fundamental parameter method (1) does not need any standards. The accuracy of the results depends on the accuracy with which the nuclear data is available.

A comprehensive compilation of the branching intensities of gamma rays from Pu isotopes and their daughter products have been published by Gunnink et al. (2,3). The peak due to the ^{238}Pu signature at 43.477 keV has invariably the contribution from the 43.40 keV line from ^{241}Am as the two cannot be resolved. It is thus essential to know the branching intensity of the ^{241}Am gamma line accurately for the

estimation of ^{238}Pu isotopic ratios. As per the earlier compilation of Gunnink et al. (2) the line has a branching ratio of 9.10E-04, whereas in the later compilation (3) the gamma line is attributed only to ^{237}U with a branching ratio of 5.90E-09.

A re-examination of the 26 to 60 keV region in the ^{241}Am gamma spectrum was made using a LEPS detector system having a resolution of 470 eV at 122 keV. The relative efficiency function was obtained from the photopeak counts at 26.344 keV, 43.40 keV and 59.536 keV. The intensity of 9.10E-04 given by Gunnink et al. (2) does not fit with the smooth relative efficiency curve. The relative efficiency at 43.40 keV from this curve was used to arrive at its branching intensity. The evaluation was done using two different americium sources giving a mean value of 6.95E-04 $\pm$ 2 %.

References

(1) H. Eberle et al., Safeguards Technology, IAEA, vol. 2, p. 27 (1979)

(2) R. Gunnink et al., Report UCRL 51096 (1971)

(3) R. Gunnink et al., Report UCRL 52139 (1976)

+Bhabha Atomic Research Centre, Bombay, India

5.1.4 The ^{235}U Enrichment Monitor: In-Plant Installation and First Operational Experiences

S. Baumann+, H. Eberle, and P. Matussek

The in-line assay system designed for continuously monitoring the ^{235}U enrichment of uranium oxide powder prior to pelletizing (1) has been installed at the RBU facility in July 1979. Having passed initial tests and calibrations, the system is now being active for routine measurements since March 1980. In the present stage, the computerized system services two enrichment measurement stations, with the enrichment monitors being installed ahead of the pellet presses in two different process lines. Hardware and software provisions are made for connecting of up to eight independent enrichment measurement stations to the PDP 11/04 computer.

A 1000 sec count time has been chosen for a single enrichment assay at the in-line positions. Up to now, several thousand enrichment measurements have been completed under real in-plant conditions. So far, the system has proved to meet the design goals of assaying the ^{235}U enrichment within the typical enrichment tolerances for LWR fuel. At the 3 % enrichment level, the enrichment is measured with a precision of about 0.4 % (1). Built-in features such as corrections for gain variations and monitoring of the resolution of the NaI detectors assure a high reliability of the measured enrichment data.

```
**********************************************************
**********************************************************

          2. LINIE              OPERATORNR. :        3422.

DATUM     18/ 3/80
UHRZEIT    7:27: 3

AUFTRAGSKENNZ. :                      KKG-G
PULVERLOSNR. :                                      6.
PELLETLOSNR. :                                      4.

**********************************************************

GEM. ANREICHERUNG (MITTELWERT) :              3.309383 %
STAND. ABWEICHUNG (ABSOLUT)    :              0.011325 %

**********************************************************

ANREICHERUNG SOLLWERT :                         3.300 %
TOLERANZGRENZE (ABSOLUT) :                      0.050 %

MAX. GEM. ANREICHERUNG :                      3.339170 %
MIN. GEM. ANREICHERUNG :                      3.270441 %

ANZAHL DER MESSUNGEN :                          353.
   UNTERHALB DER TOLERANZ :                       0.
   OBERHALB DER TOLERANZ :                        0.

MATERIALHERKUNFT :                    UF 6 AUS UDSSR
SCHROTTANTEIL :                                10. %
GEW. PULVERLOS :                              123. KG

**********************************************************
**********************************************************

ZUSATZINFORMATION :

   1172.410889     284.424255      0.848910      0.850510
     11.315621       9.370334      0.022762      0.017807
```

Table 1: Example of a Summary Protocol Obtained from In-Line Measurements of the ^{235}U Enrichment.

Table 1 presents a reprint of the summary protocol which the system delivers upon the completion of the processing of a certain batch of material. In the present example 353 enrichment analyses have been performed during the processing of the particular batch. The summary protocol records the mean value of the measured enrichments with the associated standard deviation as well as the minimum and maximum enrichment values measured from a batch of material. Additional information is given on the mean values of the countrates in the peak and background windows for the 185.7 keV line, and on the energy resolution of two reference peaks from the measured gamma spectrum. The batch-specific data given in the protocol have to be entered via teletype by the operator on a question-answer basis before he starts the processing of a new batch.

The initial calibration has been performed at the in-line position with bulk quantities of uranium oxide powder of two different enrichments. Once established, the calibration constants have been continuously improved by using the measured countrates from the actually processed materials together with the enrichments from corresponding laboratory sample analyses. This 'dynamic' calibration procedure has proved to work reasonably well. The attempt to calibrate the system off-line with small amounts of uranium oxide in dummy containers partly failed, and it needs further evaluation.

References

(1) P. Matussek, H. Allex, Proceedings of the 1st Annual Symposium on Safeguards and Nuclear Material Management, European Safeguards and Development Association (ESARDA), Brussels, April 25/27, 1979, ESARDA Report 10 (1979) p. 303

+Reaktorbrennelement Union GmbH (RBU), D 6450 Hanau, Germany

5.1.5 Note on the Contribution of ^{238}U Daughter Products to the 185 keV Gamma-Ray Intensity Observed from Low-Enriched Uranium

H. Ottmar

The gammaspectrometric ^{235}U enrichment analysis makes use of the proportionality between the measured intensity of the most prominent ^{235}U gamma ray at 185.7 keV and the abundance of the ^{235}U isotope. Low-abundant gamma rays of similar energy, however, are also emitted by the ^{238}U daughter products ^{234}Pa and ^{234m}Pa, thus introducing a small nonlinearity into the ^{235}U enrichment measurements.

In the present note we are quantifying the interference of those gamma rays from the ^{238}U daughter products which cannot be resolved from the ^{235}U gamma line at 185.7 keV in typical gamma measurements with solid state detectors. The data given are based on experimental data derived from our previously reported measurements on low-enriched U_3O_8 prototype standard samples (1). The spectral informations obtained from those measurements, together with the very well known isotopic composition of the samples, have been used to redetermine the absolute branching intensities of gamma rays from ^{234}Pa and ^{234m}Pa in the energy region between 130 and 295 keV.

Table 1 summarizes the measured branching intensities of those gamma rays. The intensity values have been normalized to the absolute branching intensities of ^{231}Th and ^{235}U gamma rays reported by Gunnink (2). On the average, the intensities of the ^{234}Pa gamma rays turn out to be 10 % higher, and those for the ^{234m}Pa gamma rays about 20 % lower than the adopted values in the Nuclear Data Sheets (3). The branching intensity value of 7.65×10^{-4} for the 258.2 keV gamma ray from ^{234m}Pa is in close agreement with the value of 7.69×10^{-4} recently determined by Harry et al. (4).

The 186.0 and 184.7 keV lines from ^{234}Pa and ^{234m}Pa, respectively, have not been observed in the presence of the 185.7 keV line from ^{235}U. Their intensities have been determined relative to the intensity of neighbouring gamma rays from the same isotope using relative intensity ratios taken from the Nuclear Data Sheets (3). The last column of the Table gives the activities of the two gamma rays expressed in

Table 1: Branching Intensities of Major Gamma Rays from ^{234}Pa and ^{234m}Pa in the Energy Region between 130 and 295 keV.

		Photons/Decay			Activity (Photons /s/g ^{238}U)
		Present		ND Sheets (3)	
^{234}Pa	131.3	0.217	(4)[a]	0.20	
	152.7	0.064	(6)	0.067	
	186.0	0.022	(10)	0.020	0.356
	226.4	0.053	(5)	0.059	
	227.2	0.073	(4)	0.055	
	248.9	0.034	(6)	0.028	
	272.2	0.015	(15)	0.013	
	293.7	0.044	(12)	0.039	
^{234m}Pa	184.7	1.60×10^{-5}	(10)	1.2×10^{-5}	0.199
	258.2	7.65×10^{-4}	(4)	5.70×10^{-4}	

a) Error in per cent

photons/sec/g ^{238}U, assuming secular equilibrium for the ^{238}U daughter products. These values have to be compared with the activity value of $4.490\ 10^{4}$ photons /sec/g ^{235}U for the 185.7 keV line from ^{235}U when calculating the contribution of the protactinium gamma rays to the gamma-ray inten-

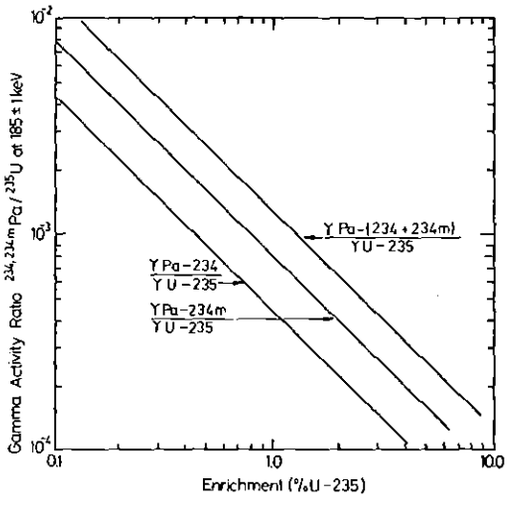

Fig. 1:
Activity ratio of 185±1 keV gamma rays from $^{234,234m}Pa$ and ^{235}U emitted from low-enriched uranium, assuming secular equilibrium for the ^{238}U daughter products.

sity observed from LWR type fuel at 185 keV. The activity ratio A(Pa)/A(^{235}U) at 185 keV is plotted in Fig. 1 as a function of the ^{235}U enrichment. The diagram shows that the contribution of the protactinium gamma rays becomes negligible for enrichments higher than about 1 %, and that it reaches at most a value of 0.5 % for typical depleted (0.2 - 0.3 % ^{235}U) materials. The associated bias has thus to be considered only in high-precision measurements.

References

(1) H. Eberle, P. Matussek, Report KfK 2868 (1979) p. 74

(2) R. Gunnink, J.F. Tinney, Rep. UCRL-51086 (1971)

(3) Y.E. Ellis, Nuclear Data Sheets 21, 493 (1977)

(4) R.J.S. Harry, J.K. Aaldijk, J.P. Braak, Safeguarding Nuclear Materials, Vol. II, International Atomic Energy Agency, Vienna, 1976, p. 235

5.1.6 A Microprocessor-Based Plutonium Waste Monitor with Internal Matrix Attenuation Correction

P. Matussek, P.P. Chakraborty[+], R.M. Iyer[+]

A new plutonium-waste monitor has been developped in the frame of the Indo-German collaboration program. The instrument employs passive gamma spectroscopy using a 5"x2" NaI(TL) detector. The development was based on the experience made with an earlier Pu waste monitor (1) which relates the net countrate in two energy windows around 208 keV and 382 keV directly to the ^{241}Pu and ^{239}Pu content in the waste containers. This method however could not account for gamma absorption due to matrix materials in the samples.

The new method uses three windows on the three complexes at 100 keV, 200 keV and 400 keV that are observed in the Pu gamma spectrum using a NaI detector. The total Pu content is determined from these three complexes by:

$$Pu_i = A_i \cdot peak_i + B_i \cdot background_i + C_i, \qquad i = 100,200,400$$

where Pu_i are the Pu contents arrived at using the three peak regions and A_i, B_i, C_i are constants obtained from calibration with a set of

standards. $Peak_i$ and $background_i$ are the counts in the respective peak and Compton background windows. In the absence of matrix attenuation the three Pu_i values should be the same within statistical uncertainty.

In case of matrix attenuation the observed Pu_i contents differ depending on the type and thickness of the gamma absorbing medium as the attenuation cross section increases with decreasing gamma energy for almost all absorbers. If Pu is the actual plutonium content then the Pu_i values obtained from the three regions are related to it by:

$$Pu_i = Pu \cdot \exp(-\mu_i(Z) \cdot T), \qquad i = 100,200,400$$

where T is the effective absorber thickness and the $\mu_i(Z)$ are the absorption coefficients of the attenuating material Z at the three energies.

It can be shown that the material index number

$$Q(Z) = \frac{\mu_{100}(Z) - \mu_{200}(Z)}{\mu_{100}(Z) - \mu_{400}(Z)} = \frac{\ln(Pu_{100}) - \ln(Pu_{200})}{\ln(Pu_{100}) - \ln(Pu_{400})}$$

is characteristic for the absorbing medium and can be used for the identification of the attenuating material. The value of this parameter ranges from zero for no absorption to 0.19 for aluminium and 0.81 for lead. Once the medium is identified, the effective thickness can be calculated using the three Pu_i results and the true plutonium content can be derived.

Implementation of the above method in an actual measurement system, giving direct printout of the Pu content after attenuation correction is achieved by using an INTEL 8085 microprocessor. The system consists of a multichannel analyzer for recording the gamma spectrum from the sample. The counts in the three energy regions and the three corresponding background regions are accumulated in six 32 bit wide counters of the microprocessor system. Real time and life time clocks for dead-time correction are also implemented. The data acquisition is controlled by the start/stop switches of the analyzer and the processing of the data starts automatically after recognition of the end of the acquisition signal.

The microprocessor calculates the uncorrected Pu_i contents from the three energy regions and tests whether the three values are identical

within the error limits given by the counting statistics (using a chi-squared test) and the calibration-constant uncertainties. The three Pu_i values and their weighted mean value are printed out. If absorption within the sample is recognized the absorber material and its effective thickness are calculated according to the procedure described above and printed out together with the corrected Pu result. For cases of very strong absorption so as to cut the 100 keV signal completely or if gamma radiating contaminants are present in the sample the microprocessor will give an error printout.

The calibration constants and the attenuation coefficients are transferred to the computer via teletype and stored in a special battery-buffered memory. Thus power down events will not destroy the constants necessary for the calculation. At present the attenuation coefficients of four representative absorber materials (Perspex, Al, Fe and Pb) are stored in the microprocessor memory. In principle a larger number of media can be considered, but the four selected here should give a reasonable estimate for absorbers present in waste containers.

The upgraded version of the Pu waste monitor is in operation at the Bhabha Atomic Research Centre, Bombay, India, since January 1980.

References

(1) M.R. Iyer, P. Matussek, H. Ottmar, S.J. Choithramani, Report KfK 2504 (1977) p. 88

+Bhabha Atomic Research Centre, Bombay, India

5.2 NUCLEAR METHODS APPLIED TO TRACE ELEMENT ANALYSIS AND CRYSTAL PHYSICS

5.2.1 The Karlsruhe Proton Microbeam System*

D. Heck

Proton, deuteron or He-ion beams with energies up to 3.5 MeV are used to excite secondary radiations in target surfaces. Beam spot sizes down to ≤ 3 µm are generated by reduced imaging of two crossed narrow collimator slits onto the target by means of a magnetic quadrupole doublet. A deflection system with electric fields enables the scanning of the target surfaces. For multi-elemental analysis proton induced X-rays enable the detection of trace elements with $Z \geq 13$, while for the identification of light elements the emission of charged particles or gamma rays produced in nuclear reactions may be used. The application is demonstrated at an example.

*Beitr. elektronenmikroskop. Direktabb. Oberfl. 12/1 (1979) 259

5.2.2 Carbon Detection via the $^{12}C(d,p)$ Reaction with the Microbeam

H. Bletzer and D. Heck

For analysis of carbon the $^{12}C(d,p_o)$ reaction is known to be well suited with high sensitivity (1,2). The carbon concentration is determined by the number of protons generated in the (d,p_o) reaction and registered in a surface barrier detector. In our equipment we use a 450 mm^2 detector at 4.4 cm distance from the target in 130° position. It is covered with 15 µm aluminium foil to stop the scattered deuterons. By suitable choice of the deuteron energy (E_d = 1.44 MeV), the protons emitted from the interior of the sample can energetically be discriminated against those emitted from $^{12}C(d,p_o)$ at the surface and also from those emitted in the $^{16}O(d,p)$ reaction. To ensure that no interference from carbon surface contamination takes place, the samples are embedded in Wood's metal instead of epoxy resin. A cold trap inside the target chamber surrounding the sample keeps the partial pressure of carbon hydrates as low as possible.

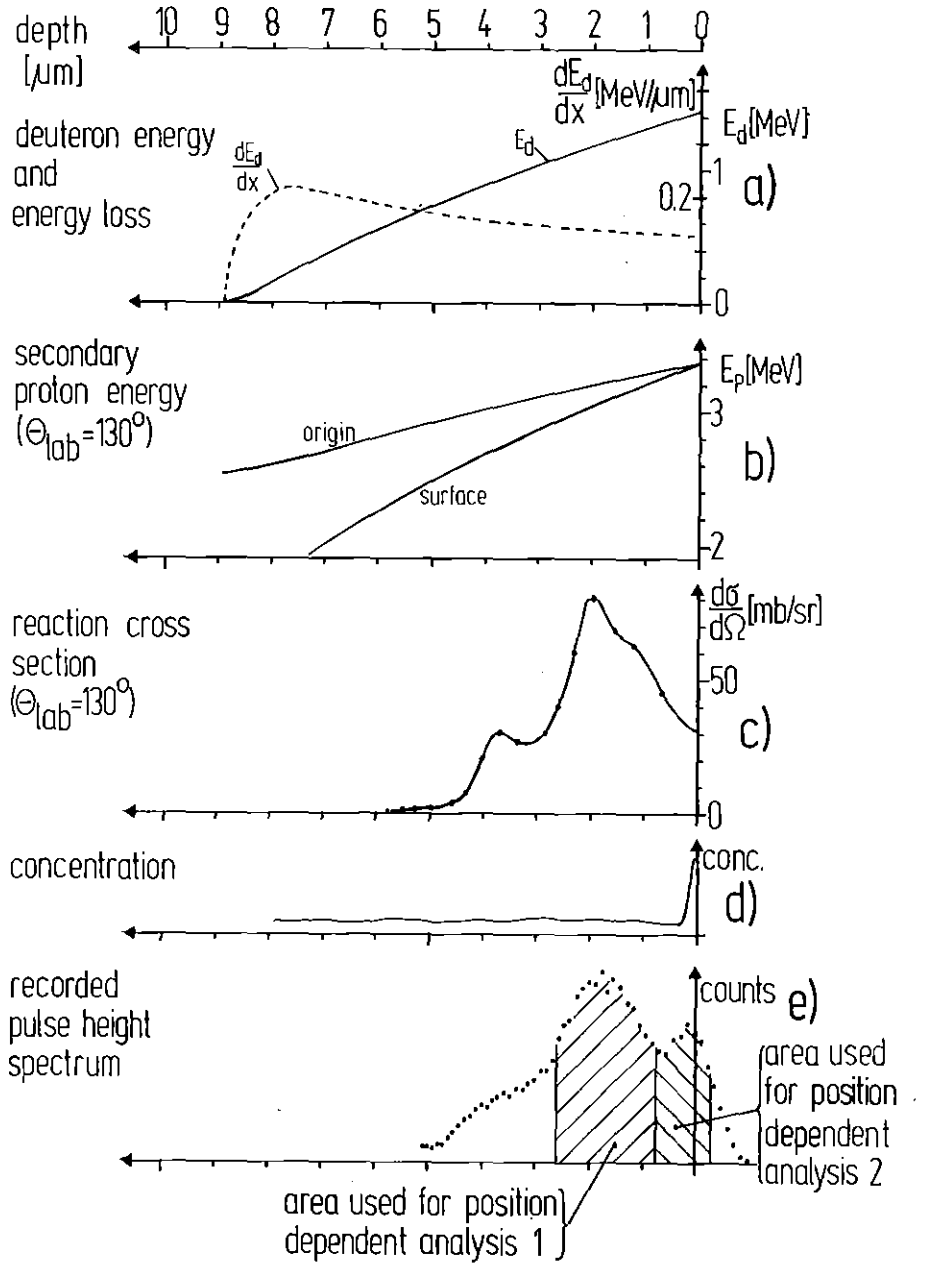

Fig. 1: Carbon detection with $^{12}C(d,p)$ reaction at E_d = 1.44 MeV.

In fig. 1 the dependence from the depth within a steel sample is shown for a) the deuteron energy and stopping power; b) the proton energy resulting from kinematics (130°) (ref. 3) without and with slowing down of the protons along the path through the sample towards the detector; c) the reaction cross section; d) a concentration profile, assuming contamination of the surface; e) the resulting pulse height spectrum, which is a folding of c) and d).

The two hatched areas in fig. 1 e indicate the proton groups coming from the interior of the target (1) and the target surface (2).

In a demonstration example an electron beam welded connection between two sheets (0.35 mm thick) of stainless steel has been analyzed for carbon concentrations. The topography of the cross section of the welding is shown in fig. 2, where the carbon concen-

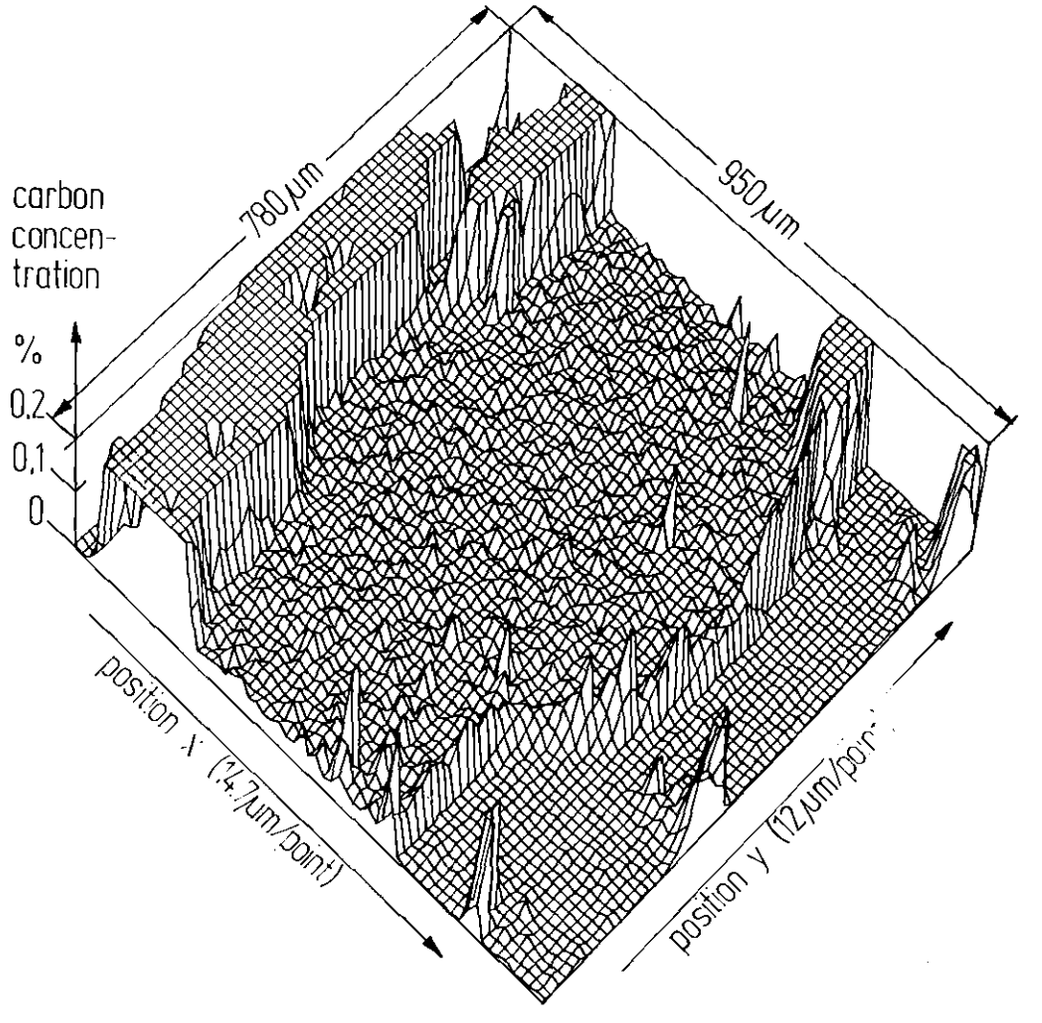

Fig. 2: Distribution of carbon across a welding connection of two stainless steel sheets.

tration (according to area 1 of fig. 1e) is plotted as a function of position. The middle part with a homogeneous concentration of $\sim$0.05 % represents the welding zone, from which the two sheets extend in $\pm$ y direction. The low carbon concentration in the region adjacent in x-direction represents

the embedding Wood's metal, while the high carbon concentration in negative x-direction results from a contamination with diamond powder used in the polishing procedure. Some high concentration spikes in the welding zone result from small diamond grains, pressed into the sample surface, which can be examined by visual inspection in a light microscope.

The distribution of protons from area 2, representing the carbon distribution at the surface, is shown in fig. 3. In comparison with fig. 2 the low carbon concentration on the steel surface is in contrast with the higher and irregular carbon contamination on the Wood's metal surface.

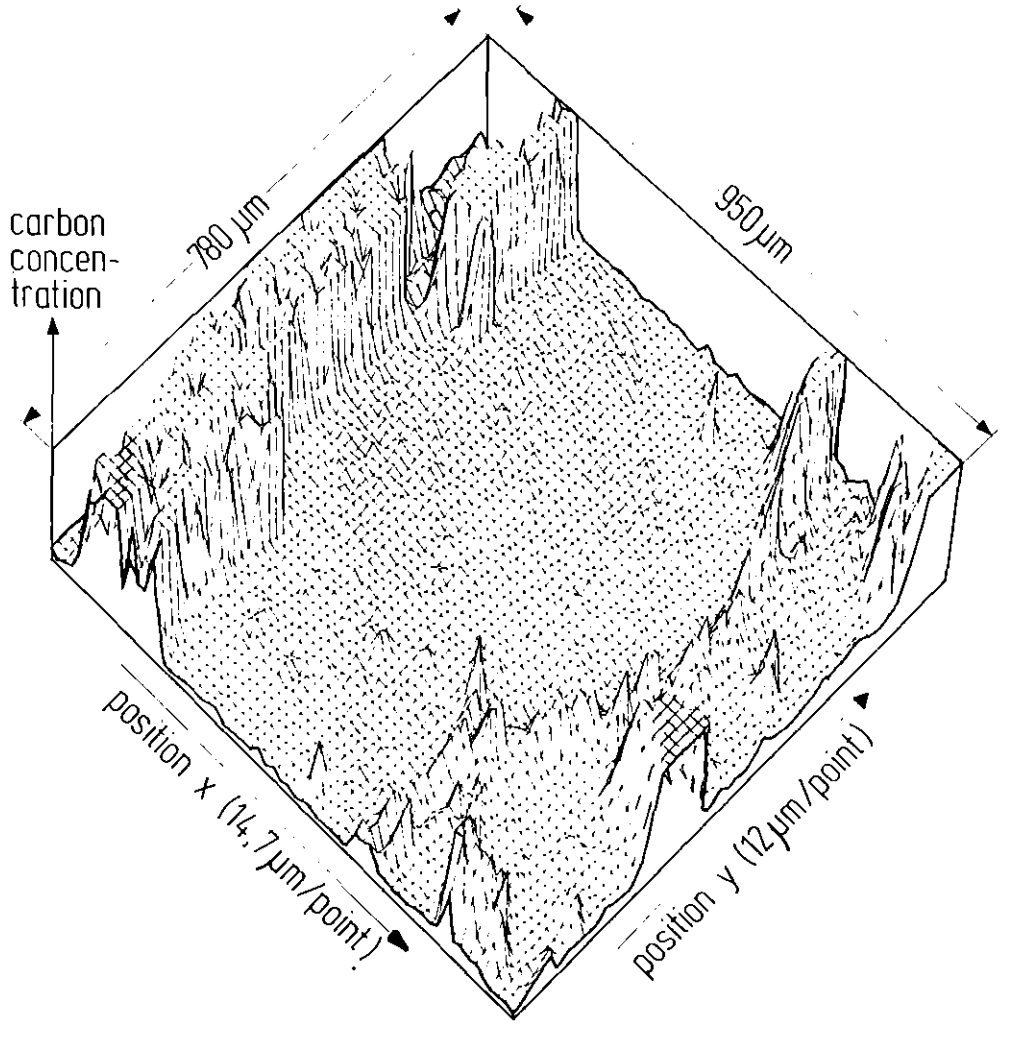

Fig. 3: Distribution of carbon on the surface of the sample of fig. 2.

In conclusion this demonstration sample shows, that with reasonable measuring times (10 sec/point) a sensitive carbon analysis can be performed with the (d,p_o) reaction with good discrimination capabilities against carbon surface contamination; interference with other (d,p) reactions is minimized by suitable choice of the deuteron energy.

References

(1) T.B. Pierce et al., Nucl. Instr. Meth. 118 (1974) 115

(2) F.C.W. Pummery and J.W. McMillan, Nucl. Instr. Meth. 168 (1980) 181

(3) L.C. Feldman and S.T. Picraux, in Ion Beam Handbook for Material Analysis, ed. J.W. Mayer and E. Rimini (Academic Press, New York, 1977) p. 231

5.2.3 The Influence of Secondary Fluorescence from Elements Adjacent to the Microbeam Spot on Local Concentration Determination with PIXE*

D. Heck

In position dependent PIXE analyses with microbeams secondary fluorescence may induce X-ray emission from elements in the micrometer-range vicinity of the beam focus spot. To study this effect in a simplified geometry, Cu/Au layer targets have been prepared. This material combination enables iterative electroplating for easy preparation of varying layer thickness with plane borders between the two materials and gives simultaneously sufficient secondary fluorescence. The proton beam spot of dimensions 6 μm x 0.75 μm is swept across the polished end face of the layer sandwich and the Cu and Au X-ray intensities are measured as a function of the distance x from the Cu-layer and of the proton energy E_p. For proton energies between 1 and 3 MeV the decrease of the copper K_α X-ray intensity outside the Cu-layer may be described by an exponential function

$$I = I_o \cdot c \cdot E_p \cdot \exp(-\alpha \cdot x)$$

with $\alpha = 0.255\ \mu m^{-1}$ and $c = 0.0272\ MeV^{-1}$.

*to be published in Nucl. Instr. Meth.

5.2.4 Implantation of ^{111}In Ions in Diamond Type Lattices for PAC Studies

H. Appel[+], J. Raudies[+], W.-G. Thies[+], B. Feurer, and A. Hanser

Electric hyperfine interaction is helpful in perhaps a unique way in determining the lattice sites taken up by implants in diamond. The quadrupole moment of a nucleus interacts with an inhomogeneous electric field in a low symmetry site of the crystal. Both the size and the symmetry axis of this electric field gradient (EFG) can be determined using the time dependent perturbed angular correlation technique (TDPAC).

Doping of diamonds can in general not be achieved by the commonly used technique of diffusion. The only way to embed foreign atoms into diamond is, as yet, by means of ion implantation.

^{111}In ions were implanted in <100> cleaved, type IIa diamonds. The radioisotope was produced via the ^{109}Ag(α,2n)^{111}In reaction at the Karlsruhe Isochronous Cyclotron. The implantations were carried out at the Karlsruhe electromagnetic isotope separator with an acceleration voltage of 60 kV. During the implantation the temperature of the diamond was 600°C. The total dose is estimated to approximately $3 \cdot 10^{13}$ ions cm^{-2}. The implanted samples were annealed for 30 min at 1350 $\pm$ 50°C in an evacuated quartz ampoule at $\lesssim 10^{-6}$ Torr. The measurements were carried out at room temperature.

The observed angular correlation can be parametrized as follows (see, e.g. Alder et al. (1)):

$$R(t) = a_o + \sum_{n=1}^{3} e^{-(n\delta t)^2/2} a_n \cos(n\omega_o t)$$

The time independent rate a_o and the relative amplitudes a_n of the three frequencies depend on the orientation of the EFG axis with respect to the γ-ray detectors. They can be calculated. The damping factor δ takes into account that the field gradient is in general not sharp. It is assumed to be smeared out following approximately a Gaussian distribution.

Data were taken for four different orientations of the sample with respect to the γ_1-detector as shown in fig. 1. The solid lines are

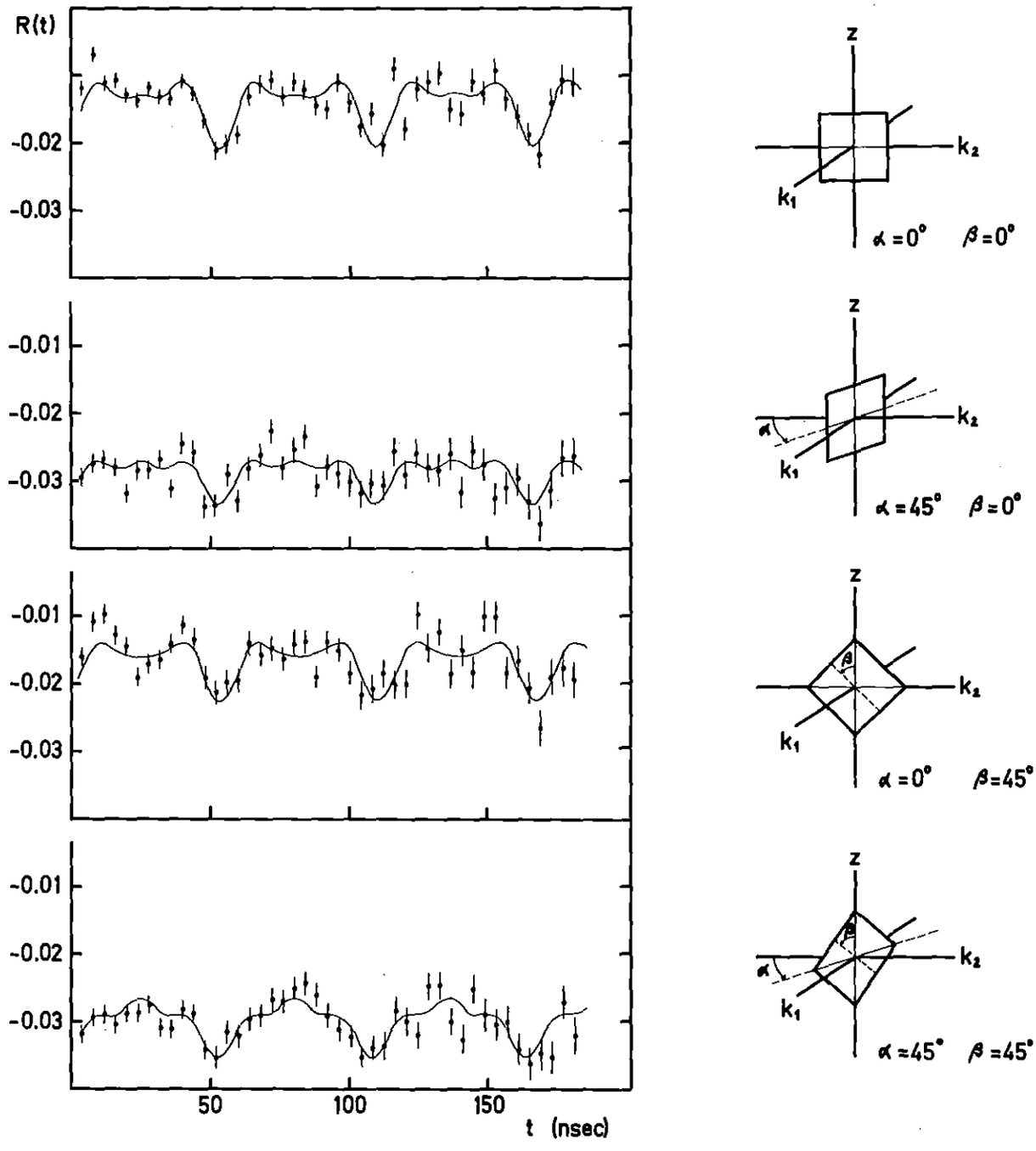

Fig. 1: R(t) measured for four different orientations of the sample with respect to the detector axes. The solid line is a fit according to Eq. (1) assuming axial symmetry of the field gradients along <111> directions.

computed fits according to Eq. (1) with fixed relative amplitudes for the a_n characteristic for each geometry. The best fit is achieved if one

assumes a symmetry axis of the EFG along the <111> direction of the crystal.

We conclude from the results that only a small fraction of 5.3 ± 0.3 % of the implanted ^{111}In ions occupy unique lattice sites along <111> directions where they experience an EFG of 6×10^{17} V cm^{-2}, corresponding to a quadrupole frequency $\nu_Q = (117.8 \pm 0.6) \times 10^6$ s^{-1}. A large fraction of the ions has obviously gone to a variety of interstitial sites, where they experience a broad spectrum of field gradients. Their contribution to the modulation pattern is smeared out towards a constant background.

The experiment is still in progress and further studies are planned in particular to explore the temperature dependence of the EFG in diamond.

Reference

(1) K. Alder et al., Helv. Phys. Acta 26 (1953) 761

+Institut für Experimentelle Kernphysik der Universität und Institut für Genetik und für Toxikologie von Spaltstoffen des Kernforschungszentrums Karlsruhe

6. TECHNICAL DEVELOPMENT

6.1 CYCLOTRONS

6.1.1 Operation Summary of the Karlsruhe Isochronous Cyclotron

F. Schulz and H. Schweickert

During the period of publication of this report the machine has been in full operation (see Table 1). The total available beam time for experiments of 7203 h for this year is practically the same number as for last year (1). This number could only be achieved by reducing the time devoted for testing new components and beam development because we needed, as reported last year, a planned shut down of 3

CYCLOTRON OPERATIONAL	WITH INTERNAL ION SOURCES		WITH EXTERNAL ION SOURCES		TOTAL	
FOR EXPERIMENTS	5865 H	80.5 %	784 H*	83.6 %	6649 H	80.8 %
BEAM DEVELOPMENT, TESTING NEW COMPONENTS, DEVELOPMENTS FOR ISOTOPE PRODUCTION	534 H	7.3 %	20 H	2.1 %	554 H	6.7 %
TOTAL TIME OF OPERATION WITH THE BEAM ON TARGETS	6399 H	87.8 %	804 H	85.7 %	7203 H	87.5 %
SCHEDULED SHUT-DOWN FOR MAINTENANCE, REPAIR AND INSTALLATION	306 H	4.2 %	11 H	1.2 %	317 H	3.9 %
UNSCHEDULED SHUT-DOWN	582 H	8.0 %	123 H	13.1 %	705 H	8.6 %
TOTAL SHIFT TIME	7287 H	100 %	938 H	100 %	8225 H**	100 %

* POLARIZED DEUTERONS 202 H
$^{6}Li^{3+}$-ION (156 MeV) 582 H

** THE REAL TIME OF 8784 H IS ACHIEVED BY ADDING A TOTAL OF 9 DAYS SHUT DOWNS 23.12.90-2.1.80; 14 DAYS IN JANUARY/FEBRUARY 80

Table 1: Statistics of the cyclotron from July 1979 to June 1980.

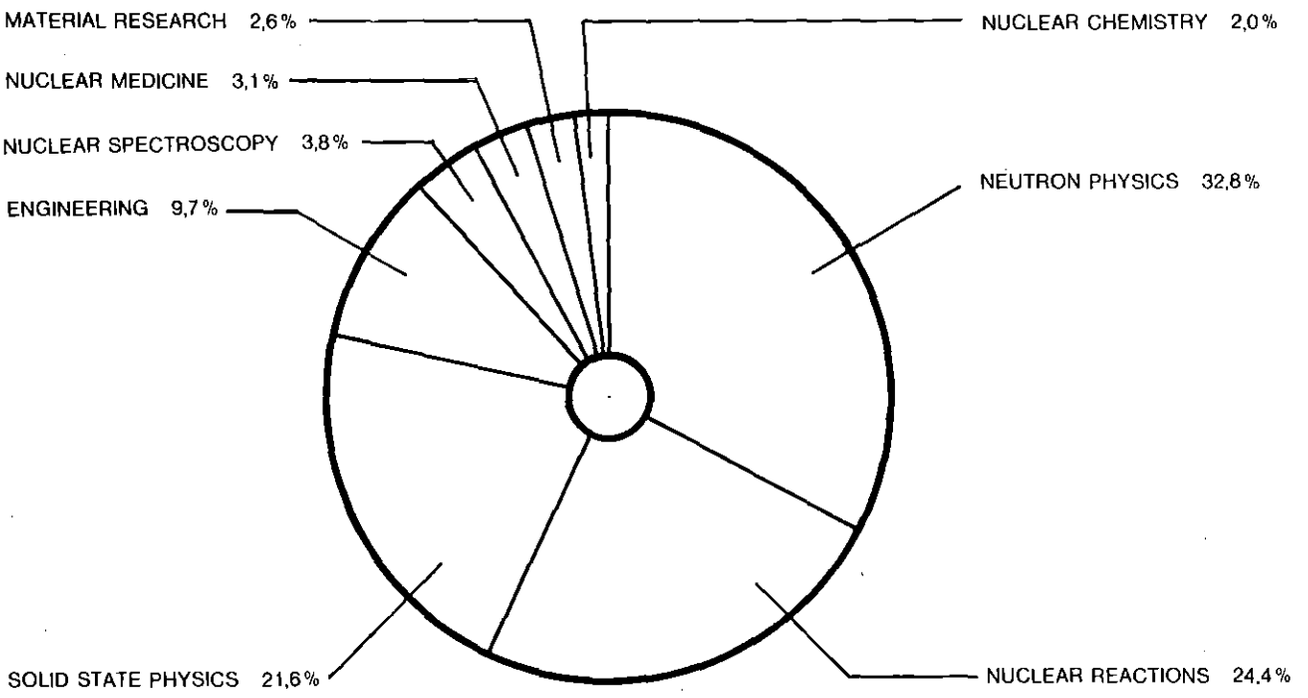

KFK-KARLSRUHE USERS

INSTITUT FÜR KERNPHYSIK	2211 h	33,3%
INSTITUT FÜR ANGEWANDTE KERNPHYSIK	1406 h	21,2%
INSTITUT FÜR TECHNISCHE PHYSIK	22 h	0,3%
LABOR FÜR ISOTOPENTECHNIK	17 h	0,2%
INSTITUT FÜR RADIOCHEMIE	15 h	0,2%
INSTITUT FÜR HEISSE CHEMIE	9 h	0,1%
TECHNOLOGIE TRANSFER	2 h	0,1%
	3682 h	55,4%

EXTERNAL USERS

MAX PLANCK INSTITUT FÜR KERNPHYSIK HEIDELBERG	600 h	9,1%
FREIE UNIVERSITÄT BERLIN	546 h	8,2%
UNIVERSITÄT MÜNSTER	516 h	7,7%
UNIVERSITÄT ERLANGEN	468 h	7,0%
UNIVERSITÄT ULM	178 h	2,7%
UNIVERSITÄT STUTTGART	140 h	2,1%
TECHNISCHE UNIVERSITÄT MÜNCHEN	128 h	1,9%
TECHNISCHE HOCHSCHULE DARMSTADT	59 h	0,9%
KERNFORSCHUNGSANLAGE JÜLICH	48 h	0,7%
UNIVERSITÄT BONN	32 h	0,5%
UNIVERSITÄT KONSTANZ	27 h	0,4%
DEUTSCHES KREBSFORSCHUNGSZENTRUM HEIDELBERG	16 h	0,2%
UNIVERSITÄT HAMBURG	8 h	0,1%
UNIVERSITÄT MAINZ	4 h	0,1%
UNIVERSITÄT LEIDEN	4 h	0,1%
	2774 h	41,7%
COMMERCIAL IODINE-123 PRODUCTION	192 h	2,9%
	6648 h	100%

Table 2: User statistics from July 1979 to June 1980 and the distribution of the 6648 h experimental time on the different fields of activity.

weeks in order to exchange too heavily corroded inner conductors of our dee system (see fig. 1). Meanwhile the replacement program for the cyclotron cooling plant and the exhaust system has also been completed.

The user statistics shows, that about 60 % of the beam time is devoted to three institutes of the Karlsruhe research center, the other 40 % being allocated to a large number of groups, mainly from different universities. The pie-diagram shows that the main activities are in the fields of neutron-physics, nuclear reactions and solid state physics. The highest growth rates have been found for both engineering (activation of engine parts) and isotope production (1).

Fig. 1: Pictures taken during the shut down from 22.1.80 to 8.2.80. The inner aluminium conductors of the dee system were replaced by copper plates. The soldering of the cooling vanes on to these plates as well as the complete installation was performed by our operators.

Reference

(1) F. Schulz and H. Schweickert, Report KfK 2868 (1979) 86

6.1.2 New Developments at the Cyclotron

H. Schweickert

As shown in the preceding contribution there is a high demand of beam time for applications, which are commercial in nature. On the other hand, because of some special facilities (large neutron time of flight spectrometer, $^{6}Li^{3+}$-ions and polarized deuterons) we found also an increasing interest in the machine for basic nuclear physics experiments and we are in the process of expanding the equipment which specially serves basic nuclear physics experiments (see fig. 1), with:

- A new experimental area for neutron physics with polarized neutrons. The charged particle beam is bent behind the neutron producing target to a beam dump in order to measure the neutrons in forward direction. This arrangement is planned to be operating at the end of 1980.
- The building-up of an ECR-source to accelerate all the light ions at least up to oxygen to energies of 26 MeV/nucleon (see contribution 6.1.6).
- In order to exploit these new ion beams efficiently a small spectrometer is being built, which will be available in 1981 (see contributions 6.2).

When these new possibilities are fully available we expect running into serious problems with the availability of beam time, which is why we have bought a so called "compact cyclotron". This machine will take over all the industrial applications in mid-1982.

The compact cyclotron will be a CP-42 from the Cyclotron Corporation (TCC). There have been two main reasons for choosing such a machine:

1. The possibility of a high external beam current (200 μA guaranteed) by stripping extraction of H^-.
2. The possibility of extracting two beams simultaneously.

The machine will be operated from the same control room and by the same operators in parallel to the "old" machine (see contribution 6.1.5).

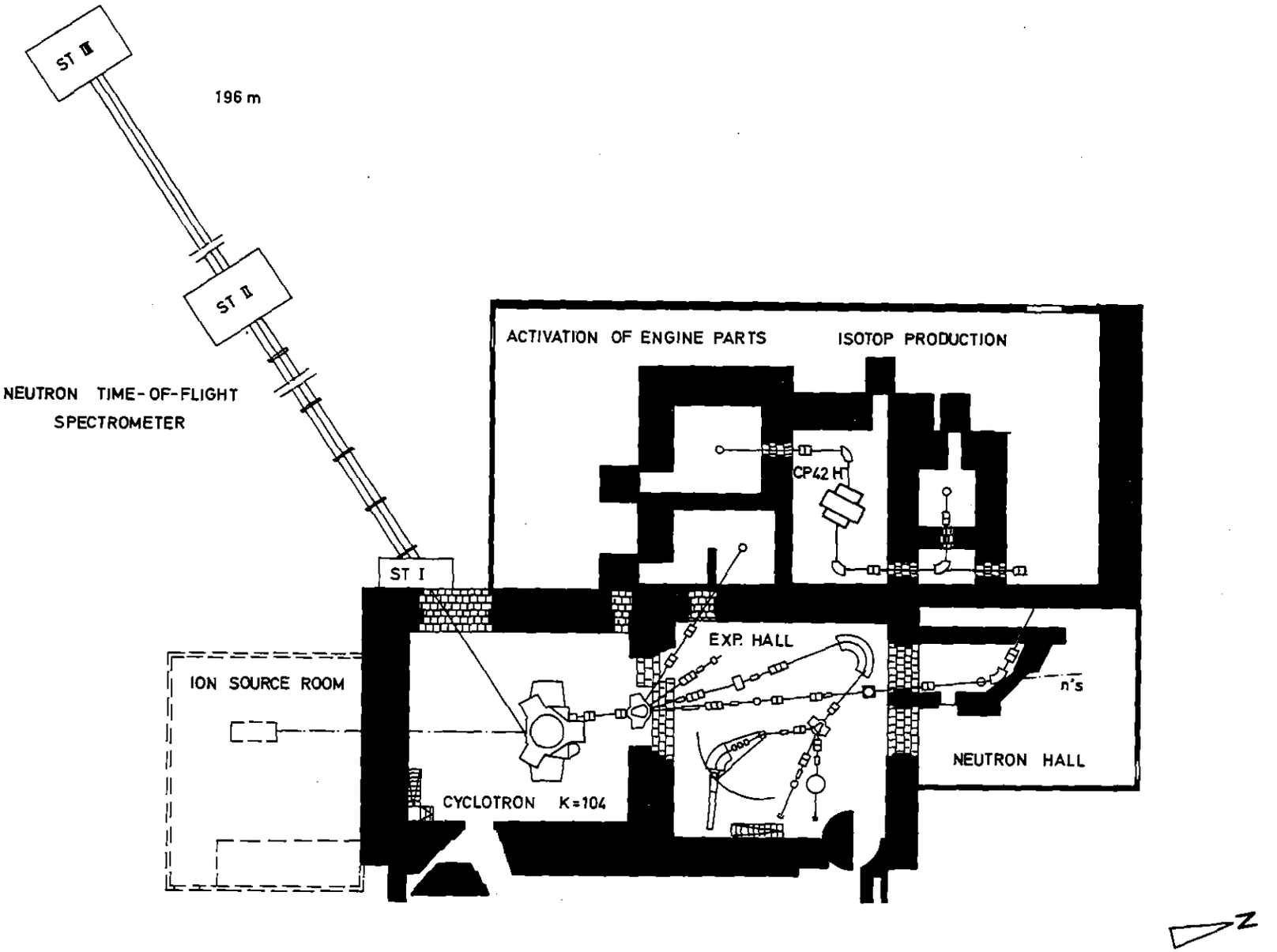

Fig. 1: Plan view of the Karlsruhe facility showing the developments in the next two years.

6.1.3 Status of the Computer Diagnostics and Control for the Karlsruhe Cyclotron

H. Heinzmann, W. Kappel, W. Kneis, B. Kögel,
G. Leinweber[+], and J. Möllenbeck

The dual computer system (1) for diagnostics and control of the cyclotron now consists of two NOVA 3/12s from DATA General with 256 k-Bytes memory. The second NOVA 3 replaces the NOVA 2/10 of the former system. This replacement has increased the reliability of the whole system because we now have two identical computers.

The diagnostic system CICERO (2) consists of many programs written in the programming language BASIC. This language is in use for reorganisation and modification of existing programs only. For development of new programs the language FORTRAN is used.

To simulate the attitude of an ion-beam within a beam-guiding system some new programs have been developed, which can now be used during beam set up (3).

The unreliable power supplies for the correction coils have been replaced by new ones which are controlled by the computer via CAMAC (3). To control these power supplies a program has been developed, which can now control, via a special control panel, the following parameters:

- sum currents
- first harmonics in magnitude and angle keeping the sum currents stable.

In addition the computer can now:

- control the temperature of a given coil by measuring its impedance
- recall a former set of parameters making the change over from one particle to another much faster.

We are now on the way to writing programs for the optimization of the phase history and the extraction rate as a function of correction coil current.

For the activation of machine parts a program has been developed, which supervises the whole process including beam current and position. Figure 1 shows a typical display picture for the operators.

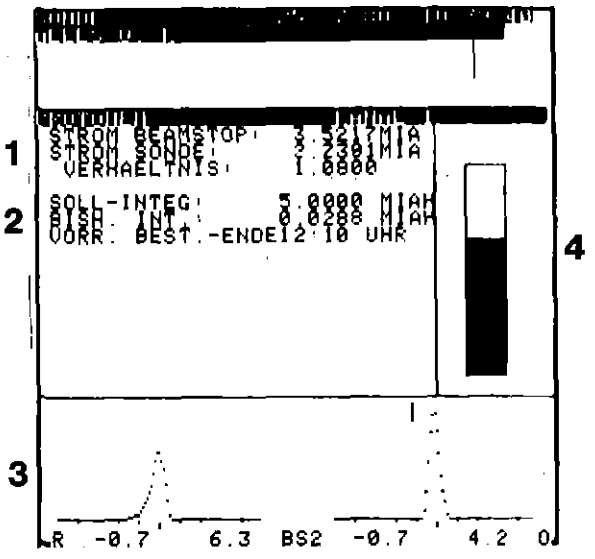

Fig. 1: Display picture during the process of activation of engine parts. Region 1 shows the last result of the calibration of the capacitive beam current probe (updated every 10 min). Region 2 gives actual and desired beam current integral in µAh. Region 3 displays the actual position of the beam in front of the target. The left number gives the position relative to the axis in mm, the right number the full width half maximum in mm. Region 4 informs the operators about the beam current.

References

(1) H. Heinzmann, W. Kappel, W. Kneis, B. Kögel, Ch. Lehmann, J. Möllenbeck, H. Schweickert, Report KfK 2686 (1978) 95

(2) W. Kappel, W. Kneis, B. Kögel, Ch. Lehmann, G. Leinweber, J. Möllenbeck, W. Segnitz, H. Schweickert, Proc of the 8th Int. Conf. on Cyclotrons and their Applications, Bloomington, USA, Sept. 1978

(3) G. Leinweber, Diplom-Arbeit (1980)

+Institut für Angewandte Informatik und Formale Beschreibungsverfahren, Universität Karlsruhe, Germany

6.1.4 Computer Controlled Beam Diagnostics and Beam Optimization at the Karlsruhe Isochronous Cyclotron*

W. Kneis

The computer-controlled diagnostic- and monitoring-system at the Karlsruhe Isochronous Cyclotron is described and discussed. The main emphasis is on the automatic beam optimization.

For the external beam guiding system of the Karlsruhe Isochronous Cyclotron two independent procedures for the automatic beam optimization were developed. As basis for these procedures the theoretical knowledge from beam transport calculations and the methods of mathematical parameter optimization with many variables were used. It is very easy to apply both procedures to other external beam guiding systems. The methods of parameter optimization used are formulated in a way not specific to the problem, so that they can be applied also to other problems like optimization of the extraction. The automatic optimization of the external beam can be performed either by using beam transport calculations (theoretical optimization) or by using the particle beam itself (experimental optimization).

*Report KfK 2835 (1979)

6.1.5 Lay-Out of the Computer Control for the CP-42 Compact Cyclotron

J. Bialy, H. Heinzmann, W. Kneis, B. Kögel, J. Peters

The CP-42 will be operated from the same control room and by the same operators as the "old" Karlsruhe Isochronous Cyclotron. The CP-42 will be delivered with a control system consisting of a LSI11 and an unibus extension system. In order to be compatible as far as possible with the "old" machine, which has in fact a rather modern control system, we have decided to use "CAMAC" for the beam guiding system and the beam diagnostics. To combine both systems, the following hardware configurations for the computer system were chosen:

The computer system consists of two identical NOVA 4-Computers from DATA GENERAL with identical peripherals, part of which is used by both CPUs (Fig. 1).

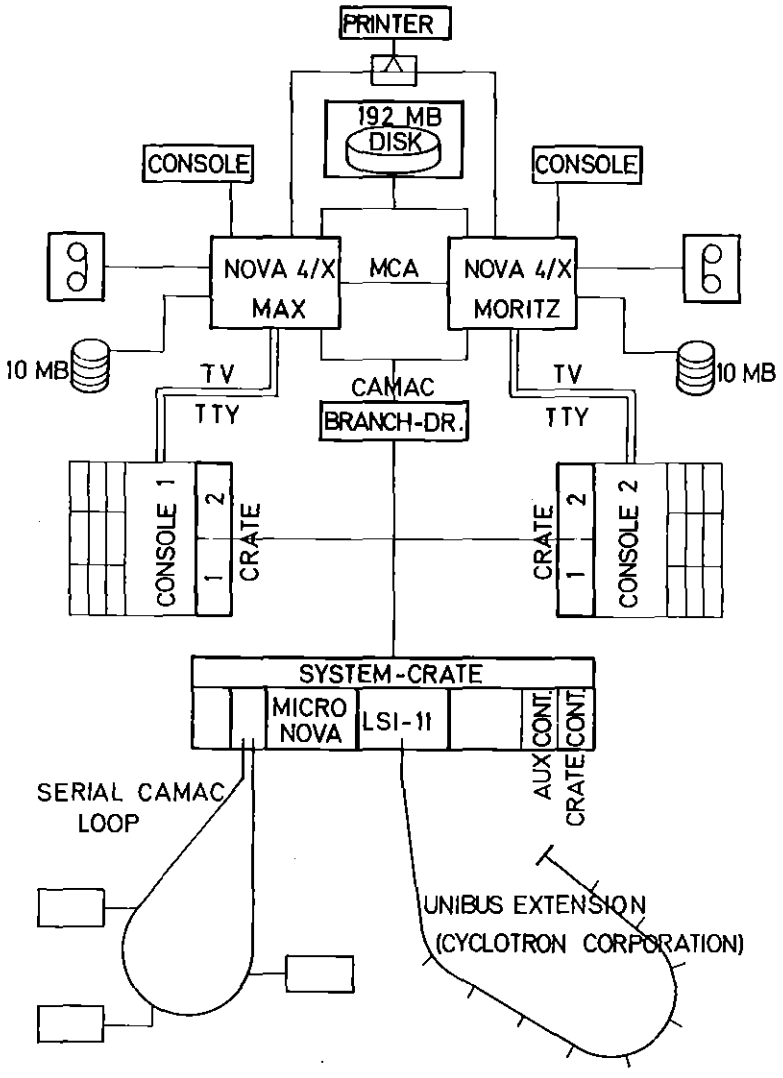

Fig. 1: Control system of the Compact Cyclotron.

The control consoles may be connected to both computers, but only alternatively.
The parameter handling of the Compact Cyclotron is performed with a LSI11 delivered by the Cyclotron Corporation. LSI11 and NOVA4 are coupled via a mailbox memory in a Camac crate. Parameters of the External Beam Guiding System are controlled via a Serial Camac Loop. In future this Serial Camac Loop shall be controlled by a second LSI11 in the System Crate.

The Compact Cyclotron is operated from an operator's console (Fig. 2). There are no control knobs as for the present machine, but only touch-panel controls.

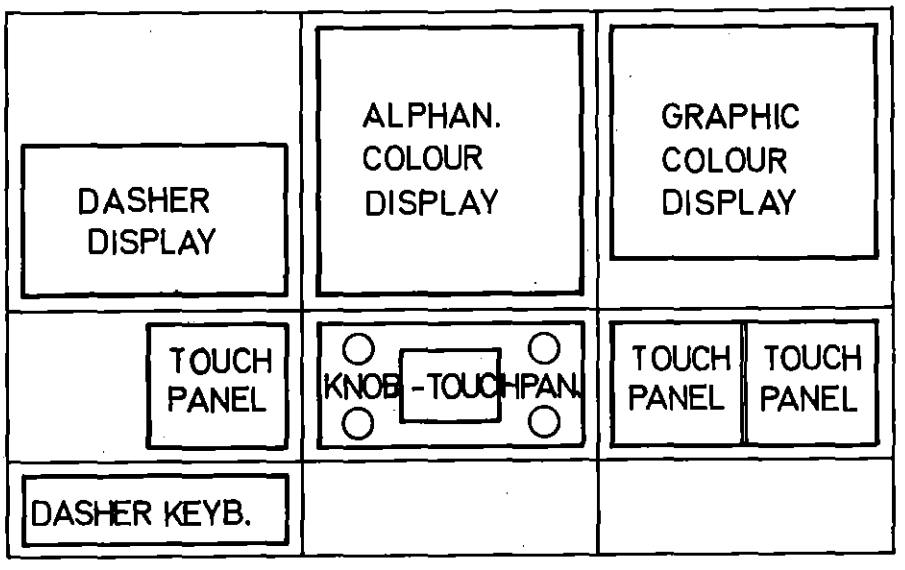

Fig. 2: Lay-out of the operator's console.

The software configuration consists mainly of an Operating System (OS). The task of the Operating System is to supervise, to control and to perform beam diagnostics. All alarms, parameters and process conditions will be reported to the OS. The supervision will be implemented as a two-level-supervision. On the first level a message is given to the operator if specified limits are violated. On the second level the computer automatically starts an adjustment program to correct the parameters out of range. If this does not succeed the operator is informed. The start of the adjustment program is also announced to the operator.
The Compact Cyclotron will be controlled exclusively by the Operating System. There is no separate manual control. Manual control is done by changing the operating conditions with series of single actions which means each switch, valve etc. must be attachable from the Operating System.

Automatic Control means to combine these single actions to so-called procedures. Examples of such procedures are turning on the vacuum system or activating the HF system. The coupling of these procedures yields automatic procedures such as setting the cyclotron in the operating state etc.

The status of this project is as follows: The whole hardware has been delivered in June 1980 and will be put together by the end of 1980. A first version of the operating system is expected to be available at the end of 1981.

6.1.6 HISKA Status Report

V. Bechtold, H.P. Ehret, L. Friedrich,
H. Schweickert, L. Wiss, P. Ziegler

A preliminary design of the ECR type ion source for fully stripped light ions has been described in (1). The main components of this source have been ordered. For the second stage the two superconducting coils and the 7.5 GHz/5 kW transmitter will be delivered at the end of this year. The permanent hexapole is under construction. The first stage 14.5 GHz/1 kW transmitter is used for ECR experiments. So it will be possible to assemble the source in 1981 if the building for all external ion sources of the cyclotron will be ready.

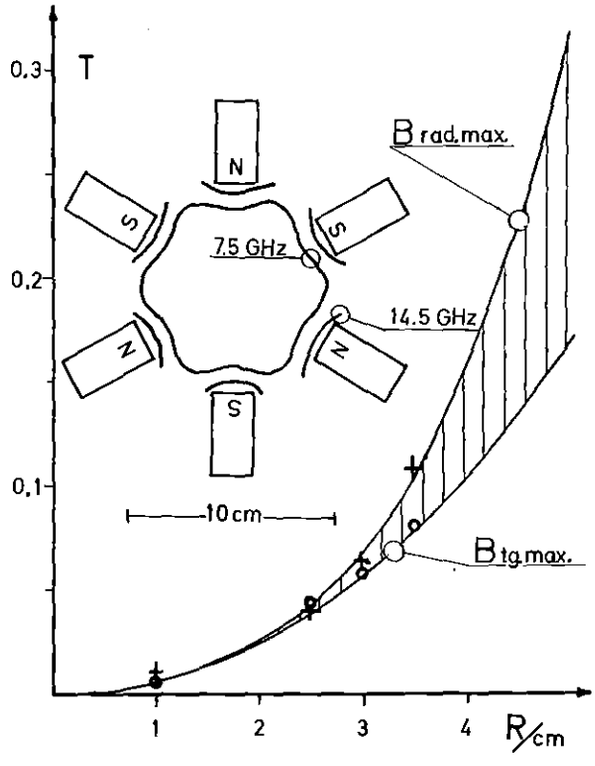

Fig. 1:
The calculated cross-sections of the 7.5 GHz and 14.5 GHz ECR-surfaces in the midplane of the permanent hexapole magnet and measurements of the radial dependence of the magnetic field are shown. Because of the high transparency of the hexapole magnet the field strength is no more constant on a certain radius but covers the range between B rad max and B tg. max.

To demonstrate acceleration of N^{7+} by the Karlsruhe cyclotron earlier and to have a test facility the small source p-HISKA (2) was completed. First experiments were started, operating the 2^{nd} stage with the 14.5 GHz transmitter (corresponding magnetic field 5.2 kG). In this case the ECR-surface is not closed inside the hexapole as it is for the 7.5 GHz resonance (corresponding magnet field 2.6 kG), fig. 1.

In spite of this unfavourable condition N^{5+} ions could be extracted.

An ECR-source using the high magnetic field inside the central bore of an axially magnetized disk of $SmCo_5$ has been developed (fig. 2).

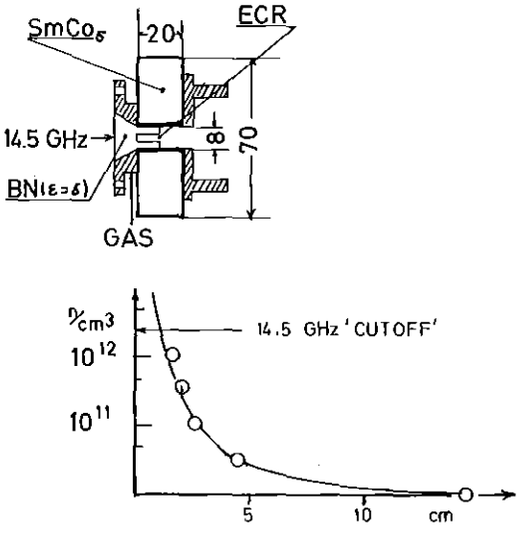

Fig. 2:
The longitudinal cross section of the first stage shows a ringmagnet with a central bore of 10 mm. In the middle of this bore an ECR plasma is produced by 14.5 GHz microwaves, which are guided into by boron-nitride. The electron density n/cm^3 was measured along the middle axis. In the ECR zone the cutoff density is achieved.

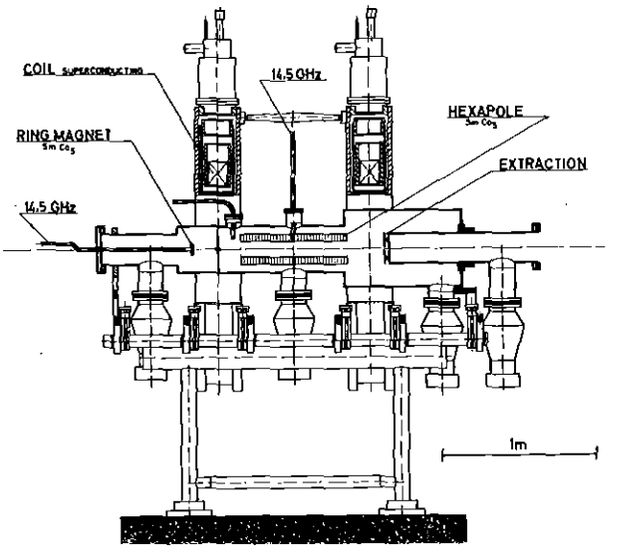

Fig. 3:
HISKA, present state of design. The first stage consist of a ring magnet made of $SmCo_5$ and a differential pumping system. The second stage is built-up with two superconducting coils and a 70 cm long permanent hexapole inserted into the vacuum chamber. The source is pumped with special diffusion pumps and can be operated at 10 kV.

This first stage and a shorter hexapole magnet of only 70 cm length enables a more compact design of the ion source HISKA (fig. 3). No more water cooled coils are used and pumping is done by special diffusion pumps with negligeable oil backstreaming.

References

(1) V. Bechtold et al., KfK Report 2868 p. 92 (1979)
(2) V. Bechtold et al., KfK Report 2868 p. 94 (1979)

6.1.7 E.C.R. Ion Source for Multiply Charged Oxygen Beams*

V. Bechtold, N. Chang-Tung[+], S. Dousson[+], R. Geller[+], B. Jacquot[+], Y. Jongen[++]

A miniaturized two stage ECR ion source (called Micromafios) is described. The ion source is based on the principle of the Electron Cyclotron Resonance (E.C.R.) and delivers completely stripped oxygen ions. This source is a small scale Supermafios (1). The hexapole of 30 cm in length is made up of permanent samarium cobalt magnets. 100 nA fully stripped oxygen ions could be extracted at 7 keV.

Reference

(1) R. Geller, I.E.E.E. Trans. Nucl. Sci., N.S.26, No. 3 (1979) p. 2120

*Nucl. Instr. Meth., in print

[+] Centre d'Etudes Nucléaires, Grenoble (France)

[++] Université Catholique, Louvain la Neuve (Belgium)

6.1.8 Status of ^{81}Rb Production at the Karlsruhe Cyclotron

N. Kernert[+], T.W. Peters, S.A. Sheikh, and H. Schweickert

Several nuclear physics laboratories have developed ^{81}Rb-^{81m}Kr generator systems over the last few years due to the growing interest in ^{81m}Kr for nuclear medicine, especially lung ventitation studies (1-3). This is principally because its γ-transition energy of 190.3 keV is well-suited for most medical cameras and collimators, and also because its short half life of 13 s enables the use of high activities (hence high count rates) while at the same time minimising the patient-radiation dose. Additionally there is the possibility of continuous use of the generator as the time between total elution of ^{81m}Kr and growth of maximum activity in the generator is only 2.28 min.

At the Karlsruhe Cyclotron ^{81}Rb is produced via the reaction ^{nat}Kr(d,xn)^{81}Rb using the Kr-gas target described by N. Kernert (5). After irradiation the target is rinsed with distilled water to extract

the Rb-isotope activities condensed on the inner walls during irradiation. By this procedure more than 90 % of the ^{81}Rb produced can be extracted (4). This distilled water containing the Rb-isotope activities is then purged through the required number of cation-exchanger generators simultaneously, which retain all the activities. At present there is provision for the simultaneous loading of upto six generators per irradiation. Fig. 1 shows the flow diagram of the whole production process.

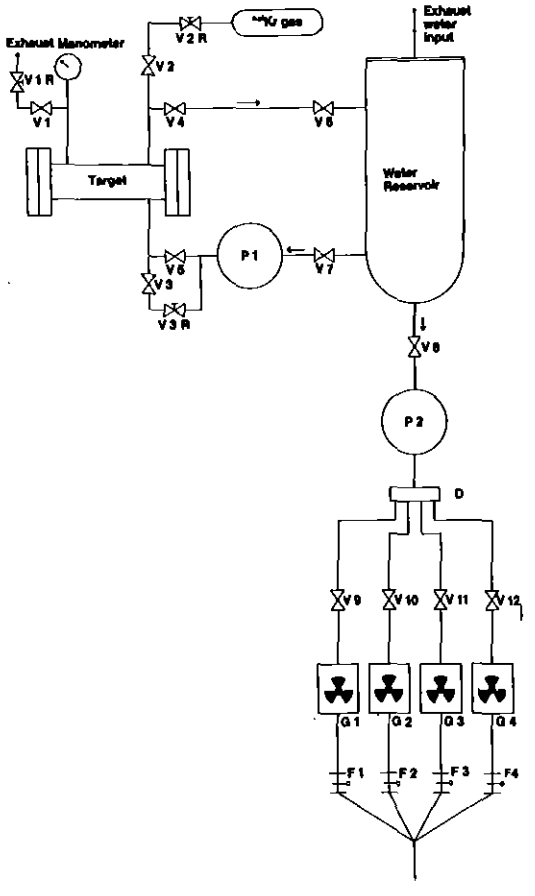

Fig. 1:
Flow diagram of the ^{81}Rb-^{81m}Kr generator production process

V1-V12	Valves
V1R-V3R	regulation valves
P1-P2	pumps
G1-G4	generator columns
F1-F4	flow meters

The cation-exchange material, the generator and shielding/container have all been carefully chosen. The best results have been obtained with a commercially available system - MINITEC, produced by Squibb & Sons, Munich - originally designed for use with ^{99m}Tc. The cation-exchange material is Dowex 50 W x 80 (200-400 mesh), which is densely packed in a plastic generator column (fig. 2).

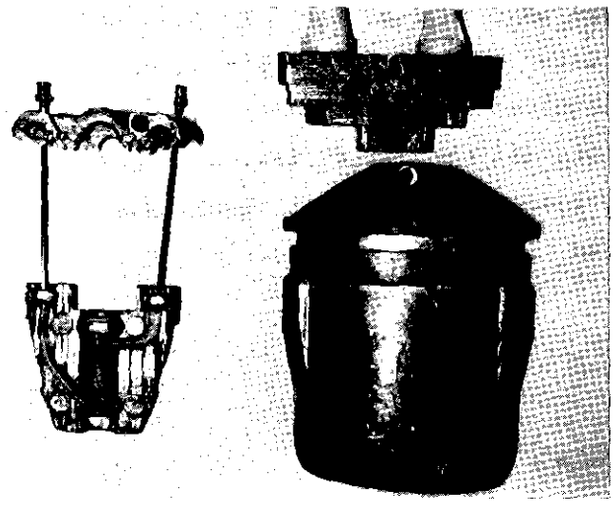

Fig. 2: Photo of the exchange column and the shielding container.

The Dowex layer itself is about 20 mm high and has been found to absorb about 99 % of the Rb activities for flow rates of upto 25 ml/min. While in use the generator column is placed upright in the lead container as shown in fig. 2. The connections to and from the generator for the loading and elution of ^{81}Rb and ^{81m}Kr, respectively, are normal medical infusion needles to ensure compatibility and easy handling during routine clinical use.

The elution of the ^{81m}Kr from the decay of ^{81}Rb in the generator column is simply carried out by blowing normal humidified air through it. The optimum pressure is of the order of a few hundred millibars.

Before the start of routine production of ^{81}Rb medical tests have as yet to be carried along with the completion of the automatic production system.

References

(1) J.F. Lamb, G.A. Baker, A. Khentigan, H.A. Moore, W.C. Neesan, and H.S. Winchell, J. nucl. med. 18 (1979) 609

(2) T.J. Ruth, R.M. Lamprecht, A.P. Wolf, and M.L. Thakur, Int. J. of Appl. Rad. & Isot., 31 (1980) 51

(3) J.H. Fremlin, K. Stammers, and F.R. Stewart, Nucl. Instr. & Meth. 156 (1978) 369

(4) G. Bauer, N. Kernert, Ch. Rämer, and H. Schweickert, KfK-report No. 2868 (1978) p. 99

(5) N. Kernert, Diplomarbeit (1980)

+Universität Karlsruhe

6.1.9 Status of the Iodine-123 Production at the Karlsruhe Isochronous Cyclotron

K.H. Assmus, W. Maier, F. Schulz, H. Schweickert

During the period of report the production of iodine-123 via the (p,2n)-reaction (1) has been used routinely to prepare 411 batches with a total of 20.3 Ci of iodine-123 for application at 7 hospitals:

Nuklearmedizin. Abtl. der Universitätsklinik Freiburg
Deutsches Krebsforschungszentrum Heidelberg, Nuklearmed. Institut
Nuklearmedizin. Abtl. der Universitätsklinik Homburg/Saar
St. Vincentius-Krankenhäuser Karlsruhe
Institut für Nuklearmedizin der Universität Köln
Nuklearmedizin. Klinik der Techn. Universität München
Städtische Krankenhäuser Saarbrücken

Following wishes of the hospitals the production frequency has now been increased to three times a week (Tuesday, Wednesday, Thursday always from 0.00 to 3.00 a.m.). Again the production could be performed with a high reliability as only 3.2 % of the scheduled deliveries were not in time.

The main improvement in the production process was in May 1980 when a new hot cell arrangement was put in operation (Fig. 1). This led to a drastic reduction in the dose of our operators for this production process to below 0.5 mrem and because of the automated mode of procedure to a higher reproducibility in the extraction process.

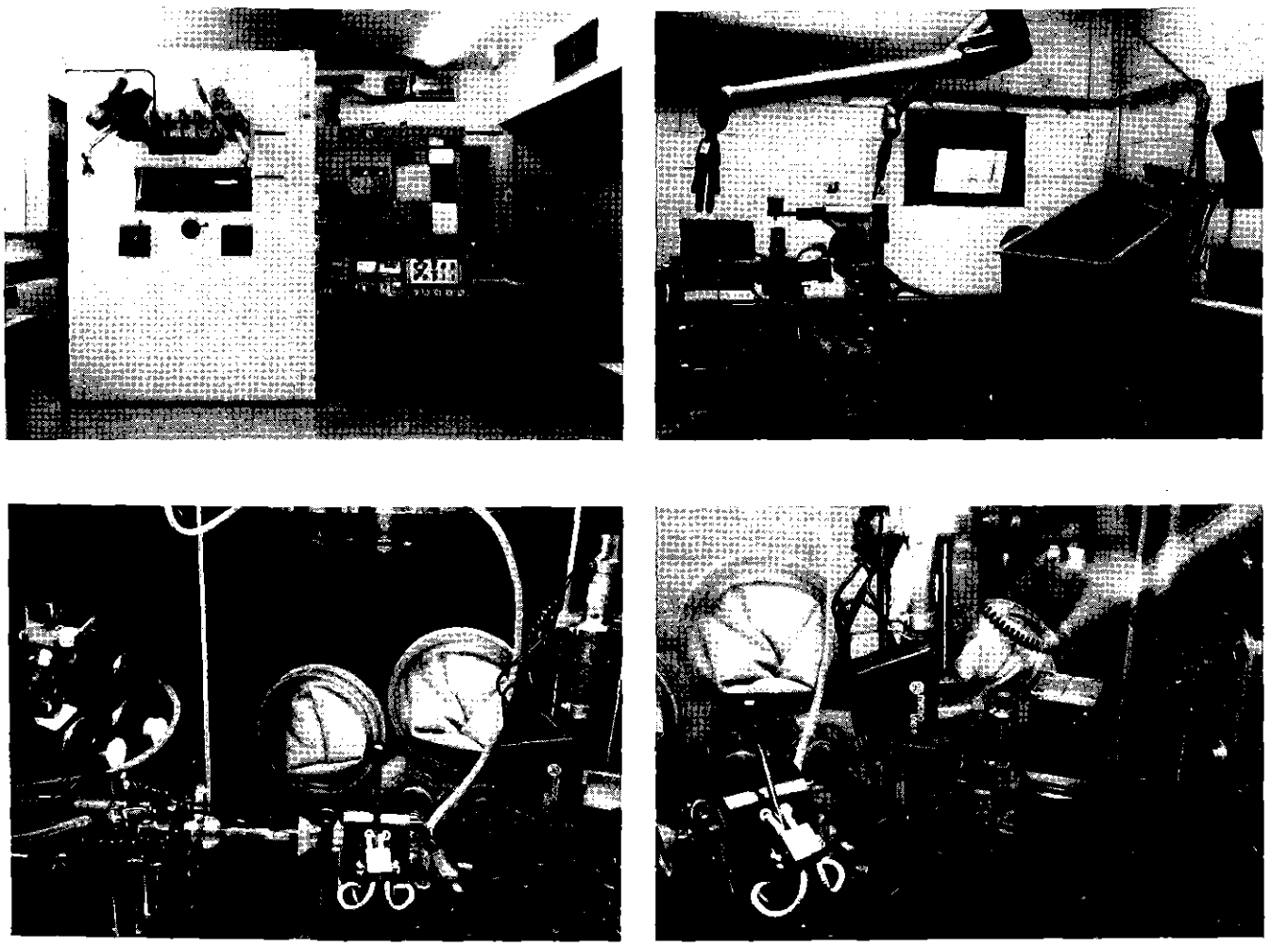

Fig. 1: New hot cell arrangement for the iodone-123 production.
Upper row left side: General view of the arrangement. The irradiated targets are transferred via a target railway to the left cell where they are dismounted by a special handling equipment. Subsequently only the TeO_2 inside the platinum backing is transferred to the right cell where the extraction and distribution process is performed.
Upper row right side: Details of the special handling equipment inside the first cell.
Lower row left side: Quartz glass apparatus and oven to heat the $^{124}TeO_2$ inside the right cell.
Lower row right side: Details of the microprocessor controlled distribution, packing and measuring equipments inside the right cell.

References

(1) K.H. Assmus, K. Jäger, R. Schütz, F. Schulz, H. Schweickert
Routine Production of Iodine-123 at the Karlsruhe Isochronous Cyclotron, 8th International Conf. on Cyclotrons and Their Applications, Bloomington, Ind., USA, September 18-21, 1978

6.1.10 Thin-Layer Activation Technique for Wear Measurements in Mechanical Engineering

R. Blank, E. Bollmann, R. Dressen, P. Fehsenfeld, B. Gegenheimer, P. Herrmann, A. Kleinrahm, H. Roth, H. Schöllhammer, and B. Schüssler

The cyclotron was used in the last year during 850 hours for thin-layer activation of engine parts. 67 % of them concern orders from the engineering industry, 19 % the development of the thin-layer activation technique proper, and 14 % the demands of the motor test test stands installed at the KfK LIT laboratory. The number of activations increased by 38 % over the number attained in the preceding year. More effective activation methods and the improvements of the technical equipment have reduced by 30 % the mean value of cyclotron operation time per activation as compared with 1978.

Development of technique and methods

The thin-layer activation technique has been adapted extensively to the more effective activation by protons. Proton activation has become the standard method. The advantages of this method are the higher yield of measured radionuclides, especially for ferrous materials, and reduced production of disturbing isotopes as compared with activation by deuterons or alpha-particles.

The technical activation equipment has been extended in order to improve the reliability and precision of irradiation and to minimize the radiation burden for the operation crew. In this way, several supplementary tools have been provided for quick and precise adjustment of the target, which often is more than 100 kg in weight. The adjusting and aiming device has been supplemented by television cameras to a remotely controlled apparatus. The cyclic system for controlling the beam posi-

tion and beam current during the irradiation of machine parts was put into operation stepwise and will soon be completed.

The failure rate of activations has been reduced to less than 3 %. The radiation burden for the operating crew has been halved.

In order to gain flexibility and effectiveness in the use of cyclotron operation time we designed an extension of the equipment for the activation of preadjusted engine parts in series. Vital components of this additional device were tested. The first stage for serial irradiation of two targets will be operable at the end of this year. The cyclotron operation time per activated engine part will be reduced by two hours as the result of this improvement.

Efforts and investments for the extensions of activation equipment seemed to be justified, considering a total loss of DM 40.000,-- to 50.000,-- for one activation failure.

The technique and methods of thin-layer activation have been adapted to the actual problems of the engineering industry, which, at present, is engaged in developing a new generation of more economical combustion engines and turbines. Thus, activations have been performed for new parts such as valve seats and valve stem guides inside the cylinder head, piston rings, piston ring grooves, and cylinder liners, and for new materials such as alloys of Ni, Cr, Co, Ti, Al, Si, Mo, W, and high-grade alloy steel.

Measurement of basic technical data

Research related to basic technical data in activation, i.e. especially measurements of the yield and activity depth distributions of irradiated technical materials, is required for the lay-out of the thin-layer activations.

The application in industry of new materials, usually complicated alloys, and the already mentioned change-over to proton activation as the standard method made it necessary to perform a lot of such measurements of basic technical data during the last year. In order to improve the transformation of the engineering problem into proper irradiation parameters, a suitable gamma spectrometer device was installed.

The equipment for the measurement of basic data is also used for routine quality control of thickness and specific activity of the

active layer on the engine part. The uniformity and correct position of the activated zone on the target are controlled by autoradiographical methods.

Investigations of technical materials

The requirements of the users for thinner active layers and the application of new materials in modern engineering made it necessary to investigate the effects of charged particle irradiation upon material wear behaviour. In first measurements, hardness tests (by Vickers- and Rockwell-B-procedures according to the DIN-regulations) were performed over the depth range of activity on a common grey cast iron and a special alloy steel (G-X165 Cr V 12). The material specimens were irradiated to more than five times the usual activity. All measurements were carried out with unirradiated material as the reference. Within an accuracy of 1 %, the measurements have shown no effects of irradiation on these materials. The program for systematic investigations of irradiation effects on wear behaviour will run over the next years.

6.2 MAGNETIC SPECTROGRAPH

6.2.1 The Magnetic Spectrograph "Little John" and the Modified Experimental Area for Nuclear Reaction Studies at the Karlsruhe Isochronous Cyclotron

H.J. Gils, J. Buschmann, S. Zagromski, H. Rebel, Ch. Rämer, G. Bauer, K. Feißt, and J. Krisch[+]

For nuclear reaction studies with charged particles a magnetic spectrograph in principle has advantages compared to semiconductor detectors and extends the number of possible experiments at a given accelerator considerably. In view of the "light" heavy ions expected by the ECR-ion source HISKA (see contribution 6.1.5) in near future, but also for improving the experimental possibilities with light ions it was decided to built up a small magnetic spectrograph at the Karlsruhe Isochronous Cyclotron. The spectrograph should fulfill the following requirements:

(1) Improvement of the energy resolution up to $\Delta E/E = 5 \cdot 10^{-4}$ for all particles ($2 \leq A \leq 20$)
(2) Considerable improvement of the peak to background ratio in particular for forward angle measurements
(3) Good mass and charge number resolution up to A = 20
(4) Spectroscopy of high energy light ions (p,d,t) up to AE/Z^2 = 300 MeV

Since the spectrograph should come into operation as soon as possible it seemed reasonable not to try to obtain a new building for it but to place it into the existing experimental hall. The restricted place there and also the restricted funds for the project led to a special design (see contribution 6.2.2). In the first stage of operation the spectrograph will consist of two quadrupole magnets, one 60° deflecting dipole magnet and one sextupole magnet. In a later stage a second sextupole should be added for correction of spherical aberrations. The main mechanical and electrical parameters of the QQDS-system are compiled in table 1.

Table 1: Parameters of the magnetic spectrograph "Little John".

Magnetic configuration	QQDS
Main orbit radius (m)	1.5
Deflection angle (degree)	60
Total weight (t)	25
Total system length (m)	8
Focal plane length (m)	0.4
Max. magnetic dipole field (kG)	16.8
Max. power (kW)	70
Angular range (degree)	90

The magnetic units, vacuum chambers and some equipment will be mounted on a support movable by 93° around the target position with a high precision of stability of the entrance optical axis (laboratory scattering angles -3 to +90°).

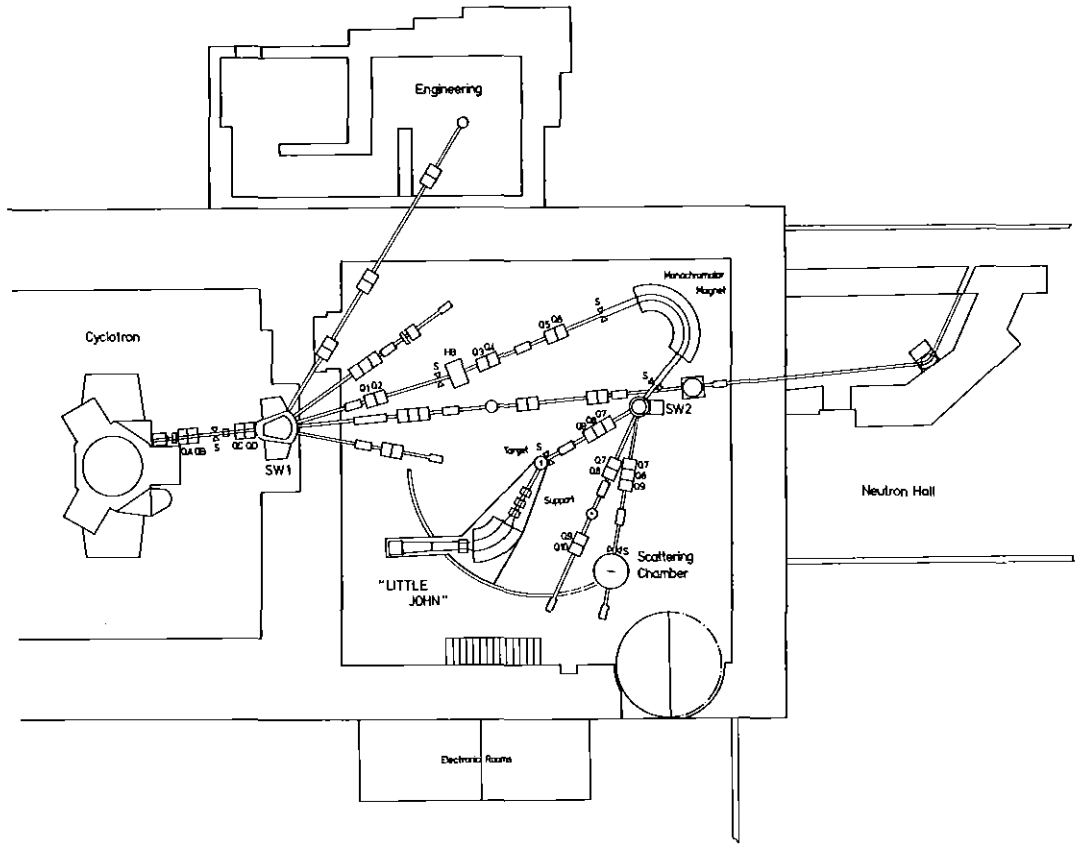

Fig. 1: Experimental area for charged particle nuclear reaction studies at the cyclotron including the magnetic spectrograph "Little John".

In order to install the spectrograph and its 7.5 m radius angular area at the monochromized beam in the experimental hall of the Karlsruhe Isochronous Cyclotron a complete rearrangement of the beam lines is necessary as shown in fig. 1. The new beam line for nuclear reaction studies (III) (which is being built up) includes a 5.5° deflection magnet, the monochromator magnet, a crossing-point with beam-line IV and an additional switching magnet feeding either the spectrograph, the large scattering chamber or a measuring place for γ-spectrosopy and coincidence measurements.

+Hauptabteilung Ingenieurtechnik

6.2.2 Ion Optical Design of the Magnetic Spectrograph "Little John"

H.J. Gils

The ion optical and magnetic requirements for the planned magnetic spectrograph "Little John" have been specified on the basis of the physical motivations compiled in the preceeding contribution (6.2.1). The final design goals shown in table 1 consider also some preconditions as e.g. the given energy resolution of the beam monochromator magnet.

Table 1: Requirements to be fulfilled by the planned magnetic spectrograph.

Mass energy-product	300
Solid angle (msr)	>1
First order momentum resolution $p/\Delta p$	>5200
Momentum acceptance (%)	$>\pm 7$
Kinematical parameter k_{max}	- 1.0 to + 0.5
Focal plane length (m)	<0.5

In order to realize the requirements in spite of the limited funds available it seemed most reasonable to use simple magnets without focussing edges, curved edges or correction coils. In addition, dispersion,

focussing and - if necessary - higher order corrections should be provided by separate magnets. A further correction of ion optical aberrations of higher order is assumed to be performed by reconstruction of the particle trajectories off-line on a computer. For that purpose the space and angular coordinates of the particle have to be determined by the focal plane detector (see contribution 6.3.1). As one of the simplest magnetic configuration fulfilling the stated features a QQDS system was selected with the two quadrupoles (Q) for horizontal and vertical focussing, the dipol (D) providing dispersion and the sextupole enabling to adjust the focal plane tilt. To reach the required mass energy product of 300 at a reasonable dipole field strength, the main orbit radius was chosen to be 1.50 m. The necessary deflection angle to obtain sufficient dispersion (and resolution) is then 60°. A schematic view of the magnetic system is shown in fig. 1 of the preceeding contribution 6.2.1.

Due to the flexible focussing system it is possible to place the focal plane at any position within a given range of 2.3 m. Thereby, the momentum dispersion of the spectrograph is varied from 2 cm/% to 4 cm/%. This enables low resolution experiments with large momentum acceptance of $\pm$ 10 % on the one hand or high resolution experiments with reduced momentum acceptance ($\pm$ 5 %) on the other. For any focal plane position the horizontal and vertical magnifications are nearly the same as shown by the characteristic trajectories in fig. 1.

The kinematic corrections can also be performed easily by the flexible focussing system. In the high dispersion mode kinematical parameters of - .25 to + 0.2 are covered whereas in the low dispersions mode the range is - 1.5 to 0.75.

Second order aberrations have been calculated by beam transport programs and have been found to be important at least for the high dispersion mode. Taking into account the expected specifications of the focal plane detector (1) the off-line correction of the most important second order effects has successfully been simulated by a ray tracing and analyzing program.

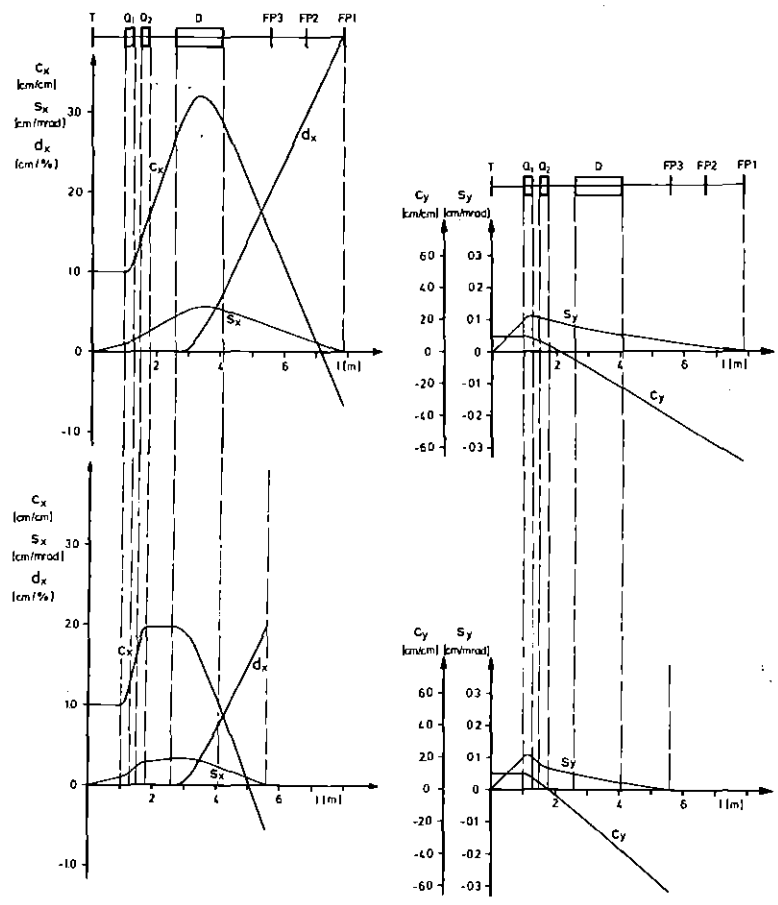

Fig. 1: Characteristic trajectories of the magnetic spectrograph for different focal plane positions.

6.3 DETECTORS

6.3.1 Design of a Position Sensitive Particle Detector for the Magnetic Spectrograph "Little John"

S. Zagromski, H.J. Gils, and H. Rebel

The focal plane detector of a magnetic spectrograph has to perform two tasks of operation: Measurement of the position of a particle traversing the focal plane and identification of charge and mass of the particle. Various types of detectors for these purposes are in use in different accelerator laboratories. For the Karlsruhe magnetic spectrograph "Little John" it seemed to be reasonable to adopt a well operating concept and to optimize it for the specific requirements. For the position sensitive part of the detector the combination of a gas proportional counter with single-wire charge division read-out for determining the x-position and a drift chamber for determining the y-position as it is used at the KVI in Groningen (1) was found to be best suited for our requirements. The design and dimensions of the detector are shown in the schematic outline of fig. 1 (see ref. 2).

Particles enter the detector through a Kapton foil of 50 x 5 cm^2 which holds a pressure difference of 1 atm. They pass through two position sensitive detectors with 10 cm distance between each other. The first one is located exactly at the focal plane of the spectrometer and provides the x-y-position of an incoming particle at this place. The second position sensitive detector gives another set of x-y-coordinates which enables the determination of the incident angle of the particle. The ΔE ionisation chamber, measuring the specific energy loss of the particle, and the E_R scintillator, stopping the particle entirely, serve for particle identification. For this purpose the time of flight of the particle between a time-start detector near the target chamber and the E_R scintillator is also measured. To minimize energy straggling and losses in the spaces between the detectors, which are filled with a (heavy) counter gas, the detector chamber is filled with He-gas at the same pressure. The pressure is adjusted on small gas-flows.

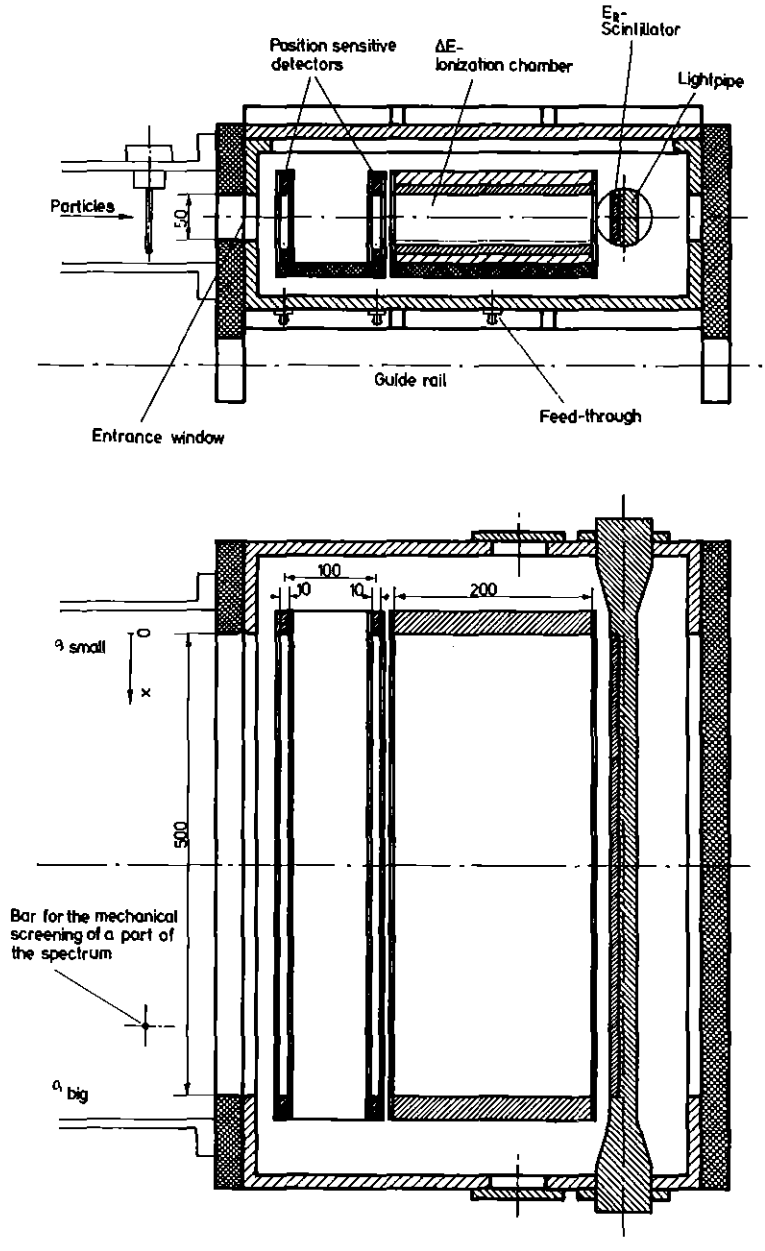

Fig. 1: Schematic cross section of the detector.

All charge sensitive preamplifiers are placed outside of the detector chamber. Feedthroughs on the bottom connect the detector elements with the electronics and high voltage supplies.

The detector is movable fixed on its support and electrically isolated against the beamline and the support.

References

(1) J. van der Plicht and J.C. Vermeulen, Nucl. Instr. and Meth. 156 (1978) 103

(2) S. Zagromski, unpublished

6.3.2 A Position Sensitive Parallel Plate Avalanche Counter for Light Particles

K. Frank[+], W. Kretschmer[+], W. Stach[+], P. Urbainsky[+], and H.G. Rebel

For the Erlangen QD magnetic spectrometer a position sensitive parallel plate avalanche detector (PSPD) was developped (1), which is designed for a high counting rate at extreme forward angles and for light particles. According to ref. 2 the PSPD consists of two foils 5-8 mm apart, where in an electric field of about 1 kV/cm an electron avalanche is produced by an ionizing particle. The corresponding signal is divided on the one foil, which is coated with a suitable resistive Cr layer of 1-3 kΩ. The detector is shown schematically in fig. 1 together with the electronic set-up. Since we plan to separate deuterons and α-particles also due to their energy loss ΔE, the detector was optimized for a maximum ΔE signal and a simultaneously good position resolution.

By the use of isobutane instead of the usual Ar-methane mixture the gas amplification was increased by a factor of about 10. The detector voltage was chosen as high as possible, but slightly below the point of sparks. The dependence of the position resolution on the electric field is shown in fig. 2 for two different resistor plates (R=0.9 kΩ and 3.3 kΩ). A position spectrum for typical working conditions (U=860 V, p=8 mbar, d=7 mm, R=3.3 kΩ) is shown for α-particles in fig. 3; the half width corresponds to a position resolution of 1 mm. The energy loss for deuterons and α-particles from deuteron induced reactions on ^{12}C, shown as two distinct peaks in fig. 4, allows a good separation of these particles. The extension of this simple detector to a two dimensional xy-detector seems to be easy and is now in progress.

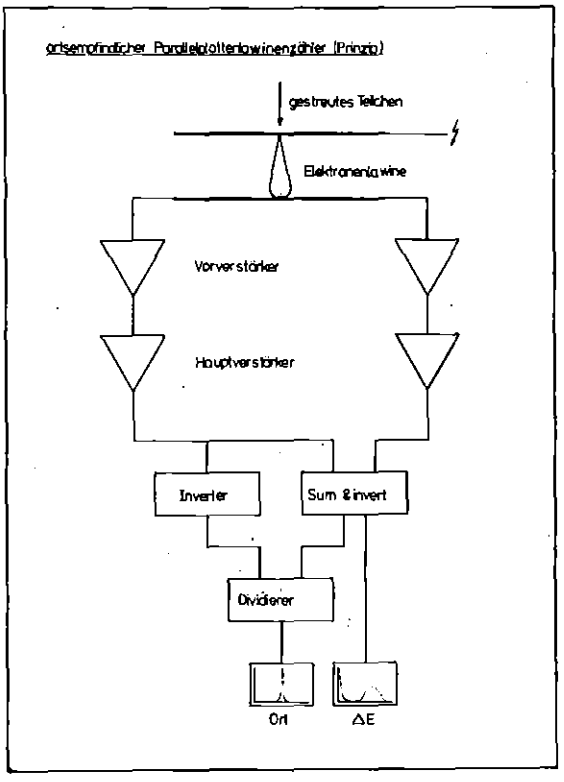

Fig. 1: Schematic picture of the PSPD.

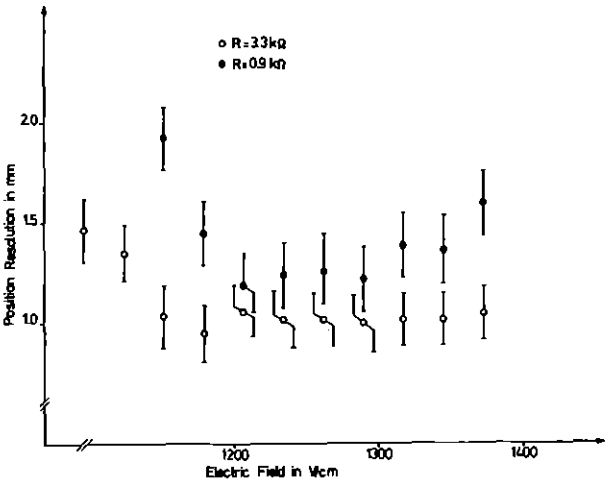

Fig. 2: Position resolution as function of the electric field.

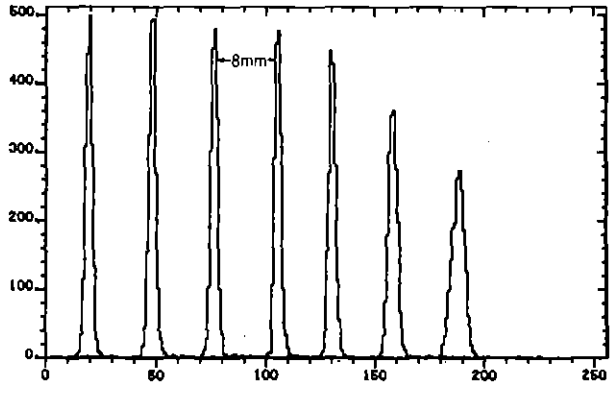

Fig. 3: Position spectrum for α-particles (distance of 8 mm for the α's).

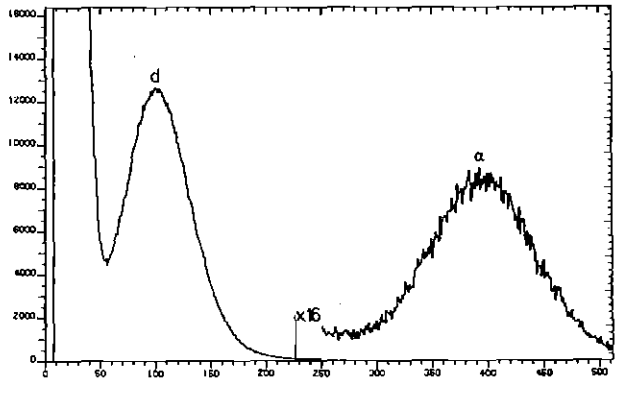

Fig. 4: Energy loss for deuterons and α-particles.

References

(1) K. Frank, Diplom thesis, Erlangen 1980

(2) R.C. Jared, P. Glässel, J.B. Hunter, and L.G. Moretto, Nucl. Instr. and Meth. 150 (1978) 597

+Tandemlabor der Universität Erlangen Nürnberg

6.4 SPALLATION SOURCE

6.4.1 Feasibility Study of High-Intensity H^- Ion Sources for a Linac

S. Göring

In order to increase the peak intensity of the neutron pulse for the projected spallation source the beam pulse of the linac must be compressed by an accumulator ring. The injection of the whole beam intensity of the linac (100 mA) into the accumulator ring is only possible by charge exchange injection of H^- ions. Therefore, the linac would have to be equipped with a H^- ion source characterized by the parameters given in the last column of table 1. It is the aim of this study, to examine the possibility to develope such an ion source.

The basis reaction for the production of a high intensity H^- ion beam is the generation of the H^- ions by interaction of H^+ ions with alkali atoms (caesium or sodium). There are two types of ion sources in use and development. The first one is the charge exchange source in which a positive ion beam is extracted from a plasma source and then converted into H^- ions in a separate charge exchange cell. The other one is the so called surface plasma source (SPS) in which the negative ions come from a cesium-coated metal surface inside a plasma ion source. For the SPS, cold-cathode magnetron and Penning type discharges are used. These compact ion sources having a discharge chamber with a volume of several cm^3 produce negative ion beams of up to 1 A with a current density of up to 4 A/cm^2. Immediately behind the extraction elektrode the H^- beam must be focused by a dipole magnet with an inhomogenious magnetic field.

Many experiences with H^- ion sources are available in the Fermi-Laboratory (FNAL), in Los Alamos (LASL), in Novosibirsk, in Argonne (ANL), and in Brookhaven (BNL). In table 1 a comparison is given between fundamental parameters of the H^- ion sources realized in these laboratories and the parameters of the ion source required for the projected linac. Successful operation of a H^- ion source at a linac (200 MeV) over more than one year was demonstrated in the Fermi-Laboratory. A comparison between the operating parameters of this source and the para-

Table 1: The parameters of H^- ion sources

Laboratory	FNAL	LASL	Novosibirsk		ANL	BNL		required parameters
Typ of ion source	M	P	P	M	DU	M	P	
Beam current[1] (mA)	200	100	200	1000	33	900	440	
Beam current[2] (mA)	50	40	-	-	27	-	-	150
Duty-cycle (%)	0.15	2	2	2	1.5	-	-	5
Duty-cycle (ms•Hz)	0.1•15	0.5•40	0.2•100		0.5•30	50 ms	3 ms	0.5•100
Emittance[3] (cm•mrad/π)	0.088	0.02	0.003		-	-	-	0.1
Emittance[4] (cm•mrad/π)	0.15	0.06	0.02			-	-	0.1
Life-time (d)	60	> 40	13	-	14	-	-	maximum
Gas flow (T•l/s)	0.03	0.25	-	-	0.13	-	-	minimum

P Penning source M Magnetron source

DU Duoplasmatron with a separate charge exchange cell

1 Behind the extraction electrode

2 Behind the preaccelerator (750 keV) or the dipole magnet

3 Normalized emittance for the plane parallel to the magnetic field of the dipole magnet.

4 Normalized emittance for the plane perpendicular to the magnetic field of the dipole magnet

\- No data available

meters of the ion source required for the projected linac shows that the H^- beam current at the end of the preaccelerator must be increased by a factor of 3 and the duty-cycle by more than a factor of 30. This requires improvements at the ion optics of the extraction system and of the dipol magnet and a more effective cooling of the cathode. Another problem arises from the expected short lifetime for the cathode of an ion source with the required H^- beam current of 150 mA at a duty-cycle of 5 %.

6.4.2 Beam Diagnostics for a Spallation Source Linac

H. Schweickert

In the frame of the project study "Spallation Source" we have started to think about the beam diagnostics for the 1.1 GeV, 6-10 mA linear accelerator. One of the main problems is that for such a high current machine the overall losses of the beam have to be in the order of 10^{-4} otherwise serious problems are encountered during the operation of such a machine (induced beam activation; radiation damage to the components etc.). There is no hope that the amount and causes of the beam losses can be foreseen to such a precision using even the most sophisticated beam dynamics codes. The only way out is, to build an appropriate beam diagnostics in order to determine at any particular stage of development the dominant causes of beam spill.

For the diagnostics system itself the key problems are: The high power of the beam and the high precision needed. The first one can be bypassed by assuming that the beam quality parameters will not change dramatically by reducing the duty cycle (100 µsec-width, up to 10 Hz repitition rate). For this case diagnostics equipment is in use at LAMPF, BNL and CERN.

Most of the beam quality parameters however will probably only be measurable for the hot spot of the beam and not for the "halos". These require a sophisticated loss measurement system with the hope to extract from time and space dependent loss patterns the causes of beam spills. Fig. 1 shows a first lay out of a beam diagnostics system for turnup and retune in the range of the accelerator.

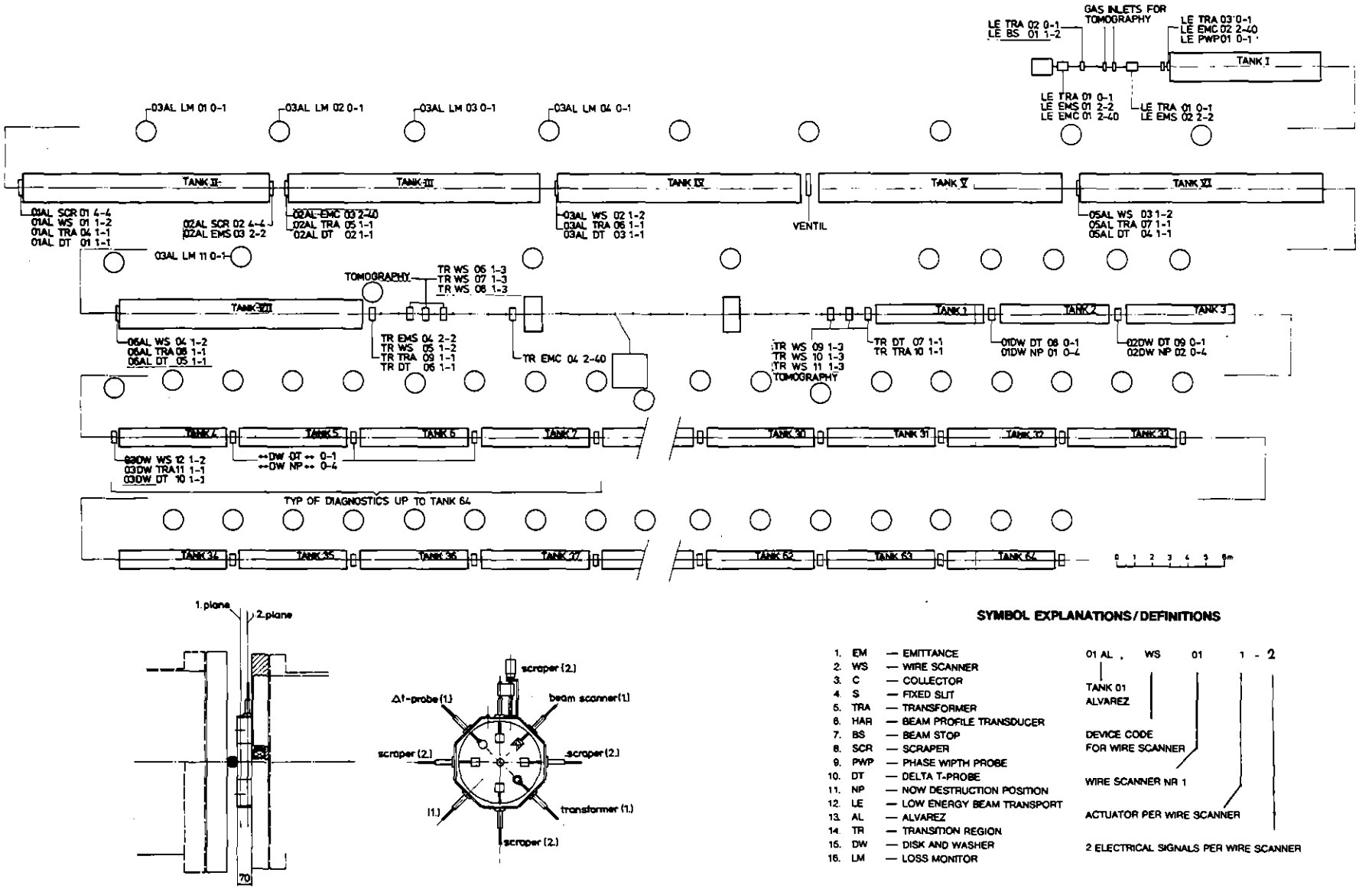

Fig. 1: First layout of a beam diagnostics system for a spallation source linac.

6.5 DATA PROCESSING AND COMPUTERS

6.5.1 GS Function Software

J. Buschmann and K. Gogg[+]

The Graphic System (GS) as developed by HDI and described in ref. 1 comprises the fundamental GS-functions to handle pictures, parts, and objects. Moreover, some supplements are available as software generators for lower case and Greek letters, dotted lines, and so on (2).

In order to enhance the usefulness of GS, more sophisticated function software was developed in the last few months and compiled in a separate manual (3). Besides a number of subroutines, UFO-programs, TSO-procedures and interface programs contributed by other authors, the following items seem to be of general interest:

AXIS1 generates a horizontal or vertical, linear or logarithmic axis;

B7 performs the allocations and initialisations needed for GS running in a TSO-environment;

CHAR1 generates a self-defining symbol;

DINH,DINQ generate a DIN-frame with or without the KfK-emblem;

GRID1 generates a grid by equidistant dotted lines, leaving out a window;

HIST1,HIST2 display an one-dimensional spectrum as a histogramm filling up a given frame;

MAP1,MAP2,MAP3 display a two-dimensional spectrum toning the contour sections or the individual cells by uniformly or statistically distributed points;

POLY1 generates a regular polygon or a circle or a sector of both;

RAST1 generates ten different overlapping point mosaics the densities of which are stepped by factors of two;

SHAD1 shades the area given by a closed or open polygon, the angle and distance of the shading lines being free parameters;

SPL1 generates the image of a polygon reflected by a vertical or horizontal straight line;

TRL1 shifts, scales, rotates, and copies a polygon.

All these functions are written in FORTRAN and exist in a subroutine version (card decks available) as well as in the UFO-program form, in general stored in private TSO-LOAD-libraries. They make use of all the special features provided by GS as attribute list, facultative arguments, checking the GS-error variable after each GS-CALL, and, in case of UFO-programs, using FT09F001 as output file.

The work will be continued.

References

(1) GS-Handbuch, Stand März 1980, edited by HDI

(2) J. Buschmann, K. Gogg, and W. Olbrich, KfK 2868 (Oktober 1979)

(3) GS-Funktions-Software, Stand Juni 1980, edited by J. Buschmann

+Hauptabteilung Datenverarbeitung und Instrumentierung, KfK Karlsruhe, Germany

6.5.2 Status of the BASIC-Compiler

G. Ehret

BASIC is a programming language which is implemented in the NOVA computer as incremental compiler of a p-maschine type intermediate code. This special form of an interpreter system (interpreting the p-code) combined with a good runtime support gives a lot of advantages to the programmer, both during the program development phase and during the debugging phase. But when development begins to stagnate and usage of programms increases the users want faster program execution. Without rewriting the whole program this can only be achieved by a compiler. Therefore the "Institut für Angewandte Informatik und formale Beschreibungsverfahren" was initiated by us to implement a BASIC-Compiler for Data General NOVA computers (1).

The work has been done in a series of 3 diploma works (2,3,4). The compiler is now operational. It is compatible with all features of the interpreter system e.g.:

The statement ENTER"filename" allows user overlays for programs too big to be loaded at one. The compiler meets all

...

behaviour of the interpreter in the case of line number mixture between the resident part and the part to be ENTERed.

Dynamic erasing of program lines is implemented to allow dynamic reduction of programs in size.

Real-time features are available using the ON ERR THEN GOSUB nnn statement extended by us (6) to fulfill the interrupt handling.

The only differences between the compiler and the interpreter system are:

1.) Dynamic allocation of fields is not implemented, but redimensioning is allowed. This means the very first dimensioning may not have the form

```
20    N=70
30    DIM A(N)
```

2.) FOR-NEXT loops must be unique. The case of one FOR and several NEXTs jumped to by IF condition is not supported.

3.) The syntax checking part is kept small. It is assumed that programs are first passed to the interpreter which monitors them for correct syntax.

4.) The SAVE statement is not implemented because there is no real need for it in programs.

The compiler is written in BASIC. It has compiled itself in an 20 hours run. The compiled compiler does the work 6 times faster. This factor applies to the text handling part of BASIC. Computational factors of 4-5 have been measured. Using virtual overlay techniques on mapped NOVA3, NOVA4 or ECLIPSE maschines, another factor of 1.6 is possible. Thus the gain is close to the factor measured formerly between BASIC and FORTRAN IV execution times.

References

(1) G. Ehret et al., IAK II Annual Report 1977/78, KFK 2686 p. 126

(2) Dornheim, Diplomarbeit Universität Karlsruhe 1978

(3) Klaus, Diplomarbeit Universität Karlsruhe 1979

(4) Schutte, Diplomarbeit Universität Karlsruhe 1980

(5) D. Hagemann, Diplomarbeit Universität Karlsruhe 1980

(6) G. Ehret et al., IAK II Annual Report 1975/76, KFK 2223 p. 126

6.5.3 Introduction of a 'Common Memory' into Mapped NOVA RDOS

H. Sobiesiak

On the older machines of type NOVA-2 we supplied the user with an program-independent memory of up to 128kB for his data-accumulation. This memory area was only accessible by data-channel transfers and could not be modified or destroyed by means of normal program execution. Additionally the user had the possibility to start his measurement with one application program, then to return to the operating-system (CLI) and do a lot of other work (e.g.: running compilers) while his data-collection was still in progress.

The introduction of the NOVA-3 series of mini-computers, which offers a main memory size of up to 256kB together with paging hard- and software, raised a serious problem for the way of data-collection mentioned above. On a mapped NOVA-3 (or NOVA-4) the memory allocation is no longer static, thus an uncontrolled data-acquisition might possibly destroy the user-program. Additionally the data-channel memory requirements have to be declared to the operating system which keeps two paging-tables (each for 32 pages) of data-channel accessible memory (page-size: 2kB). These paging tables too are set up dynamically and thus there was actually no chance to get a contigious data-channel memory of up to 64kB.

To overcome these problems a 'common-memory' area was implemeted into RDOS by making small source-code modifications to the operating-system and implementing two additional system-calls.

By means of the first call the user withdraws up to 64kB of memory from the systems pool of unused memory, stores the physical page-numbers into a special table and reserves all of the data-channel map B (the second of the above-mentioned paging tables for this 'common memory'). If the user claims for less then 64kB the rest of map-B is set to a write-protected status. This memory-allocation can only be performed from the background-program without any running foreground-program.

The second call allows the user to get the size of the 'common-memory' area (in multiples of 2kB).

Program-acces to data stored in this area can be done from both fore- and background programs by the use of standard RDOS task call .REMAP by specifing logical pagenumbers that are beyond the range of the program's own extended memory. Up till now no means are provided to protect the 'common-memory' against programmed modification by the second user.

7. COLLOQUIA AT THE INSTITUTE

25.9.79 D. Schüll, GSI Darmstadt
"Schwerionenspektrometer", insbesondere Betriebserfahrungen mit dem QQDQ-Spektrometer am UNILAC der GSI

2.10.79 R.A. Ward, California Institute of Technology
Thermalization of Long Lived Nuclear Isomeric States under Stellar Conditions

30.10.79 R. Shyam, KFA Jülich
Mechanism of fragmentation for the D-, ^{3}He and Alpha-induced reactions

7.11.79 M. Köhler, KFA Jülich
Ein zweidimensionaler ortsempfindlicher Detektor zum Nachweis geladener Teilchen in der Detektorebene des jülicher Magnetspektrographen "BIG KARL"

5.12.79 U. Trinks, Technische Universität München
SUSE: Ein supraleitendes Sektorzyklotron als Nachbeschleuniger für den Tandem in München

12.12.79 M. Brack, Universität Regensburg
Berechnung der Deformationsenergie von Atomkernen: von mikroskopischen zu semiklassischen Theorien

16.1.80 M.N. Harakeh, Kernphysisch Versneller Institut Groningen
The spectrograph focal plane detection system at the K.V.I.: present and future

23.1.80 W. Fuss, Projektgruppe Laserforschung MPG Garching
Isotopentrennung durch Multiphotondissoziation

6.2.80 D.D. Clayton, Rice-University Houston
Confirming nucleosynthesis by isotopic ananomalies in meteorites

7.3.80 R.L. Macklin, Oak Ridge National Laboratory
Re/Os and the age of the milky way

25.3.80 H. Walther, Universität München
Resonante Wechselwirkung mit Laserlicht

26.3.80 C. Jaquot, Centre d'Etudes Nucleaires Grenoble
Intense negative ion beams

23.4.80 R.W. Hamm, Los Alamos Scientific Laboratory
Radio frequency quadrupole accelerating structure research at Los Alamos

23.5.80 Dr. Markov, Laboratory of Nuclear Reactions Dubna
The Cyclotron U-400 and some other developments at the Laboratory of Nuclear Reactions at Dubna

28.5.80 Prof. Jänecke, University of Michigan
Untersuchungen von Alpha-Clustern in schweren Kernen mit Transferreaktionen

18.6.80 J.B. Garg, State University of Albany
Properties of complex spectra with high resolution neutron resonance spectroscopy

25.6.80 W. Hillebrandt, MPI für Physik und Astrophysik München
Stellare Elementsynthese durch Neutroneneinfang

4.7.80 R.L. York, Los Alamos Scientific Laboratory
H^--source developments at LAMPF (polarized and unpolarized)

7.7.80 J. Schwabe, Universität Krakau
Neuere Entwicklungen auf dem Gebiet der Beschleunigertechnik im Institut für Kernphysik in Krakau

9.7.80 E. Matthias, Freie Universität Berlin
Hochauflösende Laserspektroskopie zur Untersuchung von Kerneigenschaften

16.7.80 Ch. Batty, Rutherford Laboratory, Oxfordshire
Exotic atoms

8. PUBLICATIONS AND CONFERENCECONTRIBUTIONS

8.1 PUBLICATIONS

Beck, R.; Goetze, W.; Prelovsek, P.

Theory for the transition to self-trapping in spin-phonon systems
Physical Review.A, 20 (1979) S. 1140-51

Beer, H.; Kaeppeler, F.

Capture-to-fission ratio of ^{235}U in the neutron energy range from 10 to 500 keV
Physical Review C, 20 (1979) S. 201-11

Beer, H.; Kaeppeler, F.

Neutron capture cross sections on ^{138}Ba, ^{140}Ce, ^{142}Ce ^{175}Lu, ^{176}Lu, and ^{181}Ta at 30 keV: prerequisite for investigation of the ^{176}Lu cosmic clock
Physical Review C, 21 (1980) S. 534-44

Cierjacks, S.; Hinterberger, F.; Schmalz, G.; Erbe, D.; Rossen, P. von; Leugers, B.

High precision time-of-flight measurements of neutron resonance energies in carbon and oxygen between 3 and 30 MeV
Nuclear Instruments and Methods, 169 (1980) S. 185-98

Eberle, H.; Matussek, P.; Michel-Piper, I.; Ottmar, H.; Allex, H.

Elemental and isotopic concentration analyses on nuclear fuels using nondestructive assay techniques
Journal of Nuclear Materials, 81 (1979) S. 204-14

Eyrich, W.; Hofmann, A.; Scheib, U.; Schneider, S.; Vogler, F.; Rebel, H.

Decay of the isoscalar giant resonances in ^{208}Pb
Physical Review Letters, 43 (1979) S. 1369-72

Fröhner, F.H.; Wisshak, K.; Kaeppeler, F.

Recent work on structural material cross sections at Kernforschungszentrum Karlsruhe
KfK-2899 (September 1979)

Gils, H.J.; Friedman, E.; Majka, Z.; Rebel, H.

Nuclear density distributions of $^{40,42,44,48}Ca$ from elastic scattering of 104 MeV alpha particles
KfK-2839 (Dezember 1979)

Gils, H.J.; Friedman, E.; Rebel, H.; Buschmann, J.; Zagromski, S.; Klewe-Nebenius, H.; Neumann, B.; Pesl, R.; Bechtold, G.

Elastic scattering of 104 MeV alpha particles from $^{40,42,44,48}Ca$ and determination of the optical potentials
KfK-2838 (Dezember 1979)

Gils, H.J.; Friedman, E.; Rebel, H.; Buschmann, J.; Zagromski, S.; Klewe-Nebenius, H.; Neumann, B.; Pesl, R.; Bechtold, G.

Nuclear sizes of ^{40}Ca, ^{42}Ca, ^{44}Ca, ^{48}Ca from elastic scattering of 104 MeV α particles
I. Experimental results and optical potentials
Physical Review C, 21 (1980) S. 1239-44

Gils, H.J.; Friedman, E.; Majka, Z.; Rebel, H.

Nuclear sizes of ^{40}Ca, ^{42}Ca, ^{44}Ca, ^{48}Ca from elastic scattering of 104 MeV α particles.
II. Nuclear density distributions
Physical Review C, 21 (1980) S. 1245-51

Heck, D.

The karlsruhe proton microbeam system
Beiträge zur elektronenmikroskopischen Direktabbildung von Oberflächen, 12/1 (1979) S. 259-62

Kneis, W.

Rechnergesteuerte Strahldiagnostik und Strahloptimierung am Karlsruher Isochronzyklotron
Dissertation, Universität Heidelberg 1979
KfK-2835 (Juli 1979)

Kneis, W.; Nowicki, G.; |Ed.|

Annual Report Teilinstitut Kernphysik des Instituts für Angewandte Kernpyhsik
(July 1, 1978 - June 30, 1979)
KfK-2868 (October 1979)

Leugers, B.

Die Neutroneneinfangquerschnitte der Kryptonisotope und ihre Bedeutung für die Astrophysik
Dissertation, Universität Karlsruhe 1979
KfK-2895 (November 1979)

Mairle, G.; Knöpfle, K.T.; Riedesel, H.; Wagner, G.J.; Bechtold, V.; Friedrich, L.

The optical potential for vector-polarized deuterons of 52 MeV
Nuclear Physics, A 339 (1980) S. 61

Majka, Z.; Gils, H.J.; Rebel, H.

Saturation effect and determination of nuclear matter density distribution from optical potential
Acta Physica Polonica, B11 (1980) S. 227-31

Naqvi, A.A.

Die Fragmenteigenschaften bei der Spaltung von ^{237}Np mit schnellen Neutronen - eine experimentelle Untersuchung zur Spaltungsdynamik
Dissertation, Universität Karlsruhe 1980
KfK-2919 (März 1980)

Neumann, B.

Experimente zum Aufbruch von ^{6}Li-Ionen
KfK-2887 (Dezember 1979)

Neumann, B.; Buschmann, J.; Klewe-Nebenius, H.; Rebel, H.; Gils, H.J.

Transfer of ^{6}Li break-up fragments at ^{6}Li projectile energies far above the Coulomb barrier
Nuclear Physics, A329 (1979) S. 259-70

Rebel, H.

Isotope shifts in unstable nuclei. Invited talk presented at the IOP conference 'trends in nuclear structure physics' University of Manchester, GB, April 16-18, 1980
KfK-2974(Mai 1980)

Rebel, H.; Bekk, K.; Nowicki, G.; Schatz, G.

Atomic beam laser spectroscopy of neutron deficient Ba-nuclides
Nukleonika, 25 (1980) S. 145-63

Rebel, H.; Gils, H.J.; Schatz, G.; |Ed.|

What do we know about the radial shape of nuclei in the Ca-region ?
Proceedings of the Karlsruhe International Discussion Meeting, held at Kernforschungszentrum Karlsruhe, May 2-4, 1979
KfK-2830 (Juli 1979)

Rost, H.; Eyrich, W.; Hofmann, A.; Scheib, U.; Vogler, F.; Rebel, H.

A study of the giant resonance region of ^{40}Ca by inelastic scattering of 104 MeV α-particles
Physics Letters, 88B (1979) S. 51-54

Rullhusen, P.; Smend, F.; Schumacher, M.; Hanser, A.; Rebel. H.

Coulomb correction to Delbrueck scattering investigated at Z = 94
Zeitschrift für Physik, A 293 (1979) S. 287-92

8.2 CONFERENCE CONTRIBUTIONS

20. Annual Meeting of the Institute of Nuclear Materials Management, Albuquerque, July 16-19,1979

Ottmar, H.

Results from an interlaboratory exercise on the determination of plutonium isotopic composition by gamma spectrometry

19. Tagung für Elektronenmikroskopie und 12. Kolloquium des Arbeitskreises für Elektronenmikroskopische Direktabbildung und Analyse von Oberflächen Tübingen, September 9-14, 1979

Heck, D.

The Karlsruhe proton microbeam system

21. NEANDC Meeting, Geel, September 26, 1979

Fröhner, F.H.; Wisshak, K.; Käppeler, F.

Recent work on structural material cross sections at Kernforschungszentrum Karlsruhe. Topical Discussion on Progress in Neutron Data of Structural Materials for Fast Reactors since the NEANDC/NEACRP Specialist Meeting at CBNM Geel in December 1977

Nuclear Cross Sections for Technology, Internat. Conference, Knoxville, October 22-26, 1979

Beer, H.; Käppeler, F.

The measurement of Maxwellian averaged capture cross sections for ^{138}Ba, ^{140}Ce, ^{175}Lu and ^{176}Lu with a special activation technique

Leugers, B.; Käppeler, F.; Fabbri, F.; Reffo, G.

keV neutron capture cross sections for the s-processes isotopes of Se, Br and Kr and the abundance of krypton in the solar system

Wisshak, K.; Wickenhauser, J.; Käppeler, F.

The branching ratio in ^{242}Am after neutron capture in ^{241}Am in the keV region

Beer, H.; Käppeler, F.; Wisshak, K.

The neutron capture cross sections of natural Yb, ^{170}Yb, ^{175}Lu and ^{184}W in the energy range from 5 to 200 keV for the ^{176}Lu-chronometer

Wisshak, K.; Käppeler, F.

Determination of the capture width of the 27.7 keV s-wave resonance in ^{56}Fe

1. Meeting on ECR Ion Sources, Louvain-la-Neuve, December 12, 1979

Bechtold, V.; Ehret, H.P.; Friedrich, L.; Möllenbeck, J.; Schweickert, H.; Ziegler, P.

Status of the ECR-ion source Karlsruhe

Neutron Cross Sections of Fission Product Nuclei, Specialists' Meeting Bologna, December 12-14, 1979

Leugers, B.; Käppeler, F.

Capture cross section measurements on natural xenon, natural krypton and on various krypton isotopes between 3 and 250 keV neutron energy

INTERNAT. WINTER-MEETING ON NUCLEAR PHYSICS
BORMIO, JANUARY 21-26, 1980

Gils, H.J.; Friedman, E.

'Model independent' analysis of elastic alpha-particle scattering and determination of nuclear sizes

FRÜHJAHRSTAGUNG DPG, ATOMPHYSIK
BIELEFELD, MARCH 3-7, 1980

Andl, A.; Bekk, K.; Hanser, A.; Nowicki, G.; Rebel, H.; Schatz, G.

Isotopieverschiebung und Hyperfeinstruktur der Calcium-Resonanzlinie für die Isotope mit 40<=A<=48

FRÜHJAHRSTAGUNG DPG, KERNPHYSIK, MÜNCHEN, MARCH 17-21, 1980

Andl, A.; Bekk, K.; Hanser, A.; Nowicki, G.; Rebel, H.; Schatz, G.

Bestimmung der Kernladungsradien der Calcium-Isotope mit 40<=A<=48 mittels hochauflösender Laserspektroskopie

Beck, R.; Mihalovic, M.

Study of $^{3}He + ^{4}He$ elastic scattering with the generator coordinate method

Corcalciuc, V.; Dumitrescu, R.; Ciocanel, A.; Gils, H.J.; Rebel, H.; Zagromski S.; Stach, W.

Feinstruktur in den Winkelverteilungen der inelastischen Streuung ?

Frank, K.H.; Kretschmer, W.; Loeh, H.; Stach, W.; Urbainsky, P.; Rebel, H.

Ortsempfindlicher Parallelplattenzähler

Käppeler, F.; Beer, H.; Wisshak, K.

Untersuchung der s-Prozess-Systematik mit neuen Neutroneneinfangquerschnitten

Leugers, B.; Käppeler, F.

Die Neutroneneinfangquerschnitte der Kryptonisotope und ihre Bedeutung für die Astrophysik

Neumann, B.; Rebel, H.; Buschmann, J.; Gils, H.J.; Zagromski, S.; Klewe-Nebenius, H.

Untersuchungen zum Projektil-Aufbruch in Kernreaktionen mit 156 MeV ^{6}Li-Ionen

Rost, H.; Eyrich, W.; Hofmann, A.; Rebel, H.; Scheib, U.; Vogler, F.

Isoskalare Dipol-Zustände im Riesenresonanzbereich von (sd)-Schalenkernen

Bechtold, V.; Ehret, H.P.; Friedrich, L.; Möllenbeck, J.; Schweickert, H.; Ziegler, P.

HISKA, eine ECR-Quelle für das Karlsruher Isochron-Zyklotron

Beer, H.; Käppeler, F.; Wisshak, K.

Neutroneneinfang an ^{175}Lu und ^{170}Yb zur Bestimmung des s-Prozess-Alters über den Zerfall von ^{176}Lu

Dickmann, F.

Paarungskorrelationen in Kernen unter dem Einfluß eines Feldes ungerader Zeitspiegelungsparität

Gils, H.J.; Friedman, E.

Vorzüge und Grenzen neuer flexibler Parametriesierungen des optischen Potentials der elastischen α-Teilchen-Streuung

Kretschmer, W.; Loeh, H.; Stach, W.; Schuster, W.; Urbainsky, P.; Wango, M.B.; Rebel, H.

Untersuchung von Shape-Effekten bei der Streuung von tensorpolarisierten Deuteronen

Mairle, G.; Knöpfle, K.T.; Riedesel, N.; Wagner, G.J.; Bechtold, V.; Friedrich, L.

Das optische Potential für vektorpolarisierte Deuteronen von 52 MeV

Pesl, R.; Gils, H.J.; Buschmann, J.; Rebel, H.; Zagromski, S.; Klewe-Nebenius, H.

Streuung von 104 MeV Alpha-Teilchen an ^{48}Ca, ^{50}Ti, ^{52}Cr

Stamminger, R.; Eyrich, W.; Hofmann, A.; Rebel, H.; Rost, H.; Steuer, H.; Scheib, U.

Messung des Neutronenzerfalls der isoskalaren Riesenresonanzen im ^{208}Pb

2. ANNUAL SYMPOSIUM ON SAFEGUARDS AND NUCLEAR MATERIALS CONTROL, ESARDA
EDINBURGH, MARCH 26-28, 1980

Eberle, H.; Matussek, P.; Michel-Piper, I.; Ottmar, H.

Assay of uranium and plutonium in solution by K-edge photon absorptiometry of a continuous X-ray beam

TRENDS IN NUCLEAR STRUCTURE PHYSICS
MANCHESTER, APRIL 16-18, 1980

Andl, A.; Bekk, K.; Göring, S.; Hanser, A.; Nowicki, G.; Rebel, H.; Schatz, G.

Laser spektroscopy of radioactive alkaline earth atoms

SECOND TECHNICAL MEETING ON THE NUCLEAR TRANSMUTATION OF ACTINIDES
ISPRA, APRIL 21-24, 1980

Wisshak, K.; Käppeler, F.; Wickenhauser, J.; Hage, W.

Neutron capture and fission cross section measurements of ^{241}Am in the keV range

2. INTERNAT. CONFERENCE ON PARTICLE-INDUCED X-RAY EMISSION AND ITS ANALYTICAL APPLICATIONS, LUND, JUNE 9-12, 1980

Heck, D.

The influence of secondary fluorescence from elements adjacent to the microbeam spot on local concentration determinations with PIXE

17TH EUROPEAN CYCLOTRON PROGRESS MEETING
KARLSRUHE, JUNE 26-27, 1980

Bechtold, V.; Friedrich, L.; Schweickert, H.

HISKA Status Report

KfK-Cyclotron Group - Schweickert, H.

Status Report on the Karlsruhe Isochronous Cyclotron

POSTERS :

Gils, H.J.; Buschmann, J.; Zagromski, S.; Rebel, H.

Karlsruhe magnetic spectrograph 'Little John'

Kernert, N.; Peters, J.W.; Sheikh, S.

^{81}Rb-Production at Karlsruhe

8.3 LECTURES

Gils, H.J.

Determination of alpha-nucleus optical potentials and nuclear metter radii by elastic alpha-scattering from Ca-nuclei
Institut of Physics, Jagellonian University, Kraków, December 12, 1979

Käppeler, F.

Neutroneneinfangquerschnitte im keV-Bereich und ihre Bedeutung für die Entstehung der Elemente
Institut für Strahlenphysik, Universität Stuttgart, Juni 6, 1980

Nowicki, G.

Nuclear charge radii of calcium isotopes from high resolution laser spectroscopy
Nuclear Physics Laboratory, University of Oxford
April 14, 1980

Nowicki, G.

Laserspektroskopie an radioaktiven Erdalkali-Atomen
Institut für Angewandte Physik, Universität Bonn, Juni 3, 1980

Rebel, H.

Laser spectroscopy of unstable nuclei
Racah Institute of Physics, Hebrew, University Jerusalem, March 11, 1980

Rebel, H.

Nuclear structure studies with high resolution laser spectroscopy
Weizmann-Institut, Rehovoth, March 14, 1980

Rebel, H.

Matter distributions and neutron-proton radii differences in Ca-nuclei
Nuclear Physics Laboratory, University of Oxford, April 14, 1980

Rebel, H.

Nuclear structure studies by laser spectroscopy of alkali earth nuclides
Institut Max von Laue-Paul Langevin, Grenoble, May 8, 1980

Rebel, H.

Differences in charge and matter distributions of Ca nuclei from high-resolution laser spectroscopy and MeV alpha particle scattering
Institut Des Sciences Nucleaires, Universite de Grenoble, May 9, 1980

Schatz, G.

Laser spectroscopy of radioactive Ba atoms
Institut of Physics, Jagellonian University Kraków, December 14, 1979

Schatz G.

Laserspektroskopie an radioaktiven Erd-alkali-Atomen
Universität Kaiserslautern, April 21, 1980

Schatz, G.

Laserspektroskopie an radioaktiven Atomen
KFA JÜlich, Institut für Kernphysik,
November 26, 1979

Schatz, G.

Laser spectroscopy of minute samples of radioactive alkaline earth atoms
KVI, University Groningen, February 11, 1980

8.4 PATENT GRANT

Schulz, F.

Ionenquelle für ein Zyklotron
DE-AS 2029 571 (10.1.1980)

9. PERSONNEL

Head of the Teilinstitut Kernphysik: Prof. Dr. G. Schatz

Scientific and technical staff:

Beck, R., Dr.	Feurer, B.	Nowicki, G., Dr.
Beer, H., Dr.	Gils, H.J., Dr.	Ottmar, H., Dr.
Bekk, K., Dr.	Göring, S., Dipl.-Phys.	Rebel, H.G., Prof., Dr.
Buschmann, J., Dr.	Hanser, A., Dr.	Rupp, G.
Dickmann, F., Dr.	Heck, D., Dr.	Schmalz, G., Dipl.-Ing.
Dohrmann, H., Ing.	Käppeler, F., Dr.	Schmidt, K.A., Dipl.-Phys.
Eberle, H., Ing.	Leugers, B., Dipl.-Phys.	Wisshak, K., Dr.
Erbe, D.	Matussek, P., Dipl.-Phys.	Zagromski, S., Ing.
Feißt, K., Mrs.	Michel-Piper, I., Mrs., Ing.	

Guests and research students:

Almeida,J.,Dipl.-Phys.	Krivec, R., Dipl.-Phys.	Neumann, B., Dipl.-Phys.
Andl, A., Dipl.-Phys.	Majka, Z., Dr.	Pesl, R., Dipl.-Phys.
Friedman, E., Prof., Dr.	Mihailović, M.V., Prof., Dr.	
Kazerouni,M.A.,Dipl.-Phys.	Naqvi, S.A.A., Dipl.-Phys.	

Secretarial staff: Mrs. H.M. Friederich, Mrs. E. Maaß

Head of the Cyclotron Laboratory: Dr. H. Schweickert

Scientific and technical staff of the Cyclotron Laboratory:

Acharya, H., Mrs.	Erdel, E.	Kappel, W.-R., Ing.
Assmus, K.H.	Fehsenfeld, P., Dr.	Kauther, P.
Bauer, G.	Franz, J.	Kessel, M.
Bechtold, V., Dr.	Friedrich, L., Dr.	Kneis, W. Dr.
Bialy, J., Dipl.-Phys.	Gegenheimer, B.	Kögel, B.
Biber, J.	Günther, O.	Kuhn, H.
Blank, R.	Haushahn, G., Dipl.-Phys.	Mangold, D.
Bollmann, E., Dipl.-Phys.	Heidenreich, K.	Maier, W.
Depta, A.	Heinzmann, H., Dipl.-Inf.	Möllenbeck, J., Ing.
Dressen, R.	Herrmann, P.	Peters, J.-W., Dipl.-Phys.
Ehret, H.P.	Hirth, W.	Radtke, G., Ing.

Rämer, Ch., Miss, Ing.	Schulz, F., Ing.	Seufert, H.
Röhrl, E.	Segnitz, W.	Stöbener, E., Ing.
Schüssler, B.	Seidel, H.	Wiss, L.
Schimpf, P.	Seitz, J.	

Guests and research students:

Heasman, K.	Kernert, N.	Sheikh, S.

Workshop of the Cyclotron Laboratory:

Bleier, W.	Maier, W.	Schönstein, E.
Ernst, R.	Möck, W.	Schütz, R.
Hauer, W.	Petermann, W.	Würges, J.
Heitz, E.	Ripp, H.	
Klinger, G.	Schlenker, G.	

Secretarial staff: Mrs. E. Kirste, Mrs. R. Uchatius